NUREG/CR-1623
EGG-2052
Distribution Category: R3

A STUDY OF FILM BOILING, QUENCH, AND REWET PHENOMENA DURING HIGH PRESSURE POWER-COOLING-MISMATCH TESTING

Fred S. Gunnerson
Paul S. Dunphy

Published October 1980

EG&G Idaho, Inc.
Idaho Falls, Idaho 83415

Prepared for the
Nuclear Regulatory Commission
Washington, D.C. 20555
Under DOE Contract No. DE-AC07-76IDO1570
FIN No. A6041

ABSTRACT

The result of many postulated nuclear reactor accidents is a power-coolant imbalance where the heat generation rate of the nuclear core exceeds the heat removal capacity of the coolant. As part of the U.S. Nuclear Regulatory Commission's Program to study the behavior of fuel rods during such off-normal operation, EG&G Idaho, Inc., has conducted an extensive series of power-cooling-mismatch (PCM) tests within the Idaho National Engineering Laboratory Power Burst Facility.

This report summarizes a study of the thermal-hydraulic phenomena associated with high-pressure PCM testing within the Power Burst Facility. The primary emphasis is on departure from nucleate boiling and subsequent quench/rewet behavior.

SUMMARY

An extensive Power-Cooling-Mismatch (PCM) Test Series was recently completed as part of the U.S. Nuclear Regulatory Commission's Thermal Fuels Behavior Program. The in-pile tests were conducted by EG&G Idaho, Inc., in the U.S. Department of Energy's Idaho National Engineering Laboratory Power Burst Facility (PBF).

The test series consisted of 16 individual experiments which incorporated pressurized water reactor (PWR) type nuclear fuel rods and active fuel lengths of 0.879 to 0.914 m. Coolant pressures up to 15.6 MPa were used. Three basic test configurations were utilized: (a) single-rod tests, where a fuel rod was contained within its own coolant flow shroud, (b) four-rod tests, where each fuel rod was contained within its own coolant flow shroud, hydraulically coupled in parallel, and (c) nine-rod open bundle tests. PCM conditions were initiated by starving coolant flow, increasing test rod power, or both. All tests resulted in film boiling conditions for brief or sustained periods.

This report presents a study of thermal-hydraulic phenomena associated with the PBF Power-Cooling-Mismatch Test Series. Primary emphasis is placed on local and system conditions which influence the onset of film boiling and subsequent film boiling destabilization behavior. General considerations of power-cooling-mismatch testing, including two-phase flow patterns, typical PCM boiling cycles, and an overview of worldwide PCM testing, are also discussed.

Experimental data from the PBF/PCM Test Series are used to develop an empirical critical heat flux (CHF) correlation. Comparison with well-known reactor vendor CHF correlations indicates that, in general, the Combustion Engineering (CE-1) and LOFT correlations best model the observed onset of film boiling behavior.

Film boiling destabilization phenomena, which include quenching and rewetting, are also assessed. It is shown that quenching and rewetting are distinctly different processes involving different modes of heat transfer. Empirical and analytical correlations are presented which allow the cladding surface temperature at the onset of quenching and rewetting to be estimated from first principles.

A comparison of the thermal-hydraulic conditions at the onset of film boiling is made with the conditions at the onset of film boiling destabilization. Results indicate that the thermal-hydraulic conditions are indistiguishable and that return to nucleate boiling proceeds via the same path as boiling transition, with no signs of hysteresis.

A wide variety of temperature terminologies are used within this report, and as a result may be confusing to the casual reader. Therefore, a listing of temperature terminologies and numerical values common to the nuclear industry is given.

ACKNOWLEDGMENTS

The authors thank Mr. D. T. Sparks and Dr. R. A. Nelson, Jr. for their helpful discussions and input to portions of this study, and Mr. D. H. Schwieder for his help in correlating the experimental data.

CONTENTS

FIGURES

TABLES

NOMENCLATURE

Symbol	Description (units)
A	Area (m^2)
C_p	Heat capacity (kJ/kg·K)
F_{APF}	Axial peaking factor
F_{cw}	Cold-wall factor
G	Coolant mass flux ($kg/m^2 \cdot s$)
GWD	Gigawatt days
h_{fg}	Latent heat of vaporization (kJ/kg)
J	Nucleation rate ($m^{-3}s^{-1}$)
k	Thermal conductivity (watt/m·K)
k	Boltzmann constant (J/K)
L	Length (m)
M	Mass (kg)
MTM	Metric ton metal
N	Molecules per unit volume (m^{-3})
P	Pressure (MPa)
P_p	Peak linear rod power (kW/m)
r	Radius (m)
S	Slip parameter
T	Temperature (K), (see Appendix A)
t	Time (s)
V	Velocity (m/s)
W	Work of vapor formation (Joules)
Z	Elevation (m)

Greek Symbol	Description (units)
α	Thermal diffusivity (m^2/s)
δ	Cladding thickness (m)
θ	Contact angle (degrees)
μ	Chemical potential (Joules)
ρ	Density (kg/m^3)
σ	Surface tension (N/m^2)
ϕ	Heat flux (kW/m^2)
χ	Quality
ω	Frequency (s^{-1})

Subscripts	Description
CHF	Critical heat flux
CRIT	Property at critical point
DNB	Departure from nucleate boiling
HN	Homogeneous nucleation
i	Incipient boiling
in	Inlet
L	Liquid
Leid	Leidenfrost
MP	Melting point
max,s or ms	Maximum superheat
min	Minimum point
o	Sputtering
q	Quench
r_w	Rewet
sat	Saturation
sc	Subcooling
SN	Spontaneous nucleation
v	Vapor
w	Water of heater
ws	Maximum minus saturation

Acronyms	Definition
B&W	Babcock & Wilcox
BWR	Boiling water reactor
CHF	Critical heat flux
DNB	Departure from nucleate boiling
ECC	Emergency core cooling
FBD	Film boiling destabilization
GETR	General Electric Test Reactor
HBWR	Heavy boiling water reactor
IE	Irradiation effects
INEL	Idaho National Engineering Laboratory
LLR	LOFT Lead Rod
LOCA	Loss-of-coolant accident
LOFT	Loss-of-fluid test
LWR	Light water reactor
PBF	Power Burst Facility
PCM	Power-cooling-mismatch
PWR	Pressurized water reactor
RIA	Reactivity initiated accident
RNB	Return to nucleate boiling
SGHWR	Steam generating heavy water reactor
TC	Thermocouple
W	Westinghouse

A STUDY OF FILM BOILING, QUENCH, AND REWET PHENOMENA DURING HIGH PRESSURE POWER-COOLING-MISMATCH TESTING

1. INTRODUCTION

During normal operation of a commercial water-cooled nuclear reactor, the fuel rod cladding temperatures are usually near the saturation temperature of the water. However, an accidential increase in core power, decrease in coolant flow, or change in pressure may lead to a deterioration in heat transfer and a subsequent increase in cladding surface temperatures. The temperatures may rise to such a level that continuous coolant-cladding contact can no longer be maintained. Depending on the reference system (a pressurized water reactor or a boiling water reactor system), this phenomenon is referred to as boiling transition, the boiling crisis, departure from nucleate boiling (DNB), or dryout.

Although nuclear reactors are designed to operate under conditions where film boiling or dryout does not occur, accidents can be postulated where dryout does occur. Two of the most serious types of postulated accidents are thought to be the large-break, loss-of-coolant accident (LOCA), where the coolant inventory within the primary system is rapidly lost, and the reactivity-initiated accident (RIA), in which a sudden power increase is initiated within the nuclear core. Between these two extremes lies a wide range of off-normal power-cooling imbalance conditions, commonly referred to as power-cooling-mismatch (PCM) events. In contrast to a LOCA, a PCM event may precipitate fuel rod overheating without a deficiency in total coolant inventory. Overheating occurs when the power-cooling conditions are such that dryout or film boiling results. In present light water reactor (LWR) design and licensing efforts, considerable attention has been focused on the prevention and mitigation of film boiling occurrences.

Rigorous licensing procedures for commercial nuclear reactor operation require detailed analysis of the phenomena associated with such postulated accidents. EG&G Idaho, Inc., has recently completed an extensive series of in-pile tests as part of the U.S. Nuclear Regulatory Commission's (NRC) LWR fuel behavior program.[1,2] The tests were conducted in the Power Burst Facility (PBF) at the Idaho National Engineering Laboratory (INEL). Two categories of tests were conducted, power-cooling-mismatch (PCM) and irradiation effects (IE) tests. The PCM tests were designed to investigate the effects of thermal-hydraulic conditions on film boiling and resultant fuel rod behavior. The IE tests[a] investigated the influence of prior irradiation history and rod design on film boiling and fuel rod behavior. A partial overview of the test designs, objectives, and results are given in References 3 and 4. Details of the individual tests are given in References 5 through 16.

This report is part of a series of topical studies which were conducted to investigate a spectrum of phenomenological behavior observed during PCM testing. Previous studies have focused on fuel swelling due to retained fission gas,[17] fuel powdering within unrestructured fuel,[18] oxygen diffusion during fuel-cladding interactions,[19] molten fuel motion and cladding thermal failure,[20] high-temperature oxidation and cladding embrittlement,[21] and the behavior of defective pressurized water reactor (PWR) fuel rods during PCM testing.[22]

This report presents a study of thermal-hydraulic phenomena associated with the PBF Power-Cooling-Mismatch Test Series. Primary emphasis is placed on departure from nucleate boiling and subsequent film boiling destabilization behavior of PWR-type fuel rods.

Section 2 presents general aspects of power-cooling-mismatch testing including two-phase flow patterns, typical PCM boiling cycles, and an overview of worldwide PCM testing. In addition, a brief description of the design and conduct of the PBF/PCM Test Series is given.

---

a. The IE tests were PCM-type experiments. Within this report the general terminology PCM is used to encompass both the power-cooling-mismatch and irradiation effects experimental programs.

The third section of this report addresses the critical heat flux (CHF). Empirical CHF correlations are developed to model the PBF experimental data base. An additive or superposition correlation form, suggestive of the well-known loss-of-fluid test (LOFT) CHF correlation, was found to satisfactorily describe the experimental data. Comparisons are also made with the Combustion Engineering (CE-1), Babcock and Wilcox (B&W-2), LOFT, and Westinghouse (W-3) critical heat flux correlations.

Quench and rewet behavior are discussed in the fourth section of this report. Quench and rewet temperatures are differentiated and defined, and methods of prediction are presented. An illustrative comparison of top-spray, bottom reflood, and film boiling destabilization-type quench/rewet mechanisms is also provided.

The fifth section of this report compares departure from nucleate boiling with quenching behavior. It provides fundamental insight into the similarities and differences of the onset of film boiling and the onset of film boiling destabilization behavior. An empirical relationship, based on inlet boundary conditions, is developed to describe the associated parametric trends.

A wide variety of temperature terminologies is used in this report. To reduce confusion and possible misunderstanding, Appendix A lists and quantitively defines temperature terminologies common to the nuclear industry. Appendix B details the critical heat flux correlations used in this report. The experimental PBF data base for departure from nucleate boiling and quenching is tabulated in Appendix C. Finally, a brief discussion of the methodology and calculations used in the course of this study is presented in Appendix D.

2. GENERAL CONSIDERATIONS

The heat transfer regime that is encountered during a PCM event depends primarily on the surface temperature of the cladding. The cladding surface temperature, in turn, is dependent upon the fuel rod power distribution, the elevation on the rod, and the thermophysical nature of the local coolant. When two-phase coolant conditions are present, the flow and heat transfer become difficult to describe analytically. This is because the liquid and vapor phases do not flow at the same velocity and the void fraction or quality distribution is not necessarily uniform across the coolant channel. As a result, the relationship between the quality, the void fraction, and the volumetric flow fraction varies according to the flow pattern.

The underlying foundations for two-phase flow are a set of conservative and constitutive equations. Unfortunately, the basic set of equations are rather complex and inconvenient to use; thus, simplifying assumptions (that are somewhat controversial) are often made. This is why two-phase flow modeling is still a lively subject of research.

2.1 Two-Phase Flow Patterns During Power-Cooling-Mismatch Testing

A power-cooling-mismatch event is characterized by a power/cooling imbalance where the rate of heat generation exceeds the heat removal rate of the coolant. It may be initiated by a reduction in coolant flux, a power increase, or both. If the heat generation rate of a fuel rod exceeds the local single-phase (liquid) forced-convective heat removal rate of the coolant, vapor formation ensues.

Figure 1 illustrates the two-phase, forced convective flow regimes that are encountered during a subcooled PCM event for an overheated fuel rod located in an individual coolant flow shroud. This geometry is typical of most in-pile PCM experiments. Also illustrated in this figure is the corresponding cladding surface temperature as a function of elevation on the rod.

Initially, subcooled liquid enters the bottom of the annular coolant flow shroud (Figure 1) where it is heated as it flows upward. At some elevation, the liquid near the cladding surface reaches saturation conditions (incipient boiling) and local subcooled nucleate boiling commences. Beyond this point, quality continues to increase and subcooled nucleate boiling dominates and is characterized by a bubbly flow pattern. The calculated quality (see Appendix D) within the bubbly flow regime is about 5 to 10% (20 to 40% void fraction) and the cladding surface temperature remains approximately constant, just above the saturation temperature. At some elevation above the peak power location, subcooled film boiling ensues and the rod becomes vapor blanketed. The resultant film boiling heat transfer creates an inverse annular flow regime with local qualities (Appendix D) up to about 30% (70% void fraction). At the point where departure from nucleate boiling occurs, the cladding surface temperature rises rapidly and remains high throughout the film boiling region.

2.2 Typical Power-Cooling-Mismatch Boiling Cycle

A typical power-cooling-mismatch test consists of the following steps:

1. Establish initial subcooled, single-phase, forced convective conditions
2. Decrease the coolant mass flux or increase rod power or both until film boiling conditions are detected
3. Maintain conditions and establish a period of stable film boiling
4. Increase coolant mass flux or decrease power or both to initiate film boiling destablization (quench) and return to nucleate boiling.

The above steps are illustrated on a forced convective boiling surface in Figure 2. The boiling surface illustrated is for a time independent, fixed elevation, and constant coolant mass flux condition. Changing the coolant mass flux (as is often done in PCM testing) changes the characteristics of the boiling surface. The general steps and the representative boiling regimes, however, remain approximately as shown.

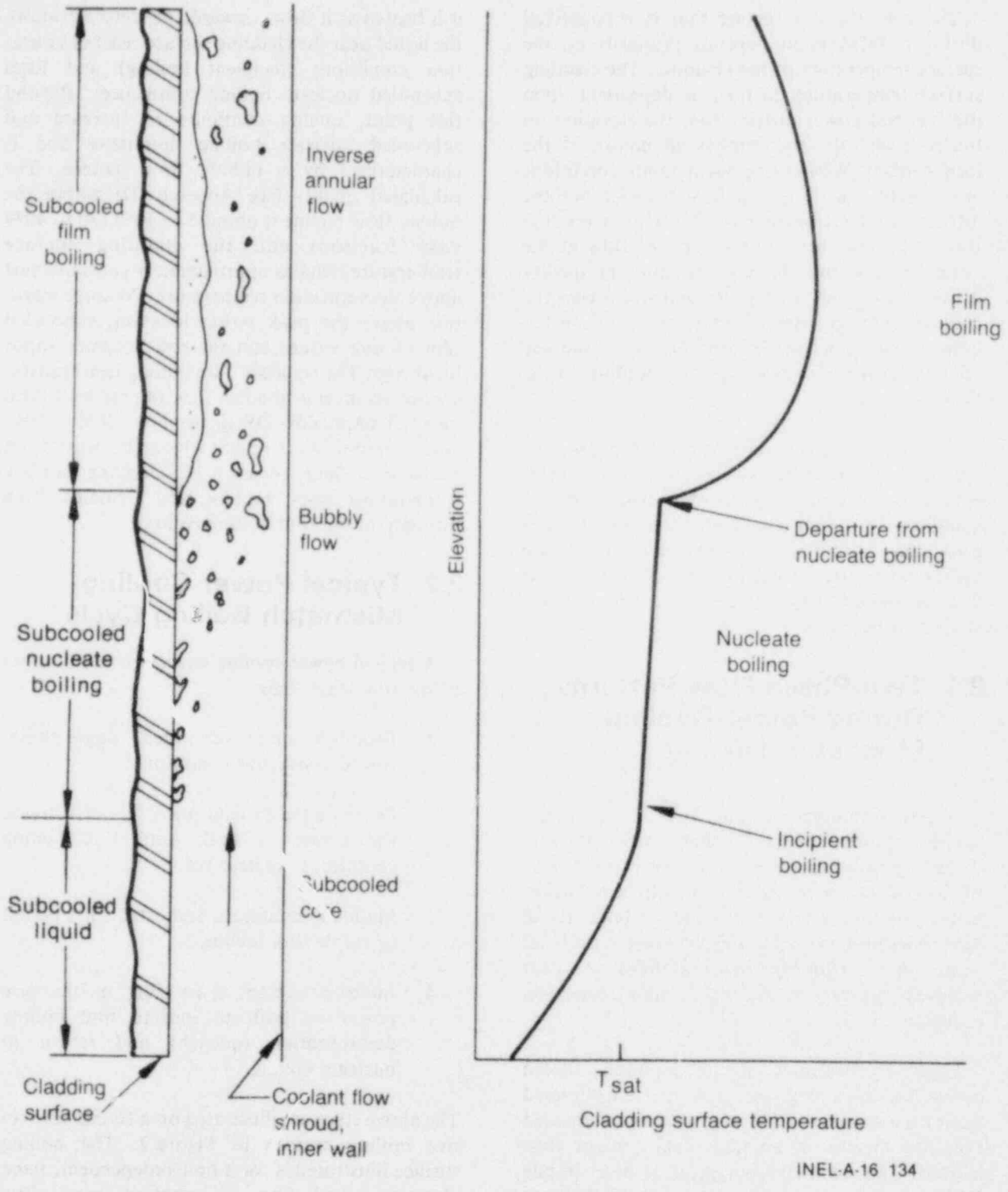

Figure 1. Forced convective flow regimes for vertical fuel rod within coolant flow shroud (with cosine power profile).

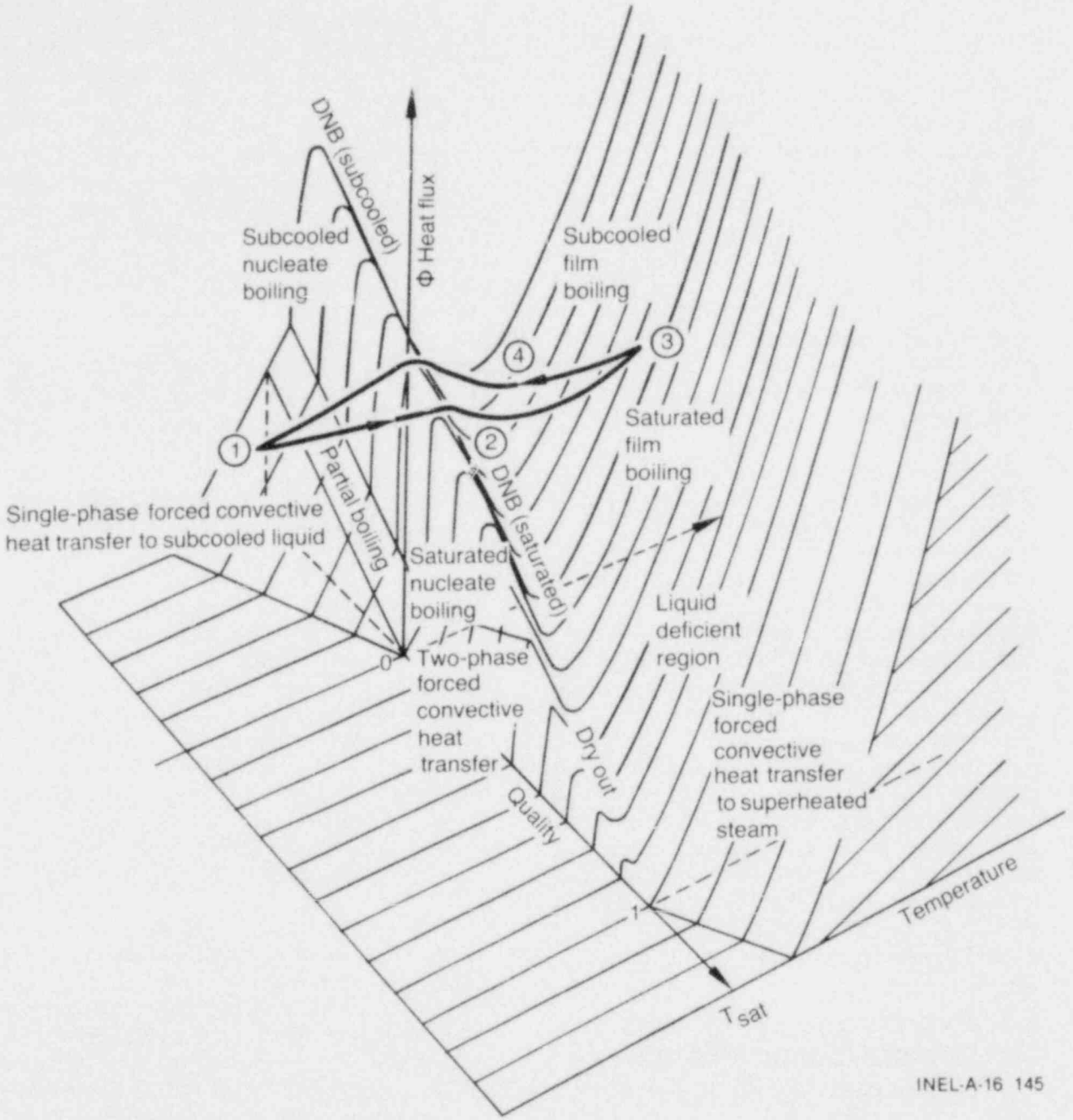

Figure 2. Power-cooling-mismatch boiling cycle on a forced convective boiling surface (constant coolant mass flux).

Figure 3 illustrates a typical PCM boiling cycle and the corresponding wall (cladding) temperature history. The boiling curve illustrated in Figure 3a is representative of a low quality (heat flux versus wall superheat) cross section from the forced convective boiling surface (Figure 2).

The PCM boiling cycle commences at departure from nucleate boiling as indicated by Point A (Figure 3). If the heating surface is heat flux controlled (approximated by a nuclear fuel rod), raising the heat flux would bring the nucleate boiling surface directly into film boiling (Path A-B) with a large increase in wall superheat. A continued increase in the heat flux (Path B-C) results in higher wall superheats and greater propensity for rod failure. At Point C (Figure 3), power input to the fuel rod is reduced or terminated, leading to a temperature turnaround or the start of rod cooling.

As the hot fuel rod cools, with minimal or no power input, some film boiling (Path C-D, Figure 3) is traversed. At Point D film boiling destabilization, or quenching, occurs, usually at wall superheat temperatures sufficiently high to prevent direct wall-coolant contact.[a] The quench is initiated by complex thermal-hydraulic interactions that are not well understood. Temperature, system pressure, liquid subcooling, heater geometry, and the thermophysical nature of the hot surface and coolant are examples of parameters which significantly influence the film boiling destabilization, or quenching process. Following quenching, the rod rapidly cools to a temperature which permits direct cladding-coolant contact, or rewetting, to occur (Point E, Figure 3), followed by subsequent return to nucleate boiling at Point F. If sufficient power to the fuel rod is reinstated, the cycle commences again.

2.3 Overview of Worldwide Power-Cooling-Mismatch Experiments

The current worldwide strategy for containment of radioactive fission products requires that the integrity of the cladding and core fuel elements be maintained during reactor operation. Since high temperature film boiling or dryout has been identified as a primary contributing agent to cladding failure, present reactor design and licensing efforts have focused attention on the prevention and mitigation of boiling transition occurrences. In support of design and licensing efforts, in-pile PCM-type test programs have been conducted in both the United States and abroad. Virtually all in-pile PCM test programs investigated fuel rod behavior under boiling water reactor (BWR) conditions. To the knowledge of the authors, the PBF/PCM Test Series has been the only in-pile program conducted under high-pressure, PWR-type conditions. Within this section, a brief overview of worldwide PCM-type tests is presented.

2.3.1 Winfrith Steam Generating Heavy Water Reactor. Dryout tests were performed at the Winfrith Steam Generating Heavy Water Reactor (SGHWR) under BWR conditions[23-25] to investigate the ability of commerical BWR rods (3.66-m in length) to withstand repeated dryout cycles and extended periods in dryout without failing. In each test, a vertical 36 rod bundle was taken into dryout by a flow reduction and subsequently quenched by restoring coolant flow. The fuel bundle successfully withstood more than 120 dryout tests at rod powers up to 90 kW/m and nine post-dryout excursions at rod powers up to 78 kW/m during which cladding temperatures up to 875 K were recorded. For most cycles, the rods were held in dryout for only a few seconds before inducing quench by a flow increase. In nine of the tests, dryout times of 60 to 150 s were reported. The maximum total dryout time for any rod in this test series was about 15 minutes.

2.3.2 Chalk River NRU Test Reactor. Dryout tests were also performed in the NRU reactor at Chalk River to provide information on the survivability of fuel rods exposed to dryout under BWR conditions.[26-29] In the Canadian tests, 19 to 37 rod fuel bundles (0.5-m in length) were subjected to power ramp and flow reduction induced dryouts. Only two of the 522 fuel rods tested failed. Rod powers in excess of 70 kW/m, peak cladding temperatures up to 1275 K, and sustained post-dryout times up to three hours occurred.

2.3.3 General Electric Test Reactor. In the General Electric Test Reactor (GETR) Test,[30] a zircaloy-clad BWR-type fuel rod was held in dryout for more than five minutes and then

a. In Section 4, it is shown that the boiling transition path (AB) and the return to nucleate boiling path (DF) coincide for the PBF/PCM tests.

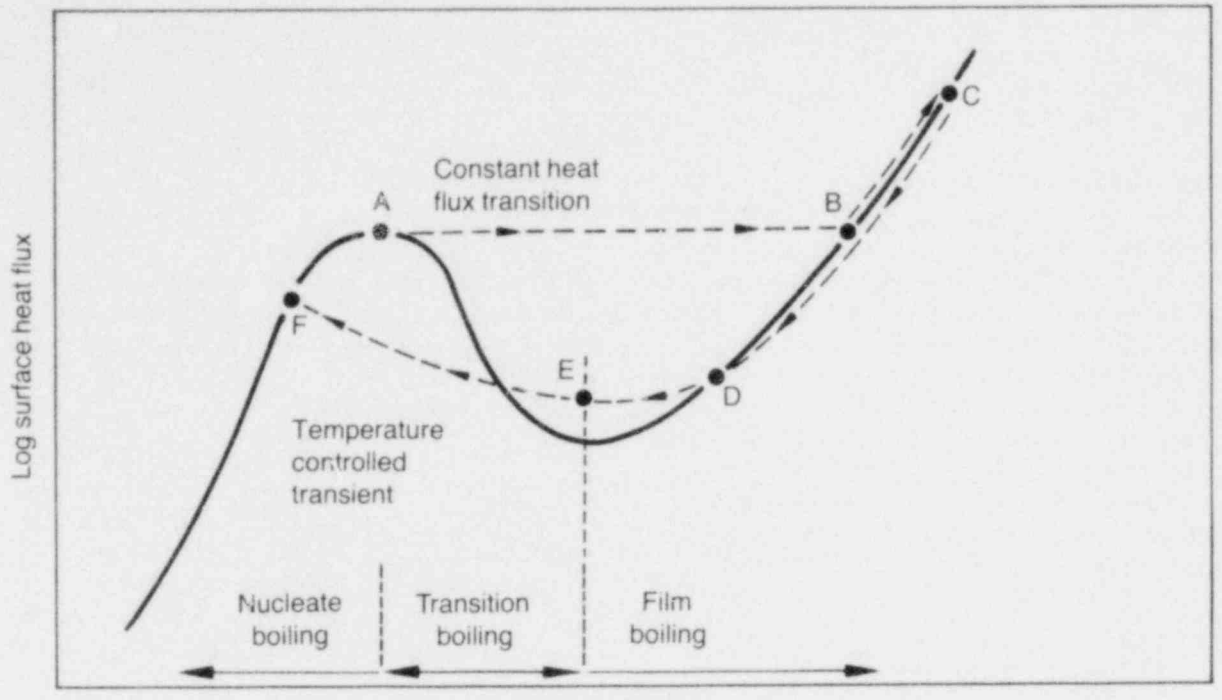

(a) PCM boiling cycle and typical low quality boiling curve

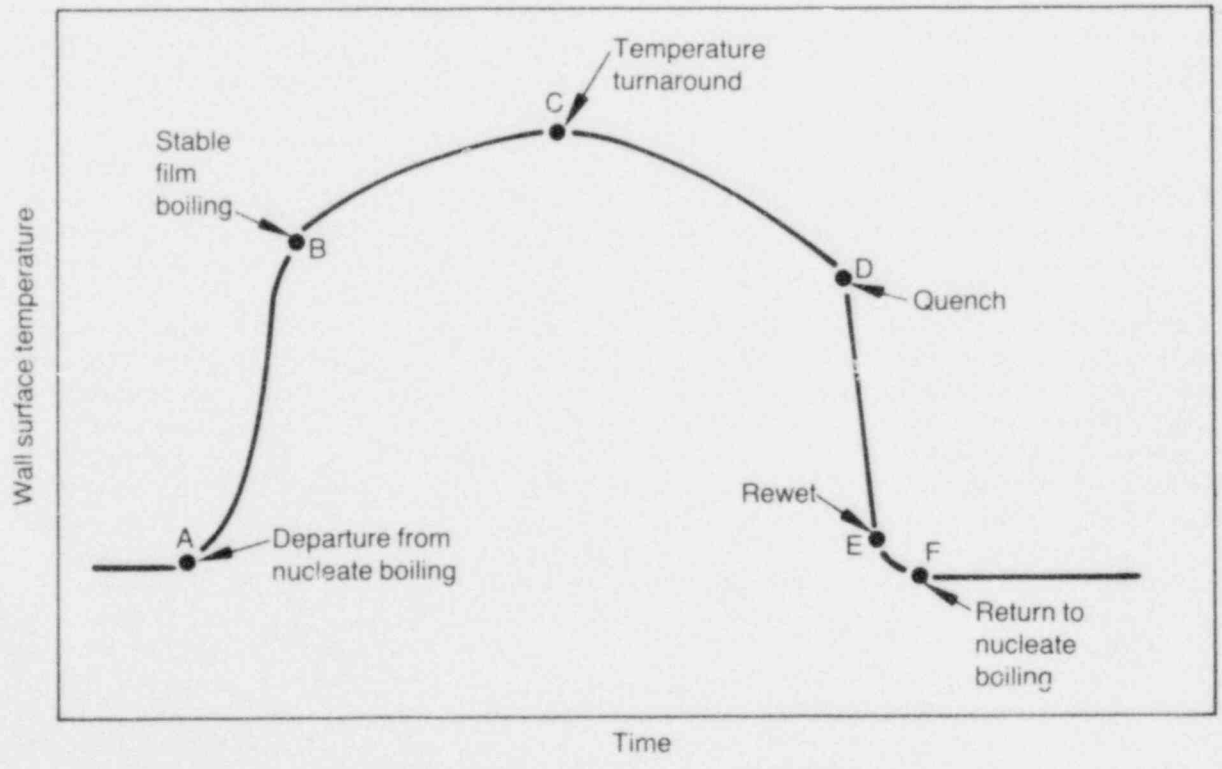

(b) Typical wall temperature history during PCM boiling cycle

INEL-A-16 149

Figure 3. PCM boiling cycle and corresponding wall temperature history.

operated at a critical heat flux ratio 1.5 for 10 days, with no sign of rod failure. The rod length was 0.5-m and peak cladding temperatures of 1375 K were recorded.

2.3.4 Halden Boiling Heavy Water Reactor. Several BWR dryout experiments have been performed in the Halden, Norway Reactor in past years[31,32] to investigate fuel rod behavior and thermal-hydraulic conditions at and beyond dryout. Seven and nine rod fuel bundles with active fuel lengths of 1.47 to 1.6 m were subjected to a series of more than 60 power ramp induced dryouts. In one test, peak cladding temperatures of about 1125 K were maintained for about five minutes without failure, despite continued irradiation to a total of about 20 GWD/MTM over the next five years.[31]

2.4 Description of Power Burst Facility Power-Cooling-Mismatch Testing

An extensive PCM test series has recently been completed at the Idaho National Engineering Laboratory (INEL) Power Burst Facility (PBF). The Test Series was designed to investigate the behavior of unirradiated and irradiated PWR-type fuel rods when subjected to departure from nucleate boiling (DNB) transition cycles. Single-rod, four-rod, and nine-rod fuel bundles were tested at peak rod powers up to 71 kW/m and peak cladding temperatures up to the melting point of zircaloy.

The Test Series consisted of 17 individual experiments (including the IE Test Series) which incorporated unirradiated and irradiated PWR-type nuclear fuel rods, with active fuel lengths of 0.879 to 0.914 m. Coolant pressures ranged from 13.6 to 15.6 MPa. Three basic test configurations were utilized:

1. Single-rod tests, where a fuel rod was contained within its own coolant flow shroud, as shown in Figure 4

2. Four-rod tests, where each fuel rod was contained within its own coolant flow shroud, hydraulically coupled in parallel

3. Nine-rod open bundle tests, where the fuel rods shared a common coolant flow channel, as shown in Figure 5.

The experiment hardware and associated instrumentation were positioned within a vertical annular test space within the PBF driver core. Test rod power, system pressure, and inlet coolant conditions were continually monitored and regulated during each test. PCM conditions were attained by starving coolant flow, increasing test rod power, or both. All tests resulted in film boiling operation for brief or sustained periods at peak rod powers up to 71 kW/m and peak cladding temperatures up to 1850 K. Behavioral information at conditions beyond fuel rod failure was also obtained.

Included in this report are results from 15 of the 16 tests conducted to date in the PCM Test Series. Data from the most recent test, Test PCM-7, were not available in time for this publication. A complete listing of all other series data can be found in Appendix C. The nominal design characteristics of the test rods are given in Table 1.

The test assemblies were instrumented to continually monitor the thermal-hydraulic conditions and fuel rod behavior during the operation of the tests. Monitored in the tests were coolant conditions, power levels,[a] cladding surface temperatures, and cladding elongation. The onset of film boiling and quench characteristics of the fuel rod were determined using the last two measurements.

The first indication of film boiling was detected by a sudden increase in either the cladding surface temperature or the cladding elongation. The linear variable differential transformer (LVDT), which responds to cladding displacement, often shows film boiling a few seconds before the external cladding thermocouples. This is because the external thermocouples were spaced approximately 5 to 10 cm apart in the film boiling region of the fuel rod.[b] If the onset of film boiling occurred between thermocouples it may have taken a few seconds for the film boiling zone to propagate up or down the rod to reach a thermocouple. The spacing of the external cladding thermocouples introduces an error factor of 6 to 17% into the calculations of critical heat flux. Other sources of error include

a. Power levels were calculated using readings from self-powered neutron detectors and results of the power calibration. Figure 4b shows the typical axial cosine flux shape.

b. The film boiling region is usually limited to the top half of the rod at elevations between 0.58 and 0.90 m from the bottom of the fuel stack.

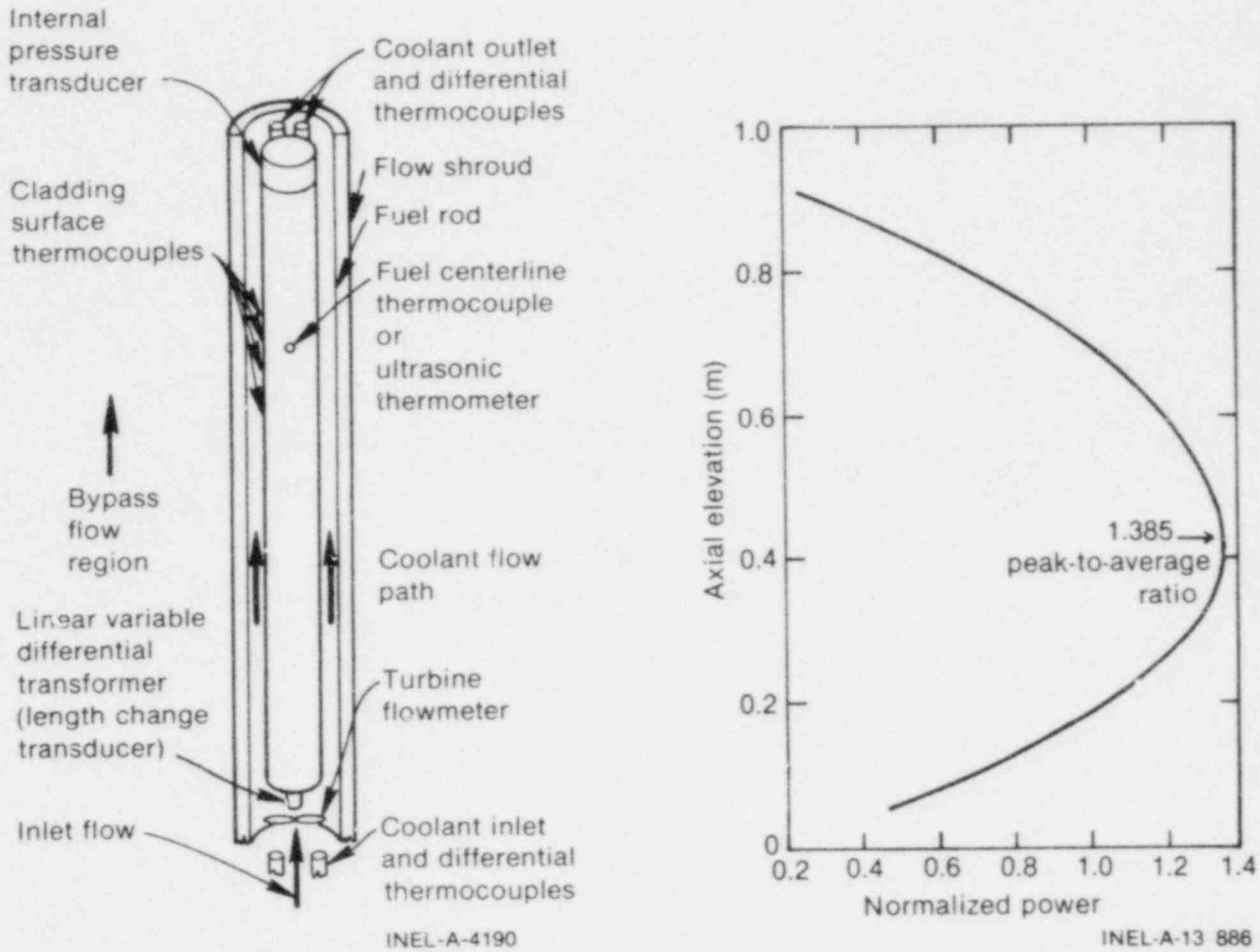

Figure 4. Single-rod test geometry and representation of typical power profile.

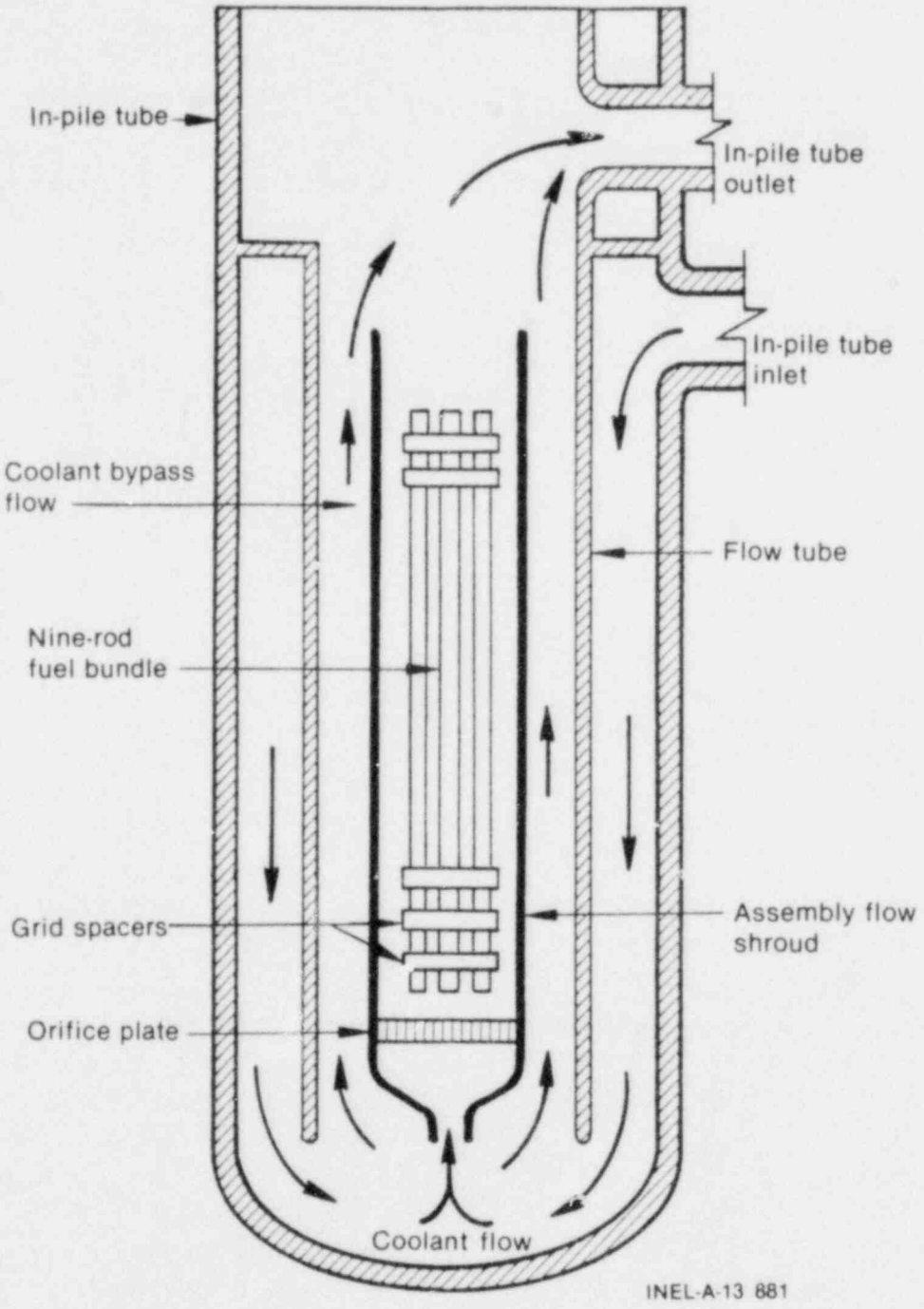

Figure 5. Schematic illustration of 3 x 3 nine-rod PCM-Test assembly.

Table 1. Nominal design characteristics of PBF/PCM tests

	8-1-RS	CHF Scoping	8-1-RF	PCM-1	PCM-2[a]	PCM-2A	PCM-3[a]	PCM-4[a]	PCM-5	PR-1[a]	IE-ST-1	IE-ST-2	IE-1	IE-2	IE-3	IE-5
Active length (m)	0.914	0.914	0.914	0.914	0.914	0.914	0.914	0.914	0.914	0.914	0.880	0.880	0.879	0.884	0.890	0.879
Pellet diameter (mm)	9.3	9.3	9.3	9.3	9.3	9.3	9.3	9.3	9.3	10.57	8.54	8.53	8.50	8.50	8.50	8.64
Cladding outer diameter (mm)	10.72	10.72	10.72	10.72	10.72	10.72	10.72	10.72	10.72	12.50	9.93	9.95	9.89	9.93[b]	9.93	9.93
Cladding thickness (mm)	0.61	0.61	0.61	0.61	0.61	0.61	0.61	0.61	0.61	0.86	0.59	0.64	0.59	0.60[c]	0.59	0.60
Cladding material	Zyr-4	Zry-4	Zry-4	Zry-4	Zry-4	Zry-4	Zry-4	Zry-4	Zry-4	Zry-2	Zr-4	Zry-4	Zry-4	Zry-4	Zr-4	Zry-4
Flow shroud inner diameter (mm)	17.9	19.2	19.4	16.3	16.3	16.3	16.3	16.3	d	19.3	19.3	19.3	16.3	16.[e]	16.3	16.3
Flow area (cm^2)	1.61	1.99	2.05	1.18	1.18	1.18	1.18	1.18	13.15	1.70	2.15	2.15	1.31	1.31	1.31	1.31
Internal pressure (MPa)	3.79	3.88	3.88	2.59	2.59	2.69	2.59[e]	2.59[e]	2.59	2.58	2.59	2.7[f]	2.6	2.6	2.6	2.58[g]
Fill gas	Helium	Helium	Helium	78% Helium 22% Argon	Helium	Helium	Helium	Helium	Helium	Helium 3 Argon 1	76% Helium 24% Argon	77% Helium 23% Argon	78% Helium 22% Argon	76% Helium 24% Argon	78% Helium 22% Argon	78% Helium 22% Argon
External thermocouple type[h]	sq[i]	sq[i]	sp	sp	sp	sp	sp	sp	sp	sp	sp spr	sp[h] spr	spr	sp[h] spr	sp spr	sp[h]

a. Values are average of four rods.

b. Rods 11 and 12 were previously irradiated and had larger diameters and smaller flow areas.

c. Values for irradiated rods were slightly higher.

d. PCM-5 was a bundle test with square flow shroud (rounded corners).

e. Three rods at 2.59, one at approximately 3.79.

f. Rod 6 was backfilled to 0.1 MPa with 100% helium.

g. Rod 19 was backfilled to 8.3 MPa.

h. sq = square tip, sp = spaded junction, spr = spring loaded.

i. Some of the external cladding thermocouples were embedded into the cladding in 0.25 mm grooves.

the power level calculation (8 to 12%), coolant flowmeter (3 to 8%), and i.: the inlet temperature thermocouple.

Four basic types of external cladding thermocouples were used in the PBF/PCM experiments, as illustrated in Figure 6. The first type (Figure 6a), the spaded junction thermocouple, was exclusively used in the power-cooling-mismatch tests. It is expected that each thermocouple geometry will uniquely influence the local coolant hydraulics, and thus, the DNB and quench behavior.

While there is some variety in the determination of quench phenomenon, quench is generally characterized by a sudden change in the slope of the cladding surface temperature versus time trace. In the few cases where a slope change was not readily visible, quench was determined in one of two ways. In some cases, quench was said to have occurred when the cladding surface temperature versus time trace reaches a slope of -200 K/s. The second technique, called "best fit of asymptotes," is to extend the prior and post-quench slope lines; their intersection is said to be the time of quench. An example of this is given in Section 4.

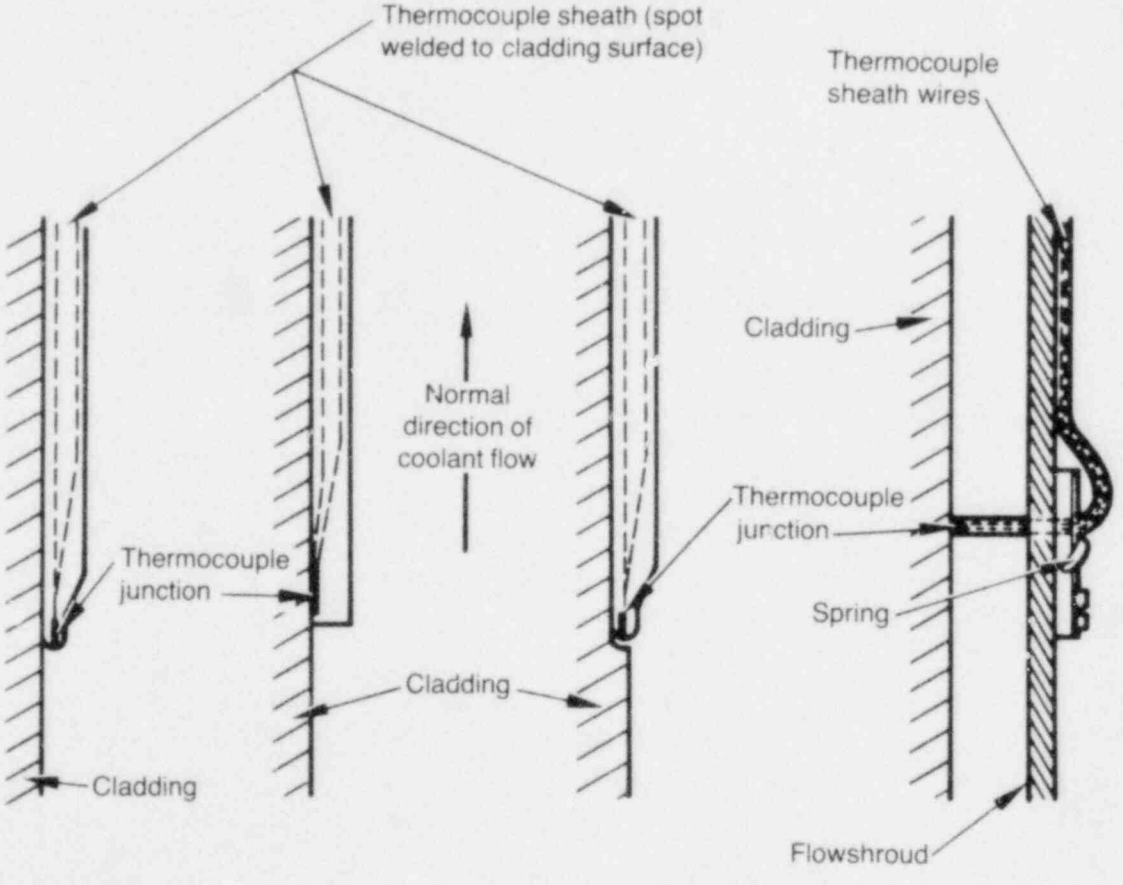

(a) Spaded junction (Tests: 8-1-RF, PCM-1, 2, 2A, 3, 4, 5, PR-1, IE ST-1, 2, IE-2, 3, 5)

(b) Grounded square junction (Tests: 8-1-RS, CHF scoping)

(c) Spaded junction in 0.25-mm groove (Tests: 8-1-RS, CHF scoping)

(d) Spring loaded (Tests: IE ST-1, 2, IE-1, 2, 3)

INEL-A-16 138

Figure 6. External cladding thermocouple geometries used in Power Burst Facility PCM and IF Testing.

3. CRITICAL HEAT FLUX

Departure from nucleate boiling (DNB) is used to describe the boiling crisis that can occur in a PWR environment. It is characterized by a sudden deterioration in the boiling heat transfer mechanism resulting in a temperature excursion of the heating surface. The surface heat flux just prior to departure from nucleate boiling is commonly referred to as the critical heat flux (CHF).

3.1 Estimating the Critical Heat Flux

Numerous departure from nucleate boiling and two-phase flow studies over the past 25 years have explored the boiling transition mechanisms so that critical heat flux predictions could be perfected. Such studies, unfortunately, have met with limited success, and presently there exists no overall analytical technique for predicting the critical heat flux. It is known, however, that DNB is a complex physical phenomena that is influenced by a wide variety of system and local parameters. Some of the more commonly accepted influencing parameters include: pressure, local enthalpy or subcooling, quality or void fraction, coolant velocity, and heater geometry. As a consequence of the inherent difficulty in modeling the critical heat flux, designers have been forced to rely on empirical correlations which have been developed for specific systems. According to one estimate,[33] several hundred thousand critical heat flux data points have been recorded, and over 200 correlations have been proposed. Generally, the critical heat flux, ϕ_{CHF}, is empirically modeled by an expression of the form

$$\phi_{CHF} = f(X_{CHF}, G, P, L/D) \qquad (1)$$

where X_{CHF} is the local quality at critical heat flux, G the coolant mass flux, P the system pressure, and D and L are the channel diameter and length of the heater, respectively. In the absence of a length effect, often considered to be for $L/D > 20$, ϕ_{CHF} may depend only on local parameters.[33]

Perhaps the best method available to date for predicting the critical heat flux for a given system is to use an empirical correlation that was developed from experimental data for a system most closely resembling the system of interest. It is well known that extrapolation of empirical correlations beyond the experimental data base often leads to erroneous results. This is why the manufacturers of boiling equipment usually develop their own empirical critical heat flux correlations through extensive experimentation. Appendix B lists several of the more common critical heat flux correlations developed for and used in the design and analysis of light water nuclear reactor technology. Reference 34 provides an excellent collection of information concerning the critical heat flux, with particular emphasis on problems in nuclear reactor design.

3.2 The Critical Heat Flux and the Power Burst Facility Power-Cooling-Mismatch Test Series

Within this section, empirical correlations are presented which model the critical heat flux behavior observed during power-cooling-mismatch testing in the Power Burst Facility. It is recognized that such correlations may be of little interest to the nuclear community outside of PBF operations. Therefore, the following general premises were used in the development of the correlations presented:

1. The PBF CHF correlations should be as simple as possible, yet accurately model the DNB behavior. This allows parametric trends to be easily recognized.

2. The design and conduct of PBF tests are often focused on transient or steady-state peak rod power, system pressure and inlet coolant conditions. Thus, a CHF correlation that is based on these readily measurable parameters would be of fundamental interest.

3. Development of PBF CHF correlations will allow convenient comparison of the PBF results with other CHF correlations that are presently being used for design and analysis of commercial reactors.

The first step in developing the critical heat flux correlations was to assume that CHF behavior may be modeled as a local phenomena. In keeping with classical precedence, coolant quality (χ) is considered to be the important local parameter. Steady state, homogeneous equilibrium quality was calculated for each datum point by the enthalpy rise technique outlined in Appendix D. The correlations were developed using linear and nonlinear, single and multivariant, least squares regression analyses, and the CHF data obtained in the manner described previously in Section 2. An additive or superposition correlation form suggestive of the LOFT critical heat flux correlation was found to satisfactorily describe the data trends.[a] The correlation included pressure (P), coolant mass flux (G), and local quality (χ) as the independent variables.

Assuming the critical heat flux is dependent on the system pressure (P), coolant mass flux (G) and local quality (χ), the following critical heat flux correlation was derived:

$$\Phi_{CHF} = 0.23\ G + 393\ P - 20.5\ P^2 - 32\ G\chi + 2\ GP\chi \quad (2)$$

where:

Φ_{CHF} = Critical heat flux (kW/m^2)

G = Coolant mass flux ($kg/m^2 \cdot s$)

P = System pressure (MPa)

χ = Local quality.

Equation (2) is identical in form to the well known LOFT critical heat flux correlation (given in Appendix B). As illustrated in Figure 7, Equation (2) correlates 94% of the experimental data with an accuracy of $\pm 30\%$.

The PBF/PCM correlation [Equation (2)] is based on experimental data from individually shrouded rods and one nine-rod open bundle test with heated lengths of 0.879 to 0.914 m and is recommended for use in the following parameter ranges:

Pressure: 13.6 to 15.5 MPa

Inlet coolant mass flux: 513 to 2750 $kg/m^2 \cdot s$

Local quality: -0.035 to 0.239

Inlet subcooling: 7 to 25 K

Critical heat flux: 840 to 2000 kW/m^2

3.3 Critical Heat Flux Correlations and Power Burst Facility Power-Cooling-Mismatch Testing

In the previous section, an empirical critical heat flux correlation was presented which models the experimental CHF data trends within the Power Burst Facility during power-cooling-mismatch testing.

Within this section, the PBF/PCM critical heat flux correlation as given by Equation (2) is compared with the LOFT, Babcock and Wilcox (B&W-2), Combustion Engineering (CE-1) and Westinghouse (W-3) CHF correlations. Appendix B presents these correlations and details the recommended parametric ranges of application.

Figure 8 illustrates a comparison of critical heat flux correlations at a constant coolant mass flux of 1100 $kg/m^2 \cdot s$ and a system pressure of 15.1 MPa. Such conditions are indicative of PBF/PCM testing with low coolant mass flux. As shown, the Combustion Engineering (CE-1) CHF correlation best models the experimental PBF/PCM data trends at lower coolant mass fluxes and positive qualities. The LOFT and CE-1 correlations best model the data at lower coolant mass fluxes and negative qualities.

Figure 9 illustrates a comparison of the critical heat flux correlations at a coolant mass flux of 2000 $kg/m^2 \cdot s$, and the same system pressure. Such conditions are typical of PBF/PCM testing with high coolant mass flux. With all qualities illustrated, the LOFT and CE-1 correlations best model the PBF/PCM data trends.

a. Many other CHF correlation forms, both additive and multiplicative, were empirically fitted to the PBF data. The LOFT form, however, with a nonlinear pressure dependence and $GP\chi$ product term provided the best accuracy.

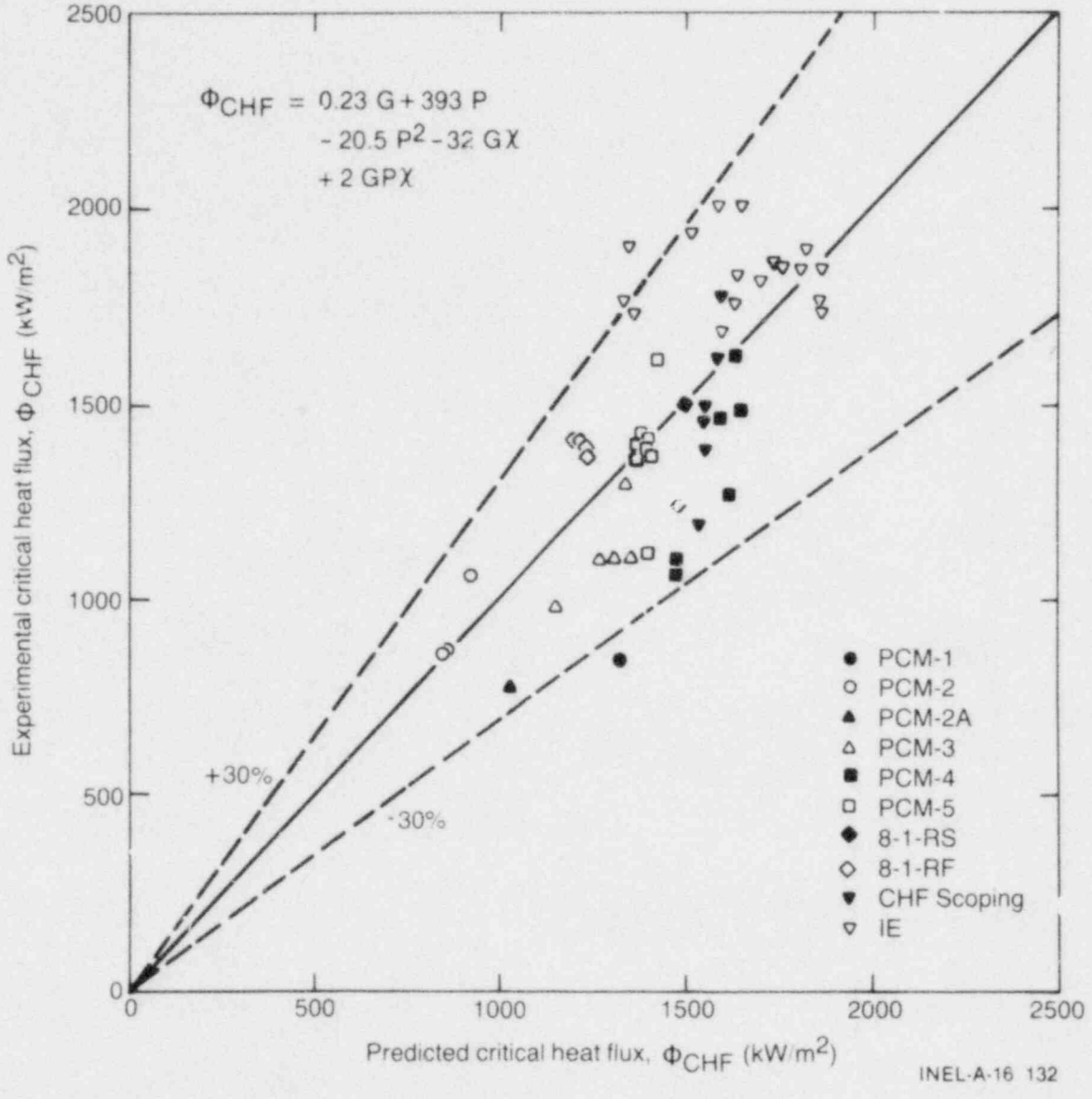

Figure 7. Comparison of experimental versus predicted critical heat flux.

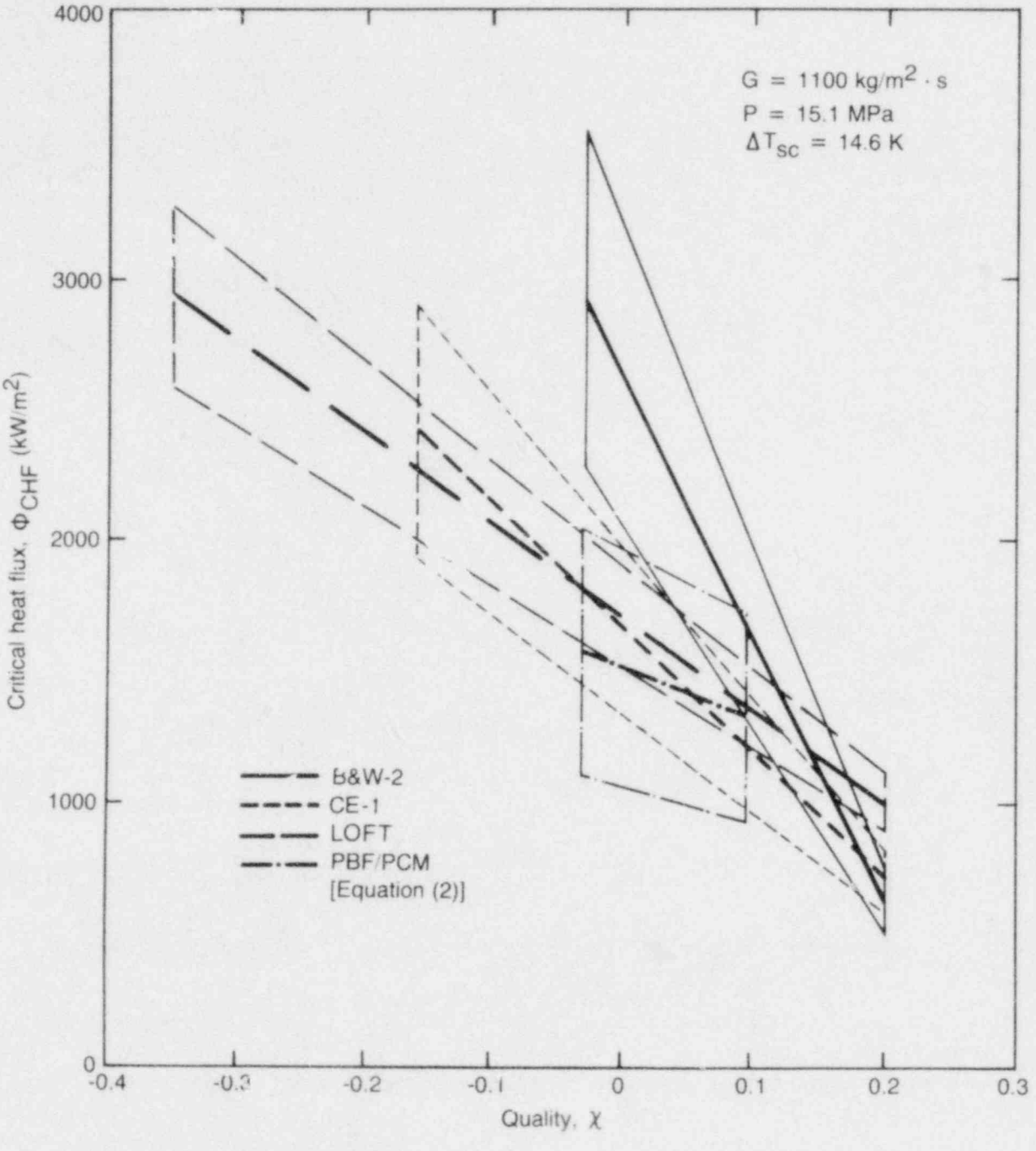

Figure 8. Comparison of critical heat flux correlations-I.

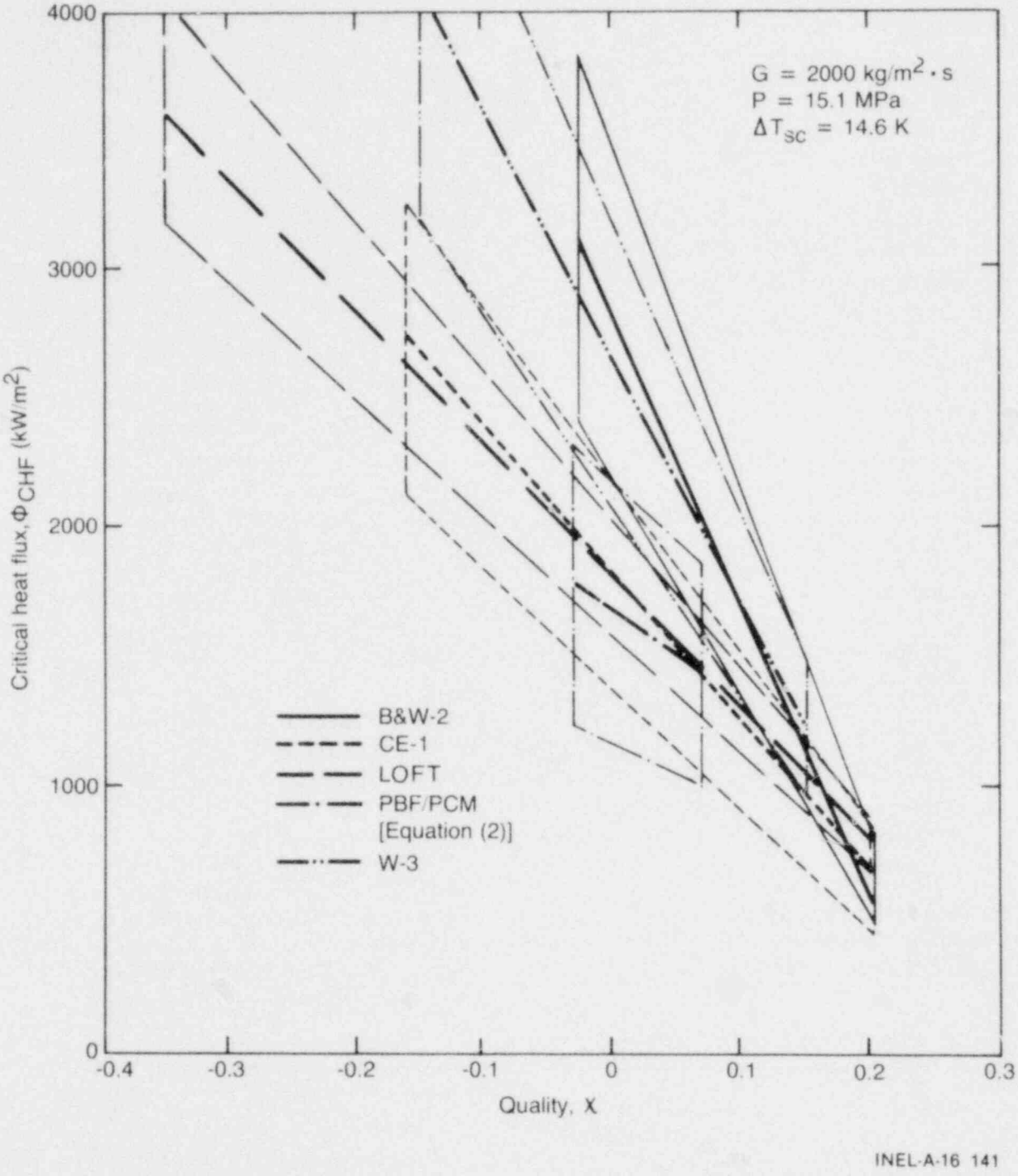

Figure 9. Comparison of critical heat flux correlations-II.

A plot of the critical heat flux versus quality can be misleading because any experimental error in the CHF is also incurred when calculating quality, so that the effect of the error is magnified by such a plot. Figure 10 illustrates a comparison of the critical heat flux correlations to coolant mass flux (G). The ranges of uncertainty of the correlations have been omitted for clarity, but range from 20 to 30%. As shown, the LOFT and CE-1 correlations again best model the PBF/PCM data trends correlated by Equation (2).

3.4 Correlating the Thermal-Hydraulic Conditions at the Onset of Film Boiling

The thermal-hydraulic conditions at the onset of film boiling (departure from nucleate boiling) have been empirically correlated for the PBF/PCM test series data (listed in Appendix C). The independent variables selected for the correlation are those readily measured and controlled during testing and include the peak rod power (P_P), inlet coolant mass flux (G) and inlet subcooling (ΔT_{sc}). The purpose of such a correlation is twofold:

1. To provide a "rule of thumb" for quick and simple predictions of the thermal-hydraulic conditions that promote the onset of film boiling during PBF/PCM testing

2. To provide a comparison of the conditions at DNB with the conditions at quench (see Section 5).

Using a nonlinear, multivariant, least squares regression analysis of the PBF/PCM data, the following correlation is obtained:

$$P_P = 8.24\ G^{0.25}\ \Delta T_{sc}^{\ 0.057}$$

(Onset of film boiling) (3)

where P_P is the peak rod power (kW/m), G is the inlet coolant mass flux ($kg/m^2 \cdot s$), and ΔT_{sc} is the inlet subcooling (K). As illustrated in Figure 11, Equation (3) accurately predicts (±20%) the inlet/power conditions at the onset of film boiling.

3.5 Parametric Trends in the Critical Heat Flux

Presented in this section is a discussion of the influence of certain system parameters on the critical heat flux and the onset of film boiling. Primary emphasis is placed on the effects observed during PCM testing within the Power Burst Facility.

3.5.1 Pressure Effect. The influence of system pressure on the critical heat flux is most easily recognized in Equation (2). For high pressure PCM testing, the critical heat flux decreases with increasing pressure. This observation is consistent with the findings of other investigators. As stated by Bergles, "The critical heat flux increases with pressure at low pressure, is relatively constant over an intermediate range of pressure, and decreases at high pressure."[33]

Qualitatively, the effect of system pressure on the critical heat flux is illustrated in Figure 12. Based on experimental studies with water,[35,36] the maximum critical heat flux appears to be located between a pressure range of about 3.5 MPa (∿500 psi) and 7 MPa (∿1000 psi).

3.5.2 Quality and Length Effects. The influence of local quality on the critical heat flux is seen from Equation (2) where for high pressure, low quality PCM testing, the critical heat flux decreases with increasing quality. Other critical heat flux correlations exhibit this general trend as well, as illustrated in Figures 8 and 9.

Figure 13 illustrates the L/D effect on the critical heat flux experimentally determined by Silvestri[37] using a two-phase water mixture in a uniformly heated tube at a pressure of 7.02 MPa (1018 psi) and a coolant mass flux of 1088 $kg/m^2 \cdot s$ (0.8×10^6 bm/ft^2-hr). As shown, increasing L/D has two main influences:

1. The burnout power increases with increasing L/D, or the surface heat flux decreases with increased L/D

2. The slope of the power versus quality curves becomes less (more negative) with increased L/D values.[a]

a. The Silvestri[37] results indicate L/D effects even when L/D < 20. This is in contrast to the Bergles[33] statement where no length effects are reported when L/D > 20.

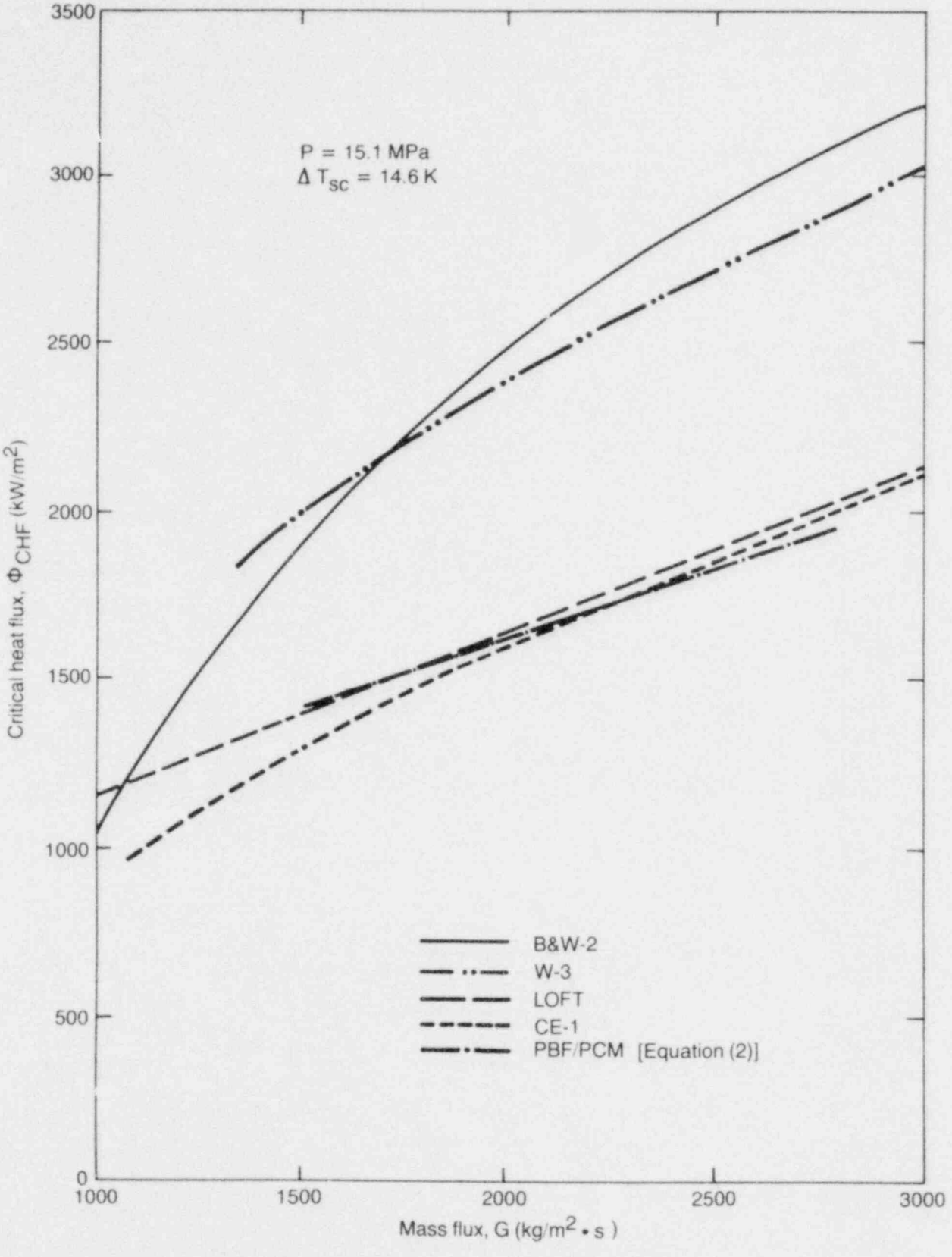

Figure 10. Comparison of critical heat flux correlations-III.

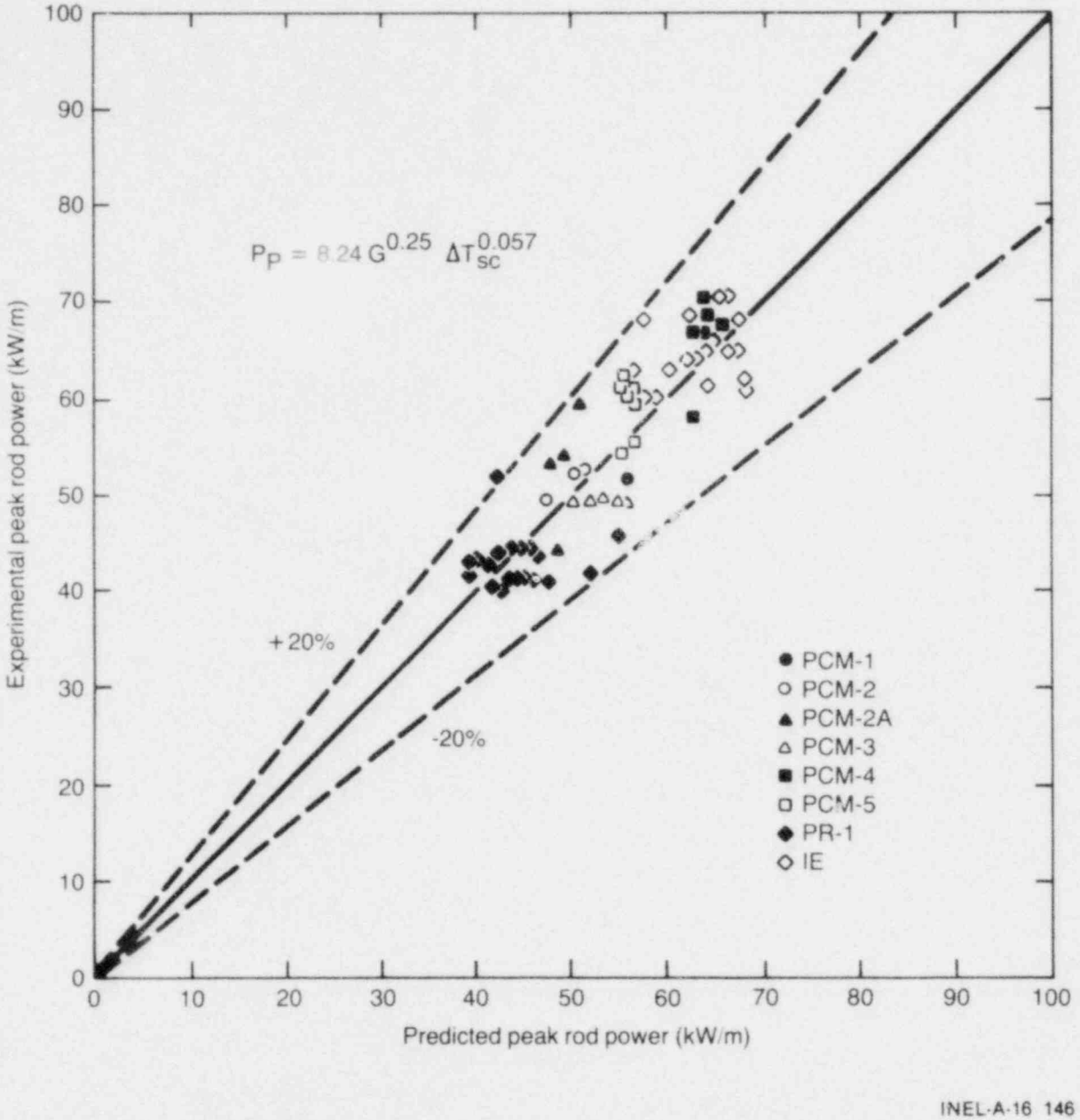

Figure 11. Measured and predicted linear peak rod power at the onset of film boiling.

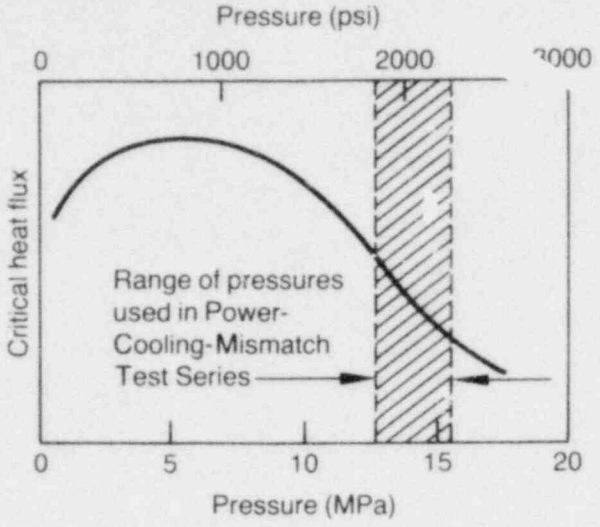

Figure 12. Effect of pressure on the critical heat flux.

The L/D range of the vendor CHF correlations is generally about 15 to 400 (Appendix B). The L/D range for the PBF/PCM data is likewise within this range, 87 to 164. If the previously stated L/D influences remain valid at higher pressures (indicative of PWR pressures), any L/D influences inherent in the PBF/PCM CHF correlation [Equation (2)] should be indistinguishable from the influences inherent within the vendor CHF correlations. This appears to be the case where, as illustrated in Figures 8 and 9, the slope of the CHF versus quality line for the PBF/PCM correlation is roughly similar to the slopes of the vendor CHF correlations. Therefore, there appears to be little or no L/D influence on the PBF/PCM CHF behavior when compared with vendor CHF behavior.

3.5.3 Cold-Wall Effect. Liquid which is not used directly to cool the heating surface usually forms a cooler film along an unheated wall. As a result, the coolant effectiveness within the coolant flow channel is somewhat reduced and the propensity for boiling transition increased. This behavior has long been recognized by previous investigators[34,38-40] and attempts to account for this phenomena have been empirically factored into critical heat flux correlations by the addition of a cold-wall factor, F_{cw} (see Appendix B).

The opposite effect, however, may have been observed during PBF/PCM testing. In Test PCM-5, which was a 3 x 3 nine-rod open bundle test where the test bundle was contained within a single flow channel, the peripheral test rods (nearest to the cooler flow channel wall) exhibited "enhanced cooling." This behavior is illustrated in Figure 14. As shown, the peripheral test rods had a higher average critical heat flux (~20% higher) than the central test rod (Rod 5, Figure 14).

During the nuclear heatup phase of test PCM-5, it is believed that the peripheral test rods bowed outward toward the higher neutron flux region.[10] Consequently, the average spacing between the peripheral test rods and the cooler flow channel wall was decreased, perhaps to the extent of contact. If bowing occurs, the boundary layer of cooler liquid flowing adjacent to the coolant flow channel will be locally disrupted and therefore available to cool the peripheral test fuel rods. In addition, the reduction of subchannel area available for coolant flow, increases local coolant velocity and enhances the local forced convective heat transfer coefficient. This also contributes to enhanced cooling.

The nine-rod bundle Test PCM-5 was conducted with the highest inlet subcooling (ΔT_{sc} = 25 K) of all PBF/PCM tests. The inlet subcooling for the single-rod PBF/PCM tests was typically 7 to 16 K. Therefore, the temperature differential across the flow channel and hence the cold wall influence may be greater for the bundle test than for the single-rod test. Furthermore, the potential for fuel rod bowing would be less for the symetrically positioned single-rod geometry.

The cold-wall factor (F_{cw}) used in vendor critical heat flux correlations (see Appendix B) is empirically based on experimental data where a "cold" guide tube was substituted in lieu of a hot rod. This geometry is considerably different than the PBF/PCM single-rod geometries where a cold-wall (flow shroud) is circumbient or surrounds the heater rod. Therefore, the applicability of a vendor produced cold-wall factor, such as F_{cw} in the Westinghouse-3 CHF correlation, to a single-rod (within a flow shroud) geometry must be questioned.

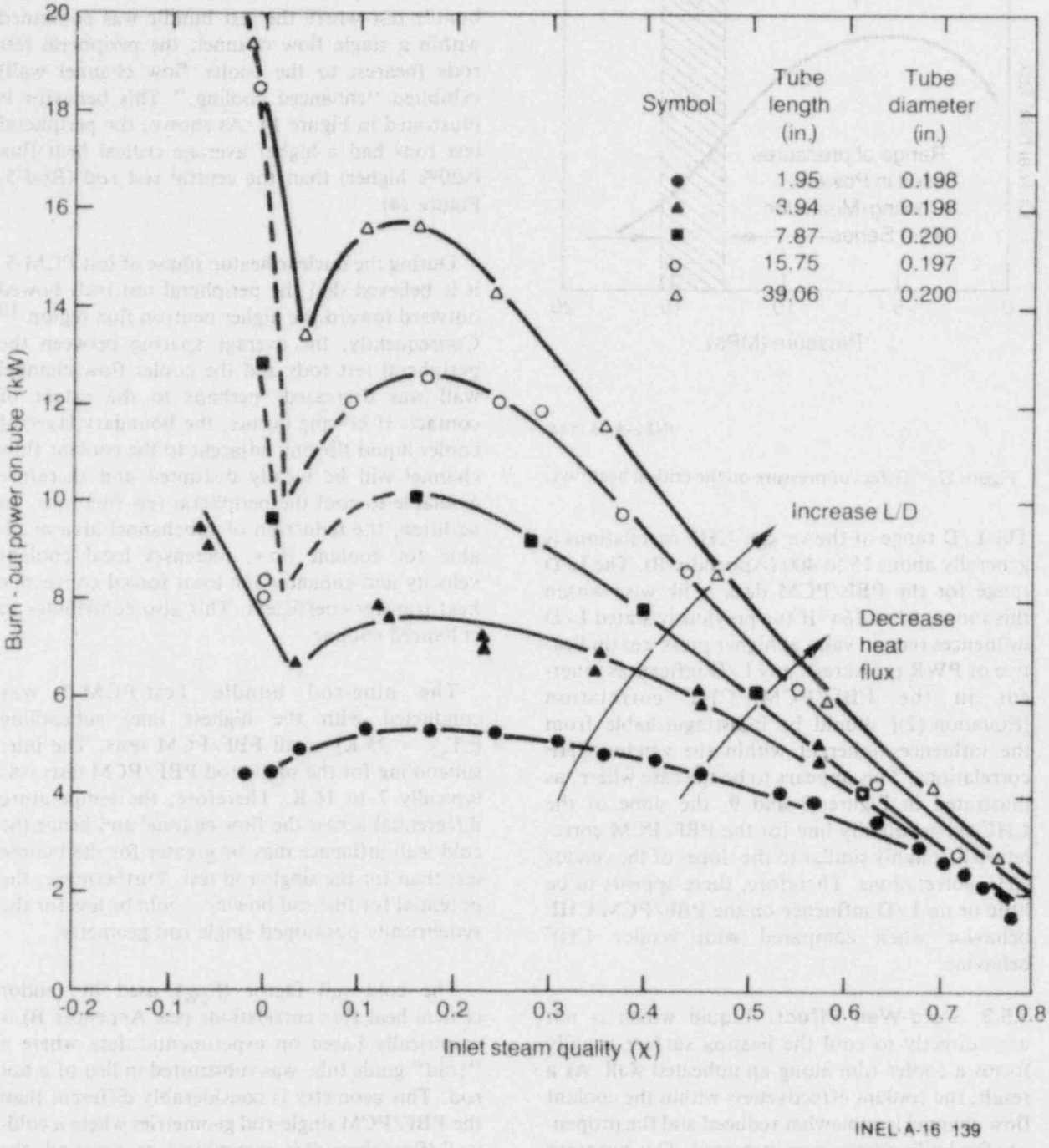

Figure 13. L/D effects on the critical heat flux.

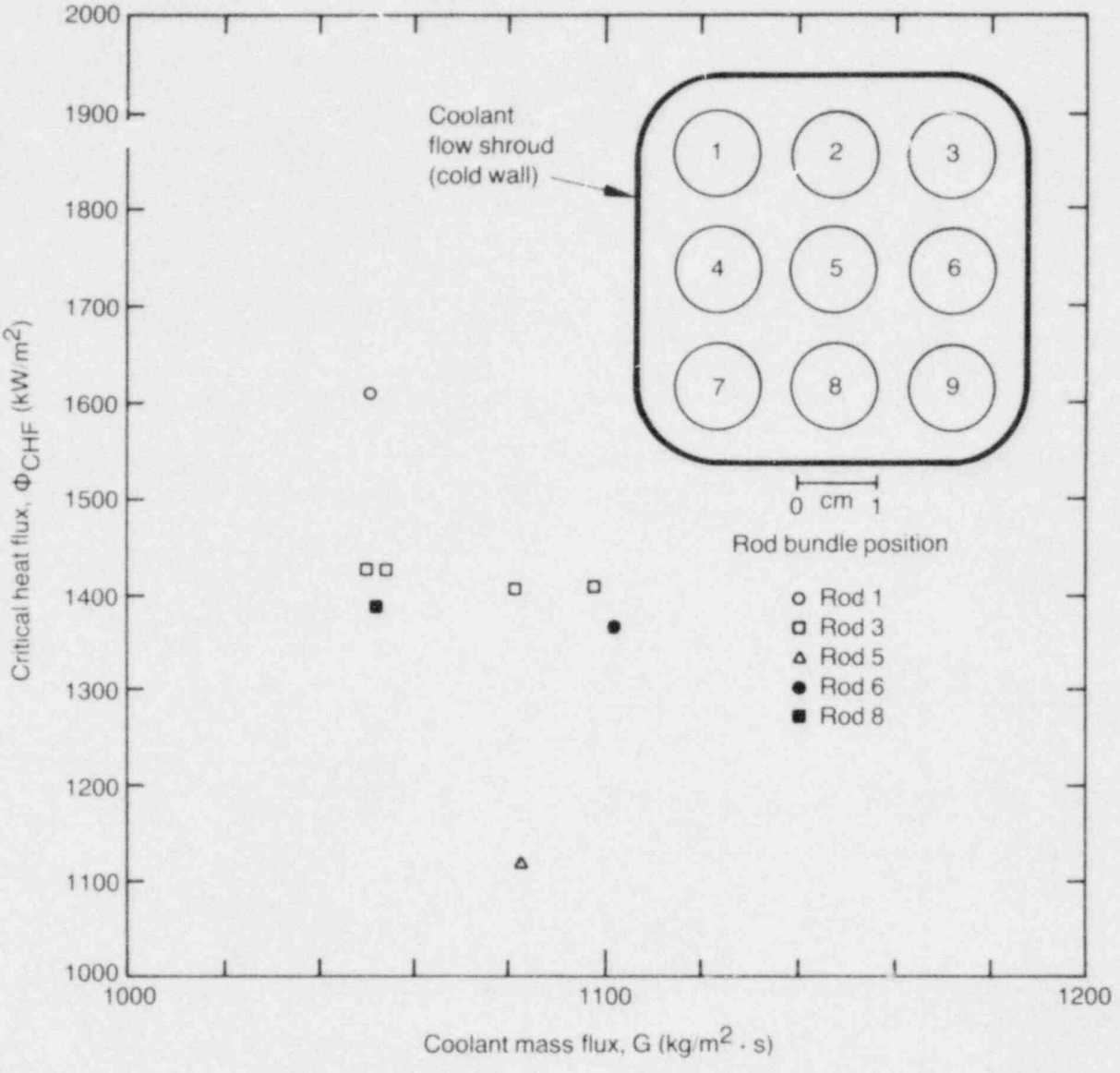

Figure 14. Possible influence of cold wall on the critical heat flux.

4. QUENCHING AND REWETTING

Many postulated nuclear reactor accidents result in dryout or film boiling within the nuclear core. In order to minimize fuel rod damage and potential rod failure, safe or lower cladding fuel temperatures must be reestablished by encouraging coolant/cladding contact. This process is commonly referred to as quenching or rewetting. Although these terms are often used interchangeably, quench and rewet are distinctly different phenomena, entailing different modes of heat transfer.

Within this section, quenching and rewetting temperatures are differentiated and defined, and methods of prediction are presented. The influence of external cladding thermocouples on these temperatures is also discussed. Results indicate that the quenching temperature and the rewetting temperature may be estimated from first principles.

4.1 Overview of Quenching Processes

Fuel rod overheating may occur during a LOCA or PCM event due to the inability to dissipate the stored heat in the fuel rod and due to continuing fission product decay heat. To prevent over heating to an unacceptable level, it is necessary to restore sufficient cooling and reestablish adequate heat removal. Generally, the time delay in reestablishing cooling allows the fuel rod temperature to rise substantially before the temperature increase is arrested.

The current strategy for containment of radioactive fission products requires that the integrity of the cladding and core fuel elements be maintained by emergency core cooling. Two techniques are commonly used for emergency core cooling in light water reactor (LWR) designs as illustrated in Figure 15. The first technique, common to

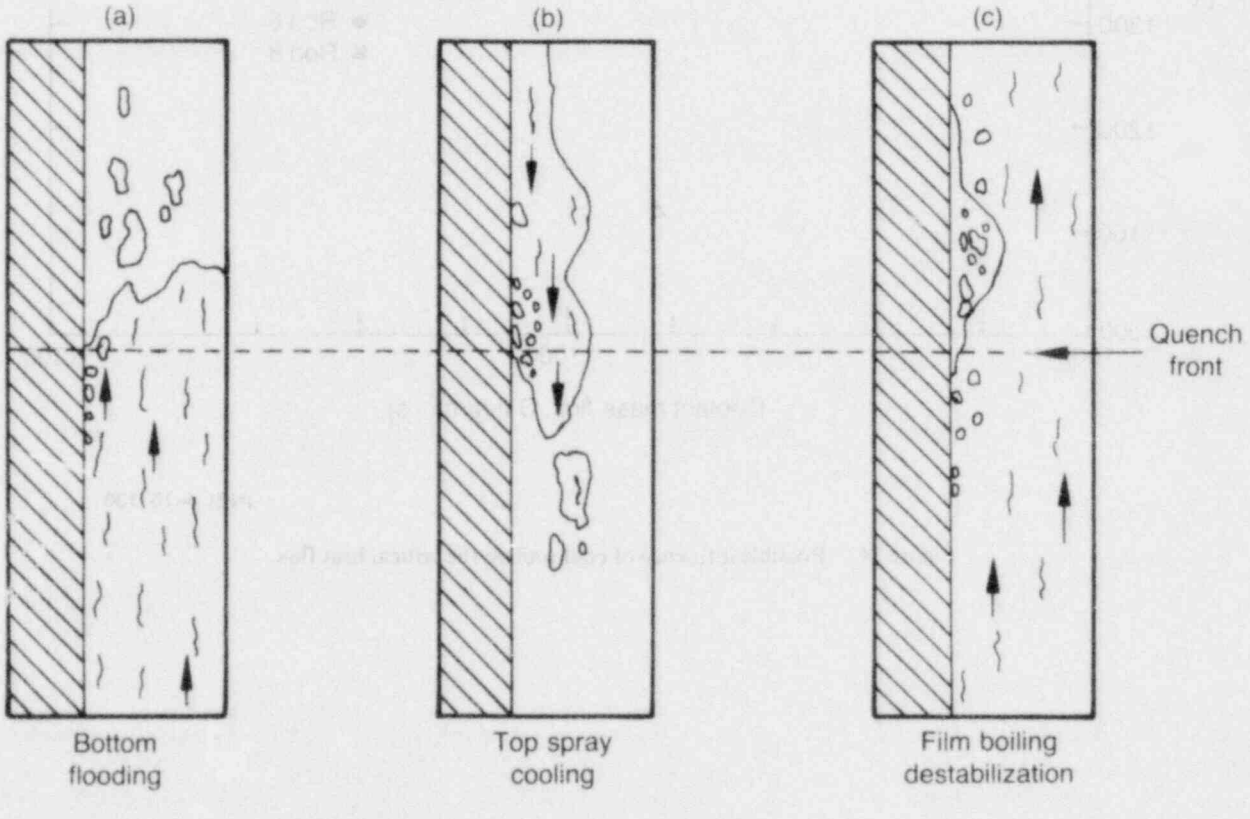

Figure 15. Quenching process.

pressurized water reactor (PWR) systems, is bottom reflood where the overheated fuel rods are quenched by the inundant process. The second technique, common to boiling water reactor (BWR) systems, is top spray cooling where the fuel rods are quenched by a falling film of water. Considerable theoretical and experimental work has been conducted to investigate the influence of the different operating parameters on the effectiveness of these emergency cooling techniques. References 41-53 provide recent overviews of the work in this area.

Presently, it is of considerable interest within the nuclear community to be able to predict and analytically describe the quench processes. Several computer codes have been developed to predict the quench process and have met with varying degrees of success. In some cases, prediction of quenching is considered fortuitous and may not actually model the physics involved.[54]

In contrast to a LOCA, a PCM event may precipitate fuel rod overheating without a deficiency in total coolant inventory. This occurs when the power-cooling conditions are such that film boiling occurs. In present LWR design and licensing efforts, considerable attention has therefore been focused on the prevention and mitigation of boiling transition occurrences. Should film boiling occur as a result of a PCM event, safe or lower fuel rod temperatures must be reestablished in order to minimize fuel rod damage and potential rod failure. This process is herein referred to as film boiling destabilization (FBD) (quench) or, under certain instances, return to nucleate boiling (RNB) (rewet). The quenching process is illustrated in Figure 16. Generally, FBD or RNB is attained by reducing core power while maintaining or enhancing coolant flow conditions without the use of the emergency core cooling system.

4.2 Quench and Rewet Temperatures

Wetting is defined and measured by the angle formed at an established liquid-solid-vapor triple interface as illustrated in Figure 16. In keeping with widely accepted terminology (References 55-58), wetting is said to occur when the contact angle (θ), as measured through the liquid phase, becomes less than 90°, with complete

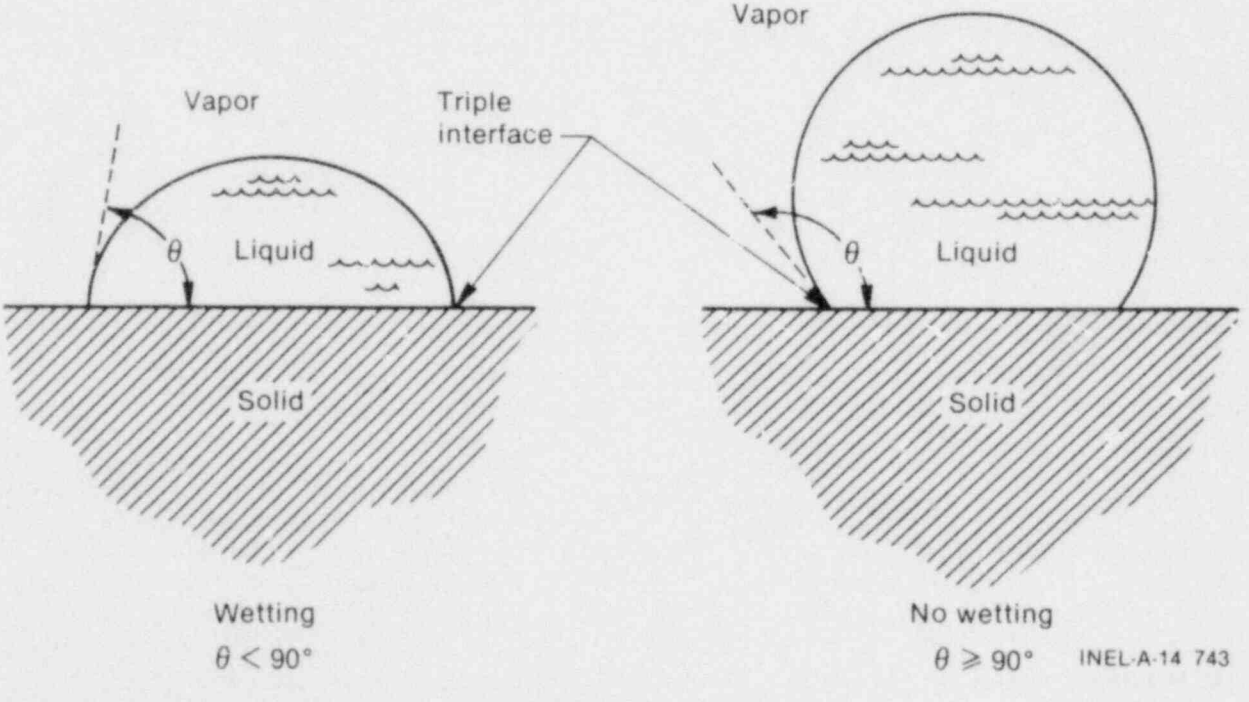

Figure 16. Contact angle and definition of wetting.

wetting corresponding to a zero degree contact angle.[a] Similarly, a contact angle of 180° corresponds to complete no-wetting. Wetting behavior is a complex phenomena influenced by many factors acting simultaneously, a few of the more common being:

1. Temperature
2. Interfacial absorption or chemisorption
3. Time
4. Thermophysical nature of the phases.

Rewetting requires that the liquid recontact the solid substrate. If the liquid-solid interface temperature attained upon contact equals or exceeds the thermodynamic limiting superheat of the rewetting liquid, the liquid is repelled from the hot surface and rewetting cannot occur.

When a liquid of uniform temperature T_L contacts a hot surface at uniform temperature T_w, the interface temperature (T_I) upon contact rapidly attains a value given by[59]:

$$T_I = \frac{T_w (k/\sqrt{\alpha})_w + T_L (k/\sqrt{\alpha})_L}{(k/\sqrt{\alpha})_w + (k/\sqrt{\alpha})_L} \quad (4)$$

Upon contact, if the interface temperature is less than or equal to the saturation temperature of the liquid, a contact angle is established. Likewise, if the interface temperature is greater than the saturation temperature of the liquid, boiling or liquid superheating will ensue. Since the limiting superheat of a liquid at a given pressure is its maximum superheat (T_{ms}), it follows from Equation (4) that the rewet temperature (T_{rw}) must obey the relationship:

$$T_{sat} < T_{rw} \leq \frac{\left[T_{ms} (k/\sqrt{\alpha})_w + (k/\sqrt{\alpha})_L\right]}{(k/\sqrt{\alpha})_w} - \frac{T_L (k/\sqrt{\alpha})_L}{(k/\sqrt{\alpha})_w} \quad (5)$$

Where all terms are defined in the Nomenclature. If $k_w/k_L >> 1$, Equation (5) reduces to:

$$T_{sat} < T_{rw} \lesssim T_{ms} \quad (6)$$

The rewet temperature [Equation (5)] depends upon the thermophysical nature of the hot surface and the contacting liquid. Theoretically, the maximum superheat of a liquid may be estimated from kinetic nucleation theory or from thermodynamic considerations. Reference 60 provides a brief review, and tabulated values, of maximum superheat temperatures for a wide variety of liquids (cryogens, refrigerants, water, liquid metals) at low pressures. At elevated pressures, the limiting superheat of a liquid approaches its thermodynamic critical temperature (T_c) and may, for a first approximation, be used in lieu of the maximum superheat in Equation (5). Appendix A provides a brief review of maximum superheat temperatures and associated values for water at various pressures.

The Leidenfrost temperature[b] (T_{Leid}) is often considered to be an upper limit for the rewet temperature. Strictly speaking, this is not necessarily true since transient liquid-solid contacts (and temporary rewetting) may exist during Leidenfrost boiling.[61,62] For general analysis and design purposes, however, macroscopic rewetting may be assumed nonexistent if the hot surface temperature exceeds the Leidenfrost temperature.

Rewetting of a hot surface by a liquid is not required for rapid cooling. Effective cooling can be attained at surface temperatures considerably above the maximum rewet temperature [Equation (5)]. This process is defined as quenching and often involves complex heat transfer phenomena. The conditions at which quench can occur vary greatly, depending upon the local fluid and hot surface conditions. This phenomenon is detailed in References 54 and 63.

Figure 17 represents a typical cladding temperature history observed during the latter stages of a LOCA with a subsequent reflood or a PCM event following a period of film boiling and

a. For liquid-liquid systems, a lens shaped interface is formed upon contact. For inclined or vertical surfaces in a gravitational field, or in the presence of forced convective shear stresses, advancing and receeding contact angles are formed.

b. The Leidenfrost temperature has its documented origins in the 18th century. It is defined as the hot surface temperature that will permit a boiling liquid drop, levitated by its own vapor, to exist for a maximum period of time (Appendix A).

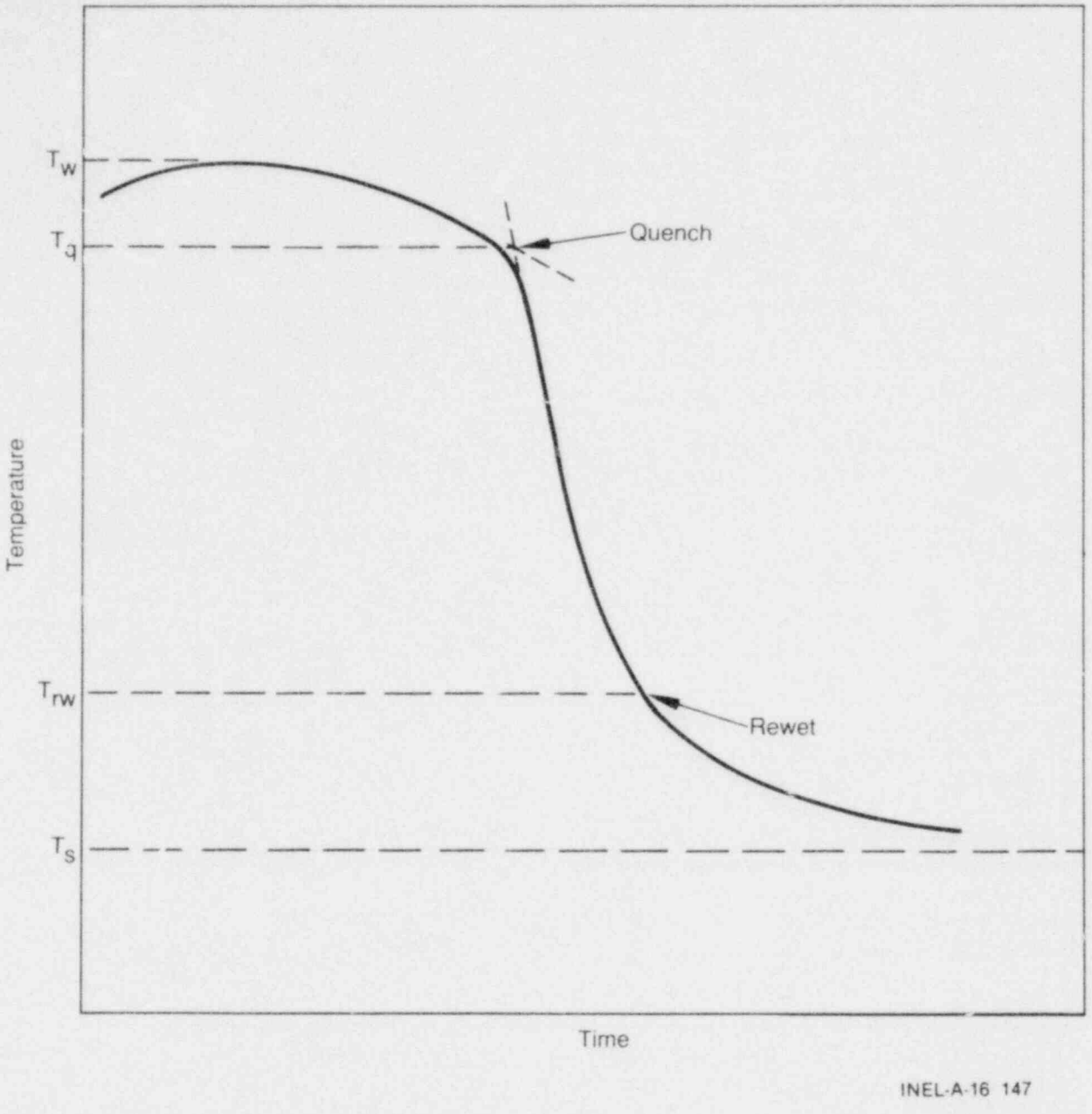

Figure 17. Cladding temperature history illustrating quench and rewet temperatures.

is used to illustrate the quench and rewet temperatures. Prior to quench, the cladding temperature history is often characterized by a period of gradual cooling. Quench is characterized by a rapid cooling of the cladding at elevated temperatures. The quench temperature (T_q) is defined as the cladding temperature at the onset of rapid cooling, where a significant increase in surface heat transfer has occurred, and is illustrated in Figure 17. Such a definition is somewhat arbitrary since the "onset of rapid cooling" is not precisely defined. For the purpose of this paper, the onset of rapid cooling, and thus quenching, is considered to occur when the temperature versus time trace (Figure 17) attains a slope of -200 K/s.

The rewet temperature is characterized by direct coolant/cladding contact and the establishment of a liquid-vapor-cladding, triple interface. Usually, the rewet temperature (Figure 17) is considerably lower than the quench temperature, and, given sufficient resolution, may be detected by a slope change in the cladding temperature versus time trace under certain conditions. Such a slope change, however, may also be caused by external cladding thermocouple-coolant interactions. Investigation into the detection of rewet and the influence of external cladding thermocouples is being done.

Many theoretical predictions of the cooling process by various models based on one, two, and three-dimensional analytical and numerical studies, require a knowledge of either the quench or rewet temperature.

4.3 Influence of External Cladding Thermocouples On Quenching

The geometry of the quench surface significantly influences the quenching process; primarily the time, temperature, and cooling rate. Recent in-pile[64] and out-of-pile[65] tests conclusively demonstrated that external cladding thermocouples attached to fuel rods or simulated fuel rods influence the quenching process during low pressure (6.9 MPa) blowdown-reflood tests. In general, the external thermocouples are accredited with inducing earlier quenches at higher temperatures. Figure 18 illustrates this behavior. It is not certain, however, whether "thermocouple effects" influence local behavior only or if their influence is felt elsewhere on the rod or adjacent rods.

External cladding thermocouples give rise to a "fin cooling effect" that may significantly decrease the local cladding temperature. Results from a recent in-pile, nine-rod PCM Test[10] indicate local cladding cooling up to several hundred degrees (K) at the point of thermocouple attachment. Therefore, it seems likely that the presence of external thermocouples may abet both quenching and rewetting phenomena.

4.4 Predicting the Quench Temperature

Very little work has been carried out to measure or predict the value of the quench temperature. To the knowledge of the authors, Kim and Lee[66] are the only researchers to have developed an empirical correlation for predicting the quench temperature. Their correlation is based on over 300 out-of-pile data points obtained in low pressure bottom reflood tests, and is given by

$$T_q = 19.51\, T_{ws}\left(\frac{T_{sc}}{T_{ws}}\right)^{0.107} \cdot \left(\frac{C_p G\delta}{k_w}\right)^{-0.162} \cdot \left(\frac{Z}{\delta}\right)^{-0.163} \cdot \left(\frac{k_w \rho_w T_{ws}}{\delta G^3}\right)^{-0.0989} + T_s \qquad (7)$$

where all terms are defined in the Nomenclature. The range of experimental parameters used in this correlation are given in Table 2. As shown in Figure 19, all correlated values of the quench temperature [Equation (6)] fall within $\pm 10\%$ of the experimental values.

Interestingly, Equation (7) appears to be valid well beyond its data base. Figure 19 illustrates a comparison of the predicted quench temperatures

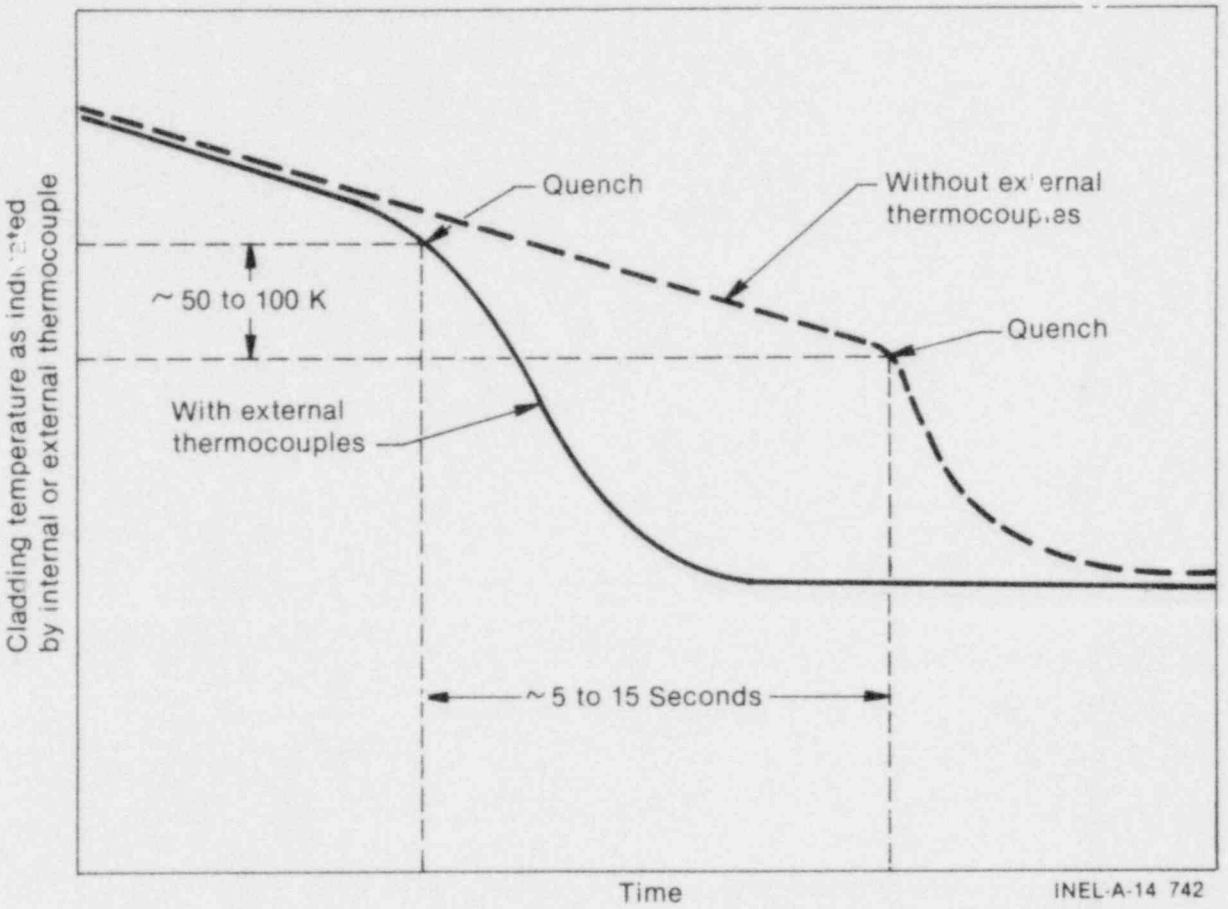

Figure 18. Influence of external cladding thermocouples on quenching process.

Table 2. Range of experimental quench parameters

	G ($kg/m^2 \cdot s$)	T_w[e] (K)	T_{sc} (K)	P (MPa)	Length (m)	Cladding	Reference
Correlation (Equation 4)	100 to 400	543 to 1073	10 to 83	0.1	2.3 to 4	SS/Inconel	66
PCM-2[a]	691 to 1435	620 to 1325	14	14.8	0.914	Zircaloy	5
PCM-2A[b]	784	866	13	14.6	0.914	Zircaloy	6
PCM-3[a]	700 to 832	890 to 1078	35	15.4	0.914	Zircaloy	8
PCM-4[a]	1063 to 1700	620 to 930	14	14.6	0.914	Zircaloy	9
PCM-5[c]	1016 to 1143	825 to 1300	25 to 29	15.5	0.914	Zircaloy	10
LLR-3[d]	1050	872	69	1.5	0.914	Zircaloy	67
LLR-5[d]	107	1000 to 1015	122	0.25	0.914	Zircaloy	67

a. Four-rod, individual coolant flow shrouds, power-cooling-mismatch (PCM) test.

b. Single-rod PCM test.

c. Nine-rod bundle PCM test.

d. LOFT-lead-rod (LLR), four-rod, individual coolant flow shrouds, LOCA blowdown/reflood test.

e. Peak cladding temperature prior to quench.

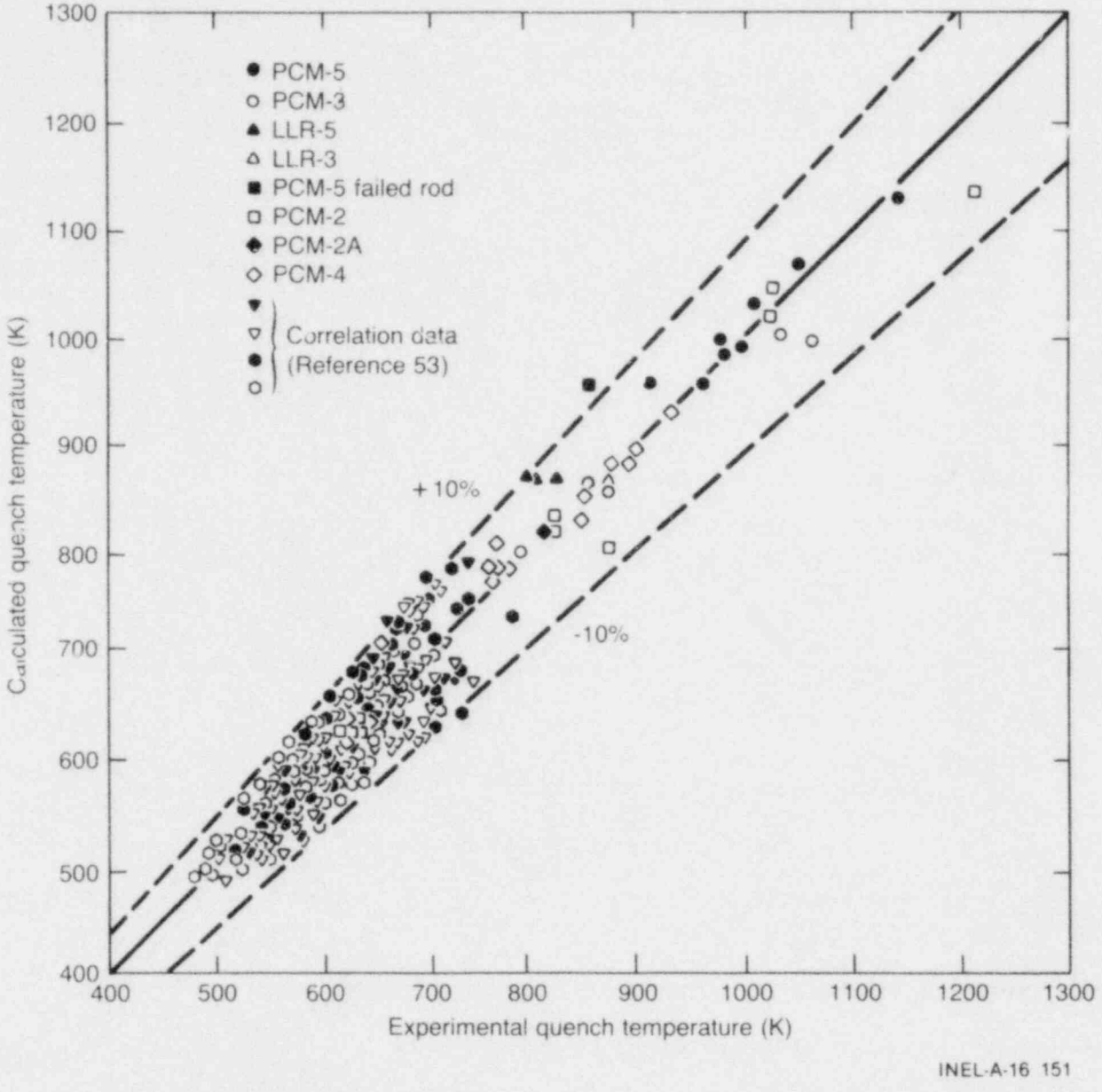

Figure 19. Correlation of quench temperatures.

[Equation (7)] with those determined experimentally from the PBF data (fuel rods with external cladding thermocouples). The range of experimental parameters for the plotted quench temperatures are given in Table 2. As shown, the empirical correlation of Kim and Lee[67] [Equation (6)] accurately predicts (±10%) the quench temperatures determined experimentally for intact fuel rods. In general, it appears that the influence of external cladding thermocouples on the quench temperature are within the range of uncertainty of Equation (7).

4.5 Predicting the Rewet Temperature

The rewet temperature is defined as the hot surface or heater temperature at which direct liquid solid contact and the formation of a liquid-vapor-solid triple interface occurs. The rewet temperature may span a wide range of values depending upon the thermophysical nature of the hot surface and the contacting liquid. From theoretical considerations, a range of rewet temperatures may be calculated and is given by Equation (5). For most applications, the maximum rewet temperature may be considered synonymous with the Leidenfrost temperature.

Table 3 provides a comparison of the predicted maximum rewet temperatures [Equation (5)] with those determined experimentally. The experimental values were based on Leidenfrost-type experiments, unless otherwise indicated. As expected, the predicted rewet temperature range encompasses experimental rewet temperatures.

Table 3. Comparison of rewet temperatures

	Rewet Temperature, T_{rw}(K)	
Fluid/Surface	Experiment[a]	Theory [Equation (5)]
Nitrogen/Aluminum	91[b]	77 to 106
Water/Stainless	537 to 593[c]	373 to 636
Water/Zircaloy-4	—	617 to 651[d]
Water/Zirconium Oxide	635 to 670[d,e]	617 to 670[d]
Mercury/Copper	967[f]	630 to 1550
Potassium/Tantalum	1588[g]	1030 to 1950

a. Based on Leidenfrost-type experiment at 0.1 MPa, unless otherwise indicated.

b. Kershock and Bell, Advanced Cryogenic Engireering, 15, Plenum,p. 271, 1970.

c. Godliski and Bell, *Proceedings of the American Institute of Chemical Engineers, 4,* 1966, p. 51,

d. Pressure of 15.5 MPa.

e. In-pile fuel rods, estimated from cladding temperature vs. time slope change (Ref. 10 and 66).

f. Poppendiek, et al., GLR-55, SAN-677-15, Geoscience, LtD., Calif., January 1966.

g. Poppendiek, et al., GLR-42, SAN-409-29, Geoscience, LtD., Calif, January 1966.

5. COMPARISON OF DEPARTURE FROM NUCLEATE BOILING AND QUENCH BEHAVIOR

In this section, a comparison is made of the thermal-hydraulic conditions at the onset of film boiling and the conditions at the onset of film boiling destabilization (quenching). Based on the experimental data from the PBF/PCM Test Series (Appendix C), it will be shown that the thermal-hydraulic conditions at the onset of film boiling are indistinguishable from the conditions at the onset of film boiling destabilization (quenching).

5.1 General Considerations of Quenching

As was discussed in Section 4, a wide variety of parameters are known to influence the quenching or film boiling destabilization process. Liquid subcooling, coolant mass flux, coolant/vapor distribution, and system pressure are examples of parameters which significantly influence this process. Film boiling may be "prematurely" destabilized by an external stimulus such as a pressure fluctuation or a physical disturbance of the stable film boiling vapor blanket. Therefore, film boiling destabilization or quenching does not necessarily occur at the "minimum film boiling point," but may occur well into the film boiling region. Appendix A briefly defines the temperature terminologies commonly used in defining these processes.

The parametric trends of the boiling transition process are often similar to the parametric trends of the film boiling destabilization process. Table 4 lists a few of the more common trends. In general, the parameters which inhibit the onset of film boiling encourage film boiling destabilization.

In order to make a valid comparison of DNB and quench behavior, similar or identical heater geometries and test conditions must be incorporated. The experiments of the PBF/PCM Test Series are ideally suited for such a purpose.

5.2 Similarities

In Section 3.4 the thermal-hydraulic conditions at the onset of film boiling were empirically correlated for the PBF/PCM Test Series data (listed in Appendix C). Using peak rod power (P_P), inlet coolant mass flux (G), and inlet subcooling (ΔT_{sc}) as the independent variables, the following empirical correlation, which is identical to Equation (3), was obtained:

$$P_P = 8.24\ G^{0.25}\ \Delta T_{sc}^{\ 0.057} \qquad (8)$$

As illustrated in Figure 11 (Section 3.4), Equation (8) accurately predicts ($\pm 20\%$) the inlet coolant/power conditions at the onset of film boiling.

Interestingly, Equation (8) also predicts ($\pm 20\%$) the PBF/PCM quench behavior as well. Figure 20 illustrates the experimentally determined peak rod powers at the onset of film boiling (open symbols) and quenching (shaded symbols) versus the predicted peak rod powers [Equation (8)]. As illustrated, the thermal-hydraulic conditions (P_P, G,ΔT_{sc}) at the onset of film boiling are virtually indistinguishable from those at quenching.

The onset of film boiling and the quenching behavior described above may also be illustrated on a forced convective boiling curve as illustrated in Figure 21. At the critical heat flux (Point A), where departure from nucleate boiling occurs, a jump discontinuity in wall temperature (to Point B) occurs. Upon cooldown, however, the system follows the same jump discontinuity and returns to nucleate boiling by way of the critical heat flux. Based on the coinciding DNB/quench data trends previously illustrated in Figure 20, little or no hystersis is expected while traversing Path A-B (Figure 21).

Return to nucleate boiling via the same path as DNB has been reported by other investigators. McEwan et al.,[67] observed this trend, and no signs of hysteresis, in tests with a heated annulus section using water at 10.3 MPa (1500 psia). Stevens et al.,[68] reported similar results using Freon-12 in a uniformly heated tube with upward vertical flow. Sterman et al.,[69,70] found, in tests using a 0.25 cm (0.63 in) diameter heated tube 1.39 cm (3.54 in) long with water at low pressures (0.20 to 0.71 MPa), that "prolonged film boiling below the burnout flux could not be maintained."

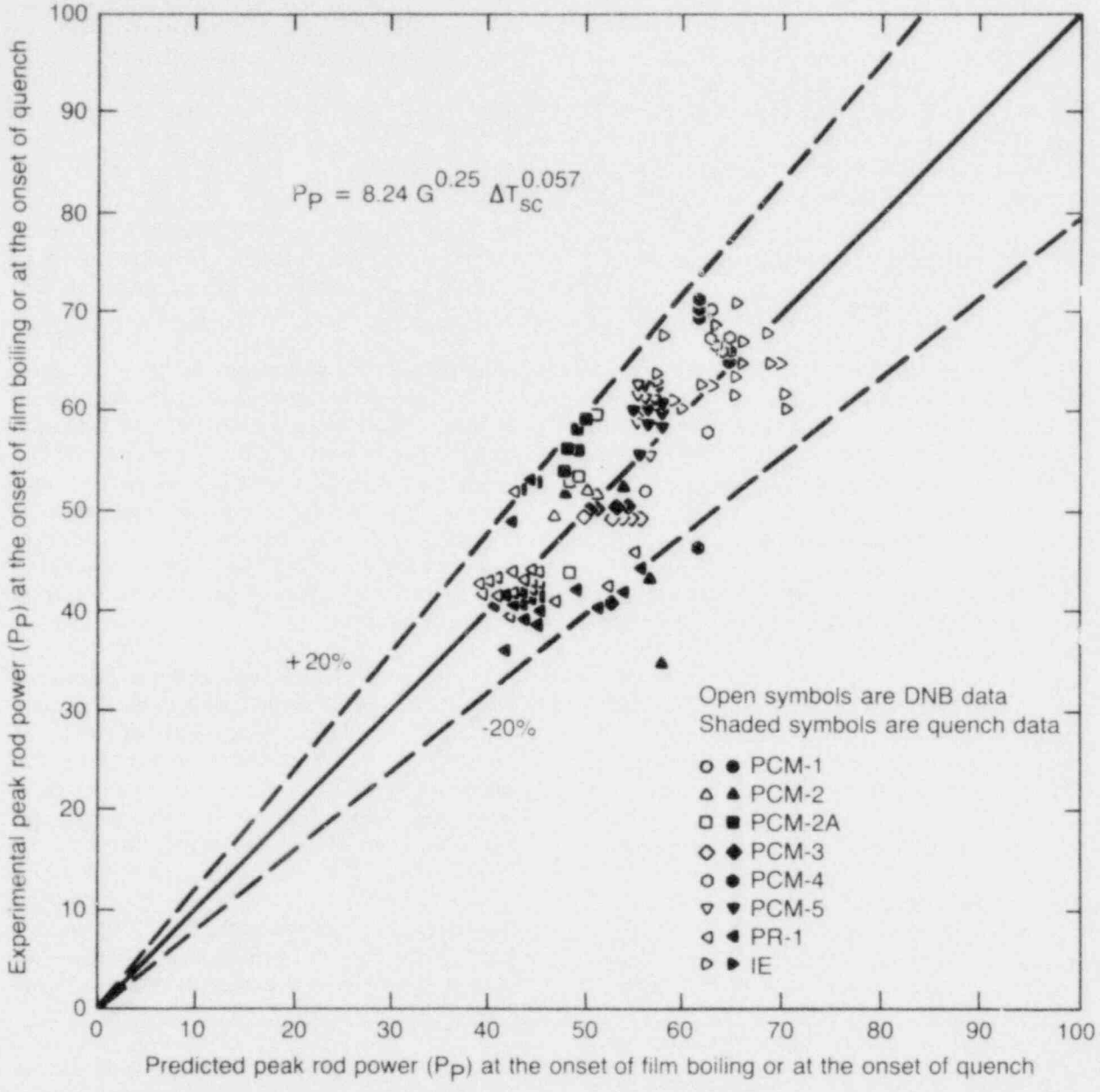

INEL-A-16 135

Figure 20. Comparison of the conditions at the onset of film boiling and quenching.

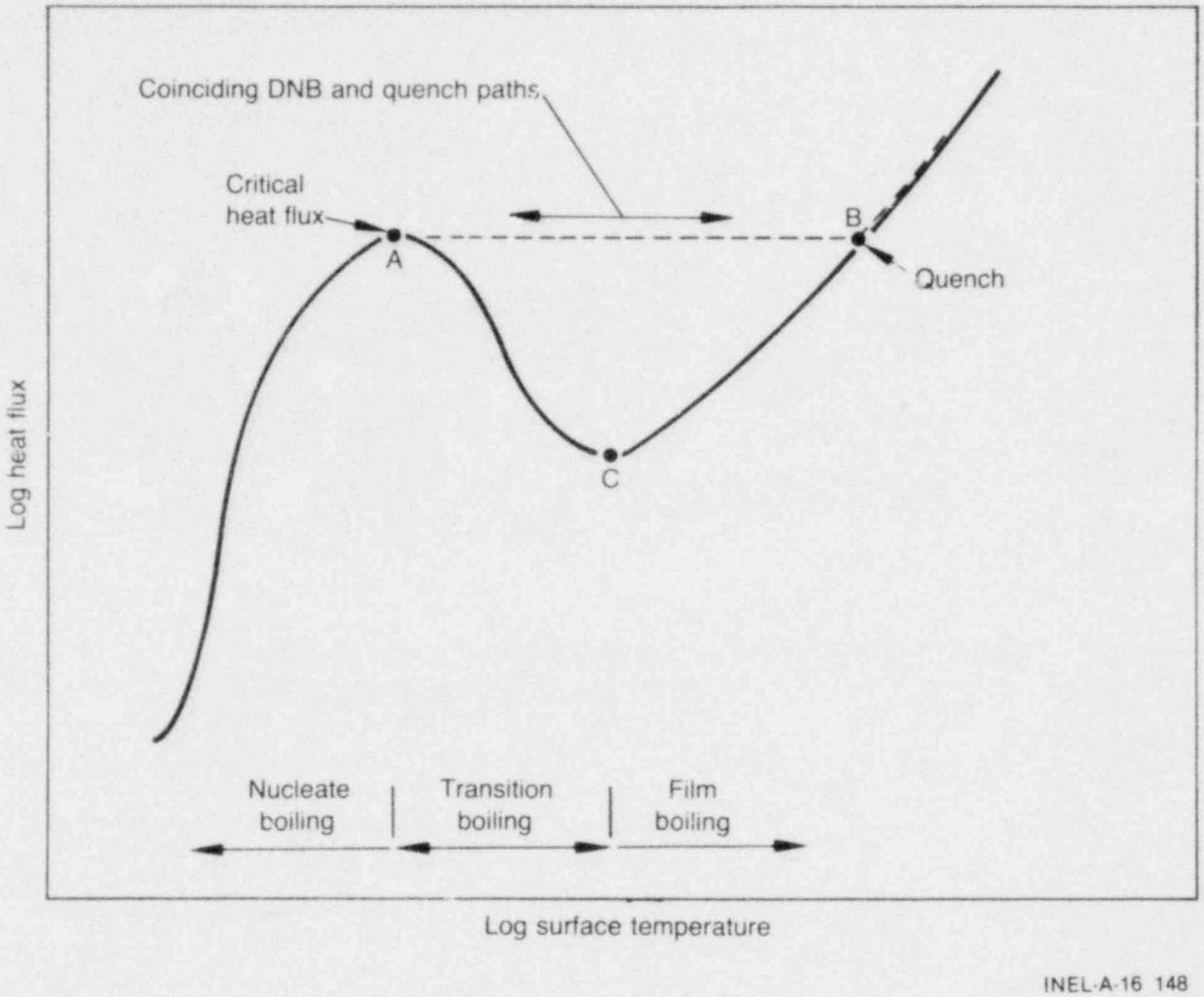

Figure 21. Classical boiling curve illustrating film boiling and quenching paths.

MacBeth summarizes this behavior by the statement: "Thus, it seems that in a forced-convection system, a region corresponding to BC (Figure 21) for pool boiling may or may not be attainable, depending on the system parameters."[71]

5.3 Differences

Obvious differences exist between the onset of film boiling and the onset of film boiling destabilization (quenching) phenomena. The parameters which hinder DNB behavior usually abet quenching behavior. This was discussed in Section 5.1 and is partially summarized on Table 4.

For PBF/PCM testing, one difference is the local coolant distribution at the onset of film boiling versus the coolant distribution at quench. A low quality (low void fraction) bubbly flow pattern (subcooled boiling) immediately proceeds the onset of film boiling as was illustrated in Figure 1. Direct coolant/cladding interactions and momentary rewetting set the stage for departure from nucleate boiling. Film boiling destabilization or quenching, however, generally occurs in a higher local quality environment where a metastable vapor film blankets the hot surface. Direct coolant/cladding contact with rewetting does not occur at the onset of quenching.

The cladding surface temperature at the onset of boiling transition is sometimes referred to as the critical heat flux temperature, T_{CHF} (see Appendix A). For PBF/PCM testing, T_{CHF} is numerically somewhat greater than the saturation temperature of the coolant. The cladding surface temperature at the onset of film boiling destabilization or quenching (T_q), however, is often several hundred degrees above the coolant saturation temperature. Therefore, the cladding surface temperature at the onset of film boiling is often several hundred degrees less than the cladding surface temperature at the onset of film boiling destabilization or quenching.

Table 4. Parametric trends of film boiling and film boiling destabilization

	Effects	
Parameter	Film Onset of Boiling (CHF)	Onset of Film Boiling Destabilization (FBD)
Increase pressure (P)	Low P: Increases CHF High P: Decreases CHF	Encourages FBD
Increase inlet subcooling (T_{sc})	Increase CHF	Encourages FBD
External cladding thermocouples	Increase and delay DNB	Encourages FBD
Increase coolant mass flux (G)	Increases CHF	Encourages FBD
Decrease power	Discourages DNB	Encourages FBD
Heater surface conditions (oxidation, roughness)	Little influence on CHF for forced convective boiling	Slightly encourages FBD in pool boiling

5.4 Anomalous Departure from Nucleate Boiling and Quench Behavior

There were two reported instances of anomalous DNB and quench behavior that occurred during the PCM Test Series. The first, was anomalous DNB behavior that occurred during the nine-rod bundle test PCM-5. The second was anomalous quench behavior that occurred during the four-rod (individual coolant flow shrouds) Test PCM-2. Within this section, these isolated cases of anomalous behavior are briefly described. It is shown that such behavior may be the result of inherent hydraulic coupling or fuel rod bowing.

5.4.1 Anomalous Departure from Nucleate Boiling Behavior and Test PCM-5. Test PCM-5 was the first nine-rod open bundle experiment in the PBF/PCM Test Series. A cross section of the 3 x 3 test fuel bundle is illustrated in Figure 14 (Section 3), and the details of this test are found in Reference 10.

Film boiling was initiated within the nine-rod test bundle by slowly increasing test rod power while maintaining an approximately constant bundle coolant mass flux. At some later period during the test, the coolant mass flux was slightly increased and the average test rod power was slightly decreased. As a result, corner rod three (see Figure 14) and center rod five quenched, and commenced return to nucleate boiling. Within seconds of when the center rod quenched, however, adjacent side rod six underwent departure from nucleate boiling and remained in film boiling for almost a minute. This behavior was unexpected since the thermal-hydraulic test conditions (increased coolant mass flux and decreased rod power) favored quench behavior and not DNB behavior. Such a phenomenon may be viewed as a hydraulically coupled rod-to-rod interaction.

Consider two adjacent fuel rods within a bundle geometry, as illustrated in Figure 22. Initially, the rods are cooled by an approximately uniform coolant distribution with no film boiling (Figure 22a). If film boiling is initiated on one of the fuel rods (Figure 22b), the coolant is redistributed and may provide enhanced cooling in adjacent regions. Such a process, of course, requires a decrease in the coolant mass flux through the film boiling vapor layer. Upon quenching and rewet on the rod (Figure 22c), the coolant is again redistributed and may result in a net decrease of the cooling capacity in adjacent regions, which in turn may induce the onset of DNB (or the continuation of film boiling) on adjacent rods. Such a phenomenon may be summarized as follows: a change in the local boiling conditions (onset of film boiling or return to nucleate boiling) alters the local coolant distribution and may influence the boiling behavior of adjacent fuel rods.

5.4.2 Anomalous Quench Behavior and Test PCM-2. Test PCM-2 was a four-rod test, where each fuel rod was contained within its own coolant flow shroud, as illustrated in Figure 4 (Section 2). The flow shrouds were hydraulically coupled in parallel with common inlet and outlet plenums. The details of this test are found in Reference 5.

Quenching was consistently initiated on three of the four test rods by either decreasing rod power, increasing coolant mass flux, or both. During the final DNB cycle, however, even with power reduction film boiling on one rod (which did not reach DNB until very low flow conditions were established) could not be terminated until the flow was increased to a higher value than that required to quench the other three rods. As shown in Figure 23, quench did not occur on this rod as flow was increased. As the flow reached the pre-DNB value of 1460 kg/m^2-s, the cladding surface temperature decreased and then gradually increased to about 1520 K. Test rod peak power was then reduced to 40 kW/m, which resulted in lower cladding temperatures, but sustained film boiling. Only after test rod power was further decreased, and the coolant mass flux further increased, did quenching occur.

This unexpected quench behavior may be the result of a hydraulically coupled interaction, as illustrated in Figure 22, or fuel rod bowing. When one (or more) test fuel rod commences film boiling, the two-phase pressure drop or flow resistance within that coolant flow shroud is increased. Since coolant follows the path of least resistance, the coolant flux is slightly redirected toward adjacent or bypass flow channels. As a result, neighboring test fuel rods may experience enhanced cooling, thereby reducing the potential for further DNB occurrences. Similiarily, film boiling destabilization or quenching reduces the pressure drop within a coolant channel, resulting in a net decrease in coolant availability for adjacent, coupled channels. Therefore, the quenching of fuel rods within hydraulically coupled coolant channels becomes successively more difficult.

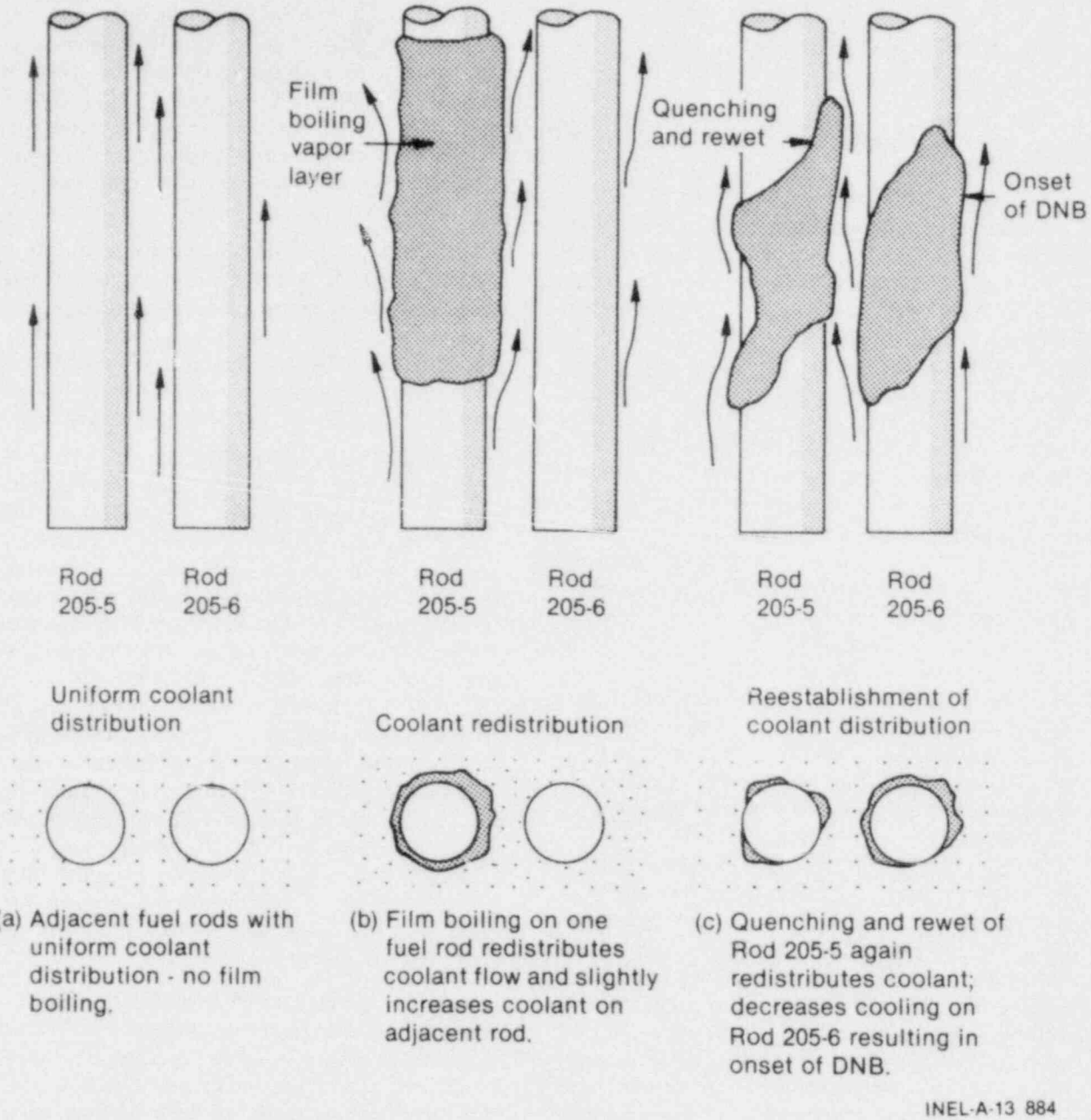

Figure 22. Conceptual illustration of thermal-hydraulic rod-to-rod interaction.

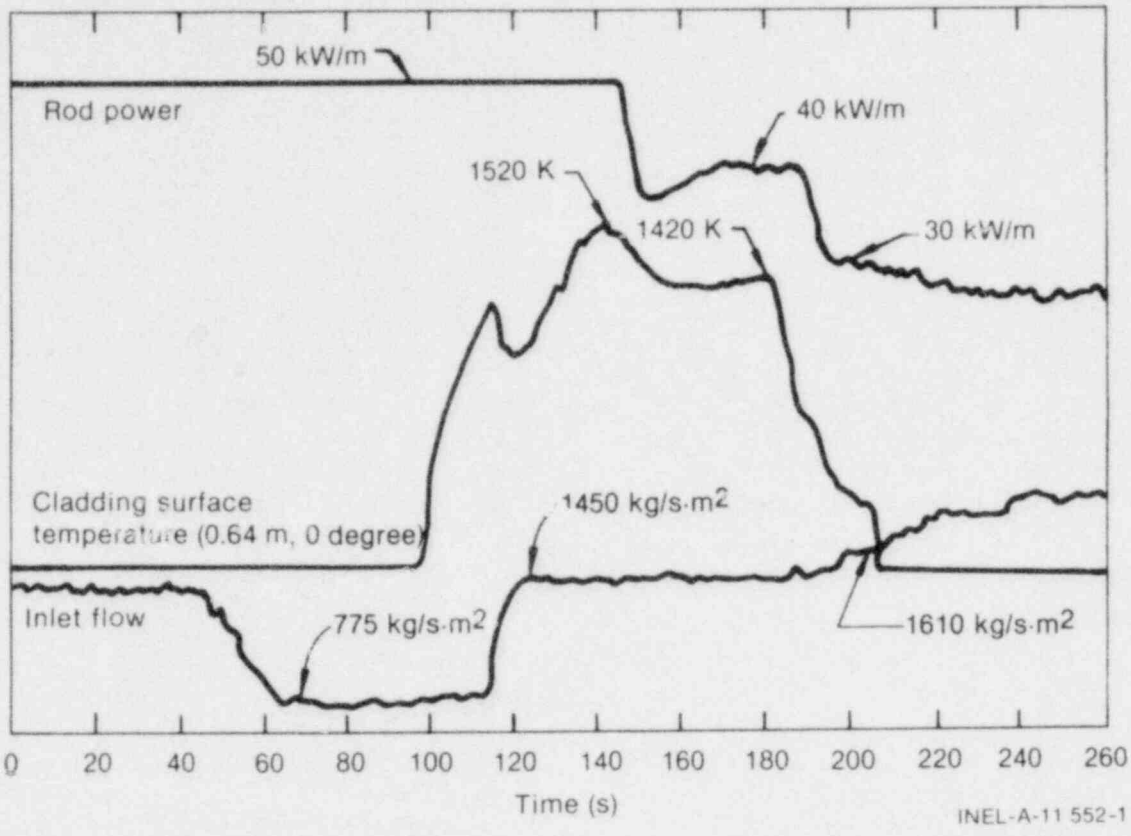

Figure 23. Anomalous rewet behavior during Test PCM-2.

The anomalous quench behavior observed in Test PCM-2 may likewise be the result of fuel rod bowing. Inherent within the four-rod geometry of Test PCM-2 is a slight power skewing, where the highest powers occur at the inner regions (0° location) of the test rods. As a result, rod bowing toward the hotter, higher power regions is expected. If the rod bowing is sufficiently great and test rod-flow shroud contact is made, localized coolant flow starvation results. This, in turn, makes film boiling destabilization or quenching more difficult to induce.

5.4.3 Closing Remarks. Many parameters influence the film boiling and quench behavior of a system. In addition to the more common thermodynamic parameters such as pressure, temperature, and volume, there are others of equal or greater importance. Geometry, for example, greatly affects the processes of film boiling and quenching. Mechanical protrusions into the flowing coolant stream (external cladding thermocouples, rod orientation or bowing, instrumentation and associated lead wires, etc.) can make a simple hydraulic system complex. The nature of the heater surface (clean, oxidized, smooth, rough, etc.) also adds an element of complexity to the understanding of two-phase heat transfer phenomena. A non-uniform radial boiling profile, inherent hydraulic coupling, and resultant localized pressure fluctuations also contribute to boiling behavior.

Unfortunately, no universal two-phase thermal-hydraulic model exists to completely describe boiling behavior. This is because the basic physical principles of boiling heat transfer, and their interdependency, are not well understood at this time. Consequently, boiling behavior which is now termed "anomalous" stems mainly from a lack of understanding of the physics which dictates boiling behavior.

6. CONCLUSIONS AND FINAL REMARKS

This report has presented a study of film boiling, quench, and rewet phenomena during high pressure Power-Cooling-Mismatch (PCM) testing within the Idaho National Engineering Laboratory (INEL) Power Burst Facility (PBF).

The results of this study led to the following observations and conclusions:

1. The critical heat flux (ϕ_{CHF}) behavior observed during PBF power-cooling-mismatch testing can best be modeled by an additive empirical correlation of the form:

$$\phi_{CHF} \ (\pm 30\%) = 0.23\ G + 393\ P - 20.5\ P^2 - 32\ GX + 2\ GPX \qquad (9)$$

   and is recommended for use in the following parameter ranges:

   Heated length (L): 0.879 to 0.914 m

   Pressure (P): 13.6 to 15.5 MPa

   Coolant mass flux (G): 513 to 2750 kg/m^2-s

   Local quality (χ): -0.035 to 0.239

   Subcooling (ΔT_{sc}): 7 to 25 K

   Critical heat flux (ϕ_{CHF}): 840 to 2000 kW/m^2

2. Comparison of observed PBF/PCM critical heat flux conditions with well-known reactor vendor correlations indicates that the Combustion Engineering (CE-1) or LOFT critical heat flux correlations best model the observed behavior.

3. Quench and rewet are distinctly different phenomena, entailing different modes of heat transfer. The cladding surface temperatures at which quench and rewet occur may be estimated from Equations (7) and (5), respectively.

4. On the basis of the PBF/PCM tests, thermal-hydraulic conditions at the onset of film boiling are indistinguishable from the conditions at the onset of film boiling destabilization (or quenching). This implies that return to nucleate boiling occurs via the same path as boiling transition, with no sign of hysteresis.

7. REFERENCES

1. T. E. Murley, L. S. Tong, G. L. Bennett, "Summary of LWR Safety Research in the USA," *IAEA International Conference on Nuclear Power and Its Fuel Cycle, Salzburg, Austria, May, 1977.*

2. U.S. Nuclear Regulatory Commission, Division of Reactor Safety Research, *Water Reactor Safety Research Program—A Description of Current and Planned Research*, NUREG-0006, February 1979.

3. P. E. MacDonald et al., "Response of Unirradiated and Irradiated PWR Fuel Rods Tests Under Power-Cooling-Mismatch Conditions," *Nuclear Safety, 19*, 1978, pp. 440-464.

4. A. S. Mehner et al., "Performance of Unirradiated and Irradiated PWR Fuel Rods Tested Under Power-Cooling-Mismatch Conditions," *ANS Thermal Reactor Safety Meeting, Sun Valley, Idaho, July 31-August 5, 1977.*

5. Z. R. Martinson and R. K. McCardell, *Power-Cooling-Mismatch Test Series, Test PCM-2 Test Results Report*, NRC/ERDA Report TREE-NUREG-1038, February 1977.

6. G. W. Cawood et al., *Power-Cooling-Mismatch Test Series, Test PCM-2A Test Results Report*, NCR-NUREG-1347, September 1976.

7. D. T. Sparks and C. J. Stanley, *Power-Cooling-Mismatch Test Series, Test PCM-1 Fuel Rod Behavior Report*, NUREG/CR-0907, TREE-1374, August 1979.

8. D. E. Owen and K. Vinjamuri, *Power-Cooling-Mismatch Test Series, Test PCM-3 Test Results Report*, NUREG/CR-0902, TREE-1335, August 1979.

9. R. L. Johnson et al., *Fuel Rod Behavior During Test PCM-4*, NUREG/CR-0903, TREE-1336, August 1979.

10. F. S. Gunnerson and D. T. Sparks, *Behavior of a Nine-Rod Fuel Assembly During Power-Cooling-Mismatch Conditions, Results of Test PCM-5*, NUREG/CR-1103, EGG-2002, November 1979.

11. W. J. Quapp, C. M. Allison, L. C. Farrar, *Irradiation Effects Test Series, Scoping Test 1, Test Results Report*, TREE-NUREG-1066, September 1977.

12. W. J. Quapp, L. C. Farrar, C. M. Allison, A. S. Mehner, *Irradiation Effects Test Series, Scoping Test 2, Test Results Report*, TREE-NUREG-1044, September 1977.

13. W. J. Quapp, L. C. Farrar, C. M. Allison and A. S. Mehner, *Irradiation Effects Test Series, Test IE-1, Test Results Report*, TREE-NUREG-1046, March 1977.

14. C. M. Allison, D. W. Croucher, S. A. Ploger, A. S. Mehner, *Irradiation Effects Test Series, Test IE-2, Test Results Report*, TREE-NUREG-1074, August 1977.

15. L. C. Farrar, D. W. Croucher, C. M. Allison, S. A. Ploger, *Irradiation Effects Test Series, Test IE-3, Test Results Report*, TREE-NUREG-1106, October 1977.

16. D. W. Croucher, T. R. Yackle, C. M. Allison, S. A. Ploger, *Irradiation Effects Test Series, Test IE-5, Test Results Report*, TREE-NUREG-1130, January 1978.

17. K. Vinjamuri, *Fuel Swelling Due to Retained Fission Gas in Molten Fuel During High Temperature Transients*, NUREG/CR-1236, EGG-2014, February 1980.

18. A. W. Cronenberg and T. R. Yackle, *An Assessment of Intergranular Fracture Within Unrestructured UO_2 Fuel Due to Film Boiling Operation*, NUREG/CR-0595, TREE-1330, March 1979.

19. A. W. Cronenberg and M. S. El-Genk, *An Assessment of Oxygen Diffusion During UO_2-Zircaloy Interaction*, TREE-NUREG-1192, January 1978.

20. M. S. El-Genk, *An Assessment of Fuel Melting, Radial Extrusion, and Cladding Thermal Failure During a Power-Cooling-Mismatch Event in Light Water Reactors*, NUREG/CR-0500, TREE-1270, May 1979.

21. S. L. Seiffert and R. R. Hobbins, *Oxidation and Embrittlement of Zircaloy-4 Cladding from High Temperature Film Boiling Operation*, NUREG/CR-0517, TREE-1327, April 1979.

22. D. W. Croucher, *Behavior of Defective PWR Fuel Rods During Power Ramp and Film Boiling Operation*, NUREG/CR-0283, TREE-1267, February 1979.

23. W. Redpath, "Winfrith SGHWR In-Reactor Dryout Tests," *Journal of British Nuclear Energy Society*, 13, 1974, pp. 87-97.

24. W. Redpath, and R. W. Read, "Critical Heat Flux Experiments in the Winfrith SGHWR," *Sixth Annual WRSR Information Meeting, Gaithersburg, Maryland, November 6, 1978* (AAEWR 1152).

25. A. Garlick, "Examination of an Instrumented Fuel Element After Dryout Tests in Winfrith SGHGWR," *Journal of British Nuclear Energy Society, 16*, 1, 1977, pp. 71-75.

26. A. S. Bain, A. W. L. Segel, and J. Novak, "Examination of Fuel Bundles Irradiated in Intermittent Dryout," *Proc., ANS Topical Meeting on Water Reactor Fuel Performance, St. Charles, Illinois, May 9-11, 1977*, (ANS).

27. D. C. Groeneveld and G. D. McPherson, *In-Reactor Post-Dryout Experiments with 36 Element Fuel Bundles*, AECL-4705, December 1973.

28. A. D. Lane and J. F. Collier, "Thermal and Irradiation Performance of Experimental Fuels Operating in Steam-Water Mixtures," *Proc. 34d UN International Conference on Peaceful Uses of Atomic Energy, A/Conf., 28/P/16/UN, Geneva, 1964.*

29. R. D. Page, "Engineering and Performance of Canada's UO_2 Fuel Assemblies for Heavy-Water Power Reactors," *Proc. Symposium on Heavy Water Power Reactors, Vienna IAEA September 1967* STI/Pub/163, Paper SM-99/48, pp. 749-77.

30. T. Sorlie, S. Levy, M. F. Lyons, J. E. Boyden, "Experience with BWR Fuel Rods," *Nucleonics, 23*, 4, April 1965, pp. 62-65, 88.

31. G. Kjaerheim, "Heat Transfer in Water Cooled Nuclear Reactors," *Nuclear Engineering and Design, 21*, 2, 1972, pp. 279-301.

32. E. Rolstad and J. Kjaerheim, "BWR Burn-Out Experiments," *Nuclear Engineering International*, December 1968, pp. 1021-1027.

33. A. E. Bergles, "Burnout in Boiling Heat Transfer. Part II: Subcooled and Low Quality Forced-Convective Systems, Two-Phase Flows and Heat Transfer, *Proceedings of NATO Advanced Study Institute, Instanbul, Turkey*, August 16-27, 1976, pp. 692-820.

34. L. S. Tong, *Boiling Crisis and Critical Heat Flux*, AEC Critical Review Series, TID-25887, 1972.

35. R. A. DeBertoli et al., *Forced Convective Heat Transfer Burnout Studies for Water in Rectangular and Round Tube at Pressure above 500 psia*, USAEC WAPD-188, 1958.

36. A. P. Ornatskiy, "The Effect of Basic Regime Parameters and Channel Geometry on Critical Heat Fluxes in Forced Convection of Subcooled Water," *Heat Transfer-Soviet Research, 1*, 3, 1969, 17-22.

37. M. Silvestri, *A Research Program in Two-Phase Flow*, CISE Report, 1963.

38. L. S. Tong, "Boundary Layer Analysis of the Flow Boiling Crisis," *International Journal of Heat Mass Transfer, 11*, 1968 pp. 1208-1211.

39. D. F. Babcock, *Heavy Water Moderated Power Reactors*, USAEC Progress Report DP-895, 1964.

40. E. Janssen and J. A. Kervinen, *Burnout Conditions for Single Rod in Annular Geometry, Water at 600 and 1400 psia*, USAEC Report GEAP-3899, 1963.

41. R. B. Duffey and D.T.C. Porthouse, "The Physics of Rewetting in Water Reactor Emergency Core Cooling," *Nuclear Engineering and Design, 25*, 1973, pp. 379-394.

42. J. H. Linehan, P. A. Howard, M. A. Grolmes, "The Stationary Boiling Front in Liquid Film Cooling of a Vertical Heated Rod," *Nuclear Engineering and Design, 52*, 1979, pp. 201-218.

43. P. Chambre and E. Elias, "Boiling Heat Transfer During Rewetting," *Nuclear Engineering and Design, 50*, 1978, pp. 353-363.

44. S. H. Chan and M. A. Grolmes, "Hydrodynamically-Contolled Rewetting," *Nuclear Engineering and Design, 34*, 1975, pp. 307-316.

45. S. A. Fairbairn, "Quenching of Hot Surfaces," *Nuclear Energy, 18*, 1979, pp. 151-159.

46. T. S. Thompson, "On the Process of Rewetting a Hot Surface by a Falling Liquid Film," *Nuclear Engineering and Design, 31*, 1974, pp. 234-245.

47. C. L. Tien and L. S. Yao, "Analysis of Conduction-Controlled Rewetting of a Vertical Surface," ASME Publication 74-WA/HT-49, 1974.

48. R. Martini and A. Premoli, "Bottom Flooding Experiments with Simple Geometries under Different E.C.C. Conditions," *Energia Nucleare, 20*, 1973, pp. 540-553.

49. K. G. Pearson, B. D. G. Piggott, R. B. Duffey, "The Effect of Thermal Diffusion From Fuel Pellets on Rewetting of Overheated Water Reactor Pins," *Nuclear Engineering and Design, 41*, 1977, pp. 165-173.

50. B. D. G. Piggott and R. B. Duffey, "The Quenching of Irradiated Fuel Pins," *Nuclear Engineering and Design, 32*, 1975, pp. 182-190.

51. B. D. G. Piggott and D. T. C. Porthouse, "A Correlation of Rewetting Data," *Nuclear Engineering and Design, 32*, 1975, pp. 171-181.

52. B. D. G. Piggott, E. P. White, R. B. Duffey, "Wetting Delay Due to Film and Transition Boiling on Hot Surfaces," *Nuclear Engineering and Design, 36*, 1976, pp. 169-181.

53. M. E. Sawan and M. W. Carbon, "A Review of Spray-Cooling and Bottom-Flooding Work for LWR Cores," *Nuclear Engineering and Design, 32*, 1975, pp. 191-207.

54. R. A. Nelson, "Forced Convective Post CHF Heat Transfer and Quenching," (to be published), *Trans. ASME, 1980 Annual Winter Meeting, Chicago, Illinois, 1980.*

55. T. Young, *Miscellaneous Works*, Vol. I, G. Peacock, ed., Murray, London, 1855.

56. A. W. Adamson, *Physical Chemistry of Surfaces*, 3rd edition, New York: John Wiley and Sons, 1976.

57. J. J. Bikerman, *Physical Surfaces*, New York: Academic Press, 1970.

58. American Chemical Society, *Contact Angle, Wettability and Adhesion*, Advances in Chemistry Series, Applied Publications, Washington, D.C., 1964.

59. H. S. Carslaw and J. C. Jaeger, *Conduction of Heat in Solids*, New York: Oxford University Press Inc., 2nd Edition, 1959.

60. F. S. Gunnerson and A. W. Cronenberg, "On the Thermodynamic Superheat Limit for Liquid Metals and Its Relation to the Leidenfrost Temperature," *Journal of Heat Transfer, 100*, 734, (1978).

61. F. S. Gunnerson, *Film Boiling Destabilization from Hydrodynamic and Thermodynamic Considerations*, Ph.D. dissertation, University of New Mexico, Albuquerque, New Mexico, 1979.

62. J. G. Comeau, *A Review of Leidenfrost Phenomena*, Master thesis, University of Ottawa, Ottawa Canada, 1979.

63. F. S. Gunnerson, "On the Prediction of Quench and Rewet Temperatures," *Transactions of ANS, 1980 Annual Meeting, Las Vegas, Nevada, June 9-12, 466*, 1980.

64. T. R. Yackle, private communication, EG&G Idaho, Inc., February 1980.

65. R. C. Gottula, *LOFT Transient (Blowdown) Critical Heat Flux Tests*, TREE-NUREG-1240, April 1978.

66. A. K. Kim and Y. Lee, "A Correlation of Rewetting Temperature," *Letters in Heat and Mass Transfer, 6*, 117, 1979.

67. L. H. McEwen, J. M. Batch, D. J. Foley, M. R. Kreiter, *Heat Transfer Beyond Burnout for Forced Convective Bulk Boiling*, ASME 57-SA-49, 1957.

68. G. F. Stevens, D. F. Elliott, R. W. Wood, *An Experimental Investigation into Forced Convection Burnout in Freon, with Reference to Burnout in Water*, AEEW-R 321, 1964.

69. L. S. Sterman and N. G. Stiushin, "An Investigation into the Influence of Speed of Circulation on the Values of Critical Heat Flows for Liquid Boiling in Tubes," *Journal of Technical Physics, (USSR) 22*, 446, 1952.

70. L. S. Sterman, N. G. Stiushin and V. G. Morozon, "An Investigation of the Dependence of Critical Heat Flux on the Rate of Circulation," *Journal of Technical Physics, (USSR) 1*, 2250, 1956.

71. R. V. MacBeth, "The Burn-Out Phenomena in Forced-Convective Boiling", *Advanced in Chemistry Engineering Progr. Symp. Series, 48*, 1968.

APPENDIX A

TEMPERATURE TERMINOLOGIES COMMON TO THE NUCLEAR INDUSTRY

APPENDIX A

TEMPERATURE TERMINOLOGIES COMMON TO THE NUCLEAR INDUSTRY

Within the nuclear community, a wide variety of terminologies are used to describe specific temperatures. Often a certain temperature is referred to by several different names; such as the minimum film boiling, Leidenfrost or rewet temperature. Confusion and misinterpretation often arise as a result of varied nomenclature.

The purpose of this appendix is to provide a listing and corresponding definitions of temperature terms common to the nuclear literature. Many of the temperatures listed have been defined or inferred in various ways by different authors. Some of the definitions which follow are, therefore, subject to the interpretation by the authors of this report.

TEMPERATURE (T): An index or measure of the molecular activity of matter which determines, in part, the transfer of heat to or from other bodies. It is a quantitative measure of the degree of "hotness" or "coldness" of a body or system. Customary units of temperature are degrees Celsius, Kelvin, Fahrenheit, or Rankine.[A-1]

APPARENT REWET TEMPERATURE: See QUENCH TEMPERATURE (T_q).

APPARENT QUENCHING TEMPERATURE: See QUENCH TEMPERATURE (T_q).

CRITICAL TEMPERATURE (T_c, T_{crit}): The temperature above which a gas cannot be liquified by pressure changes alone. It is the highest temperature at which liquid and vapor can coexist in thermodynamic equilibrium. For pure water, T_c = 647.2 K.

CRITICAL HEAT FLUX TEMPERATURE (T_{CHF}, T_{DNB}): The heater surface temperature at the critical heat flux or at the onset of boiling transition.

FOAM LIMIT TEMPERATURE: See MAXIMUM, METASTABLE SUPERHEAT TEMPERATURE.

HOMOGENEOUS NUCLEATION TEMPERATURE (T_{HN}): The maximum limit of superheat for a liquid at a given pressure, free from foreign matter and disallowing the possibility of interfacial vapor formation, as predicted from kinetic nucleation theory. Mathematically defined by the general rate expression[A-2]

$$J = \omega N \exp(-W/kT) \qquad (A\text{-}1)$$

where:

J = the number of critical size vapor nuclei per unit volume per unit time which grow to macroscopic size

ω = frequency of collision between vapor embryo and individual liquid molecules

k = Boltzmann constant (1.38×10^{-23} J/K)

N = number of liquid molecules per unit volume

The work of vapor embryo formation, W, is given by the sum of the work of surface formation, the work to overcome pressure forces, and the "molecular" work. Mathematically,

$$W = 4 \pi r^2 \sigma + 4/3 \pi r^3 (\rho' - \rho'') + 4/3 \pi r^3 \rho'' (\mu' - \mu'') \qquad (A\text{-}2)$$

where:

σ = surface tension

r = embryo radius

μ = chemical potential

liquid = single prime superscript

vapor = double prime superscript.

At the homogeneous nucleation temperature, J will increase several orders of magnitude for a change of only a few degrees in temperature, thus defining T_{HN}.

For large volume, slowly heated systems, T_{HN} occurs when $J \sim 10^{6}$ to 10^{8} (sites/cc s). For small volume, pulse heated systems, T_{HN} occurs when $J \sim 10^{12}$ to 10^{15} (sites/cc s)[A-3].

Homogeneous nucleation is an explosive type of vapor production which rarely occurs in practice since surface or heterogeneous nucleation occurs at much lower superheats. Figure A-1 illustrates a comparison of the saturation (T_{sat}), homogeneous nucleation (T_{HN}) and maximum, metastable superheat ($T_{max,s}$) temperatures as a function of pressure. As illustrated, the liquid superheat limit predicted from a thermodynamic Van der Waals-type equation of state (see MAXIMUM METASTABLE SUPERHEAT TEMPERATURE) is somewhat greater than the predicted superheat limit from kinetic theory. At atmospheric pressure, for example, $T_{max,s}$ for pure water is about 586 K and T_{HN} is about 578 K (Reference A-4). Numerically, the difference between the two values decreases with increasing pressure and are equal at the critical point (Figure A-1). Therefore, for a first approximation, $T_{HN} \approx T_{max,s}$.

INCIPIENT BOILING TEMPERATURE (T_i): The heater surface temperature at the onset of boiling or when vapor nucleation commences.

LEIDENFROST TEMPERATURE (T_{Leid}): The minimum heater surface temperature required to keep a boiling liquid droplet levitated with its own vapor (Leidenfrost boiling). Geometry independent, where from theoretical considerations[A-4]:

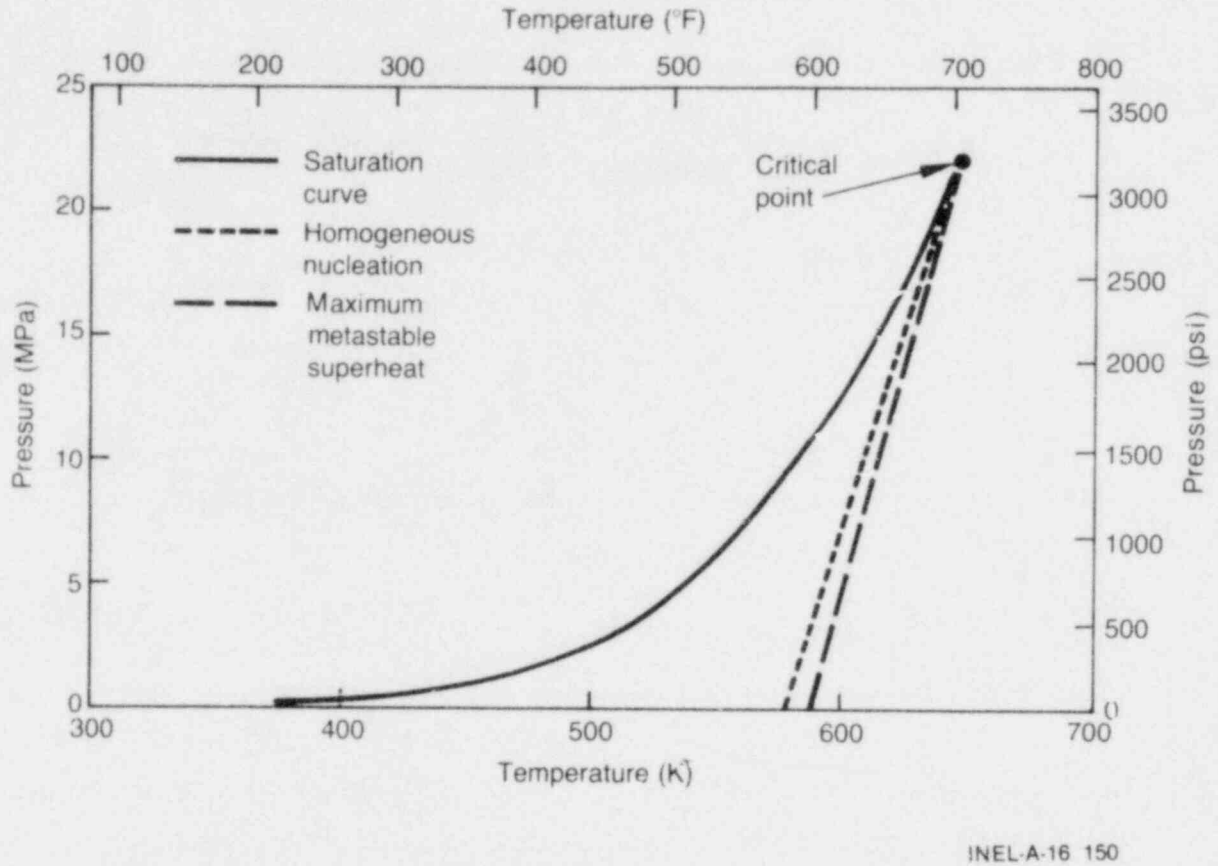

Figure A-1. Saturation and limiting superheat temperatures for pure water at various pressures.

$$T_{sat} < T_{Leid} \leq \frac{T_{ms}\ (k/\sqrt{\alpha})_w + (k/\sqrt{\alpha})_L - T_L(k/\sqrt{\alpha})_L}{(k/\sqrt{\alpha})_w} \qquad \text{(A-3)}$$

NOTE: Transient liquid-heater contact[A-5,6] and momentary rewetting may occur at temperatures above T_{Leid}. Therefore, the thermophysical natures of the boiling liquid and the heating surface influence T_{Leid}.

LIMITING SUPERHEAT TEMPERATURE: See MAXIMUM, METASTABLE SUPERHEAT TEMPERATURE, HOMOGENEOUS NUCLEATION TEMPERATURE OR SPONTANEOUS NUCLEATION TEMPERATURE.

MAXIMUM, METASTABLE SUPERHEAT TEMPERATURE ($T_{max,s}$ or T_{ms}): The maximum thermodynamic limit of liquid superheat at a given pressure as defined by the intersection of the liquid-phase spinodal and the corresponding isotherm. The liquid-phase spinodal (Figure A-2) is that curve in PVT space which separates metastable states from unstable states at densities greater than the critical density. Also referred to as the limiting superheat or foam limit temperature.[A-7] For liquids which obey the Van der Waals Equation of State (EOS), $T_{max,s}$ can be estimated by the following expression:[A-7]

$$T_{max,s} \approx \frac{27}{32} T_c \qquad \text{(at low pressure)} \qquad \text{(A-4)}$$

where T_c is the thermodynamic critical temperature. At elevated pressures, $T_{max,s}$ is more closely estimated by the empirical relationship:[A-8]

$$\frac{T_{max,s} - T_{sat}}{T_c} = \left(1 - \frac{T_{sat}}{T_c}\right) + 0.0905 \left(1 - \frac{T_{sat}}{T_c}\right)^8 \qquad \text{(A-5)}$$

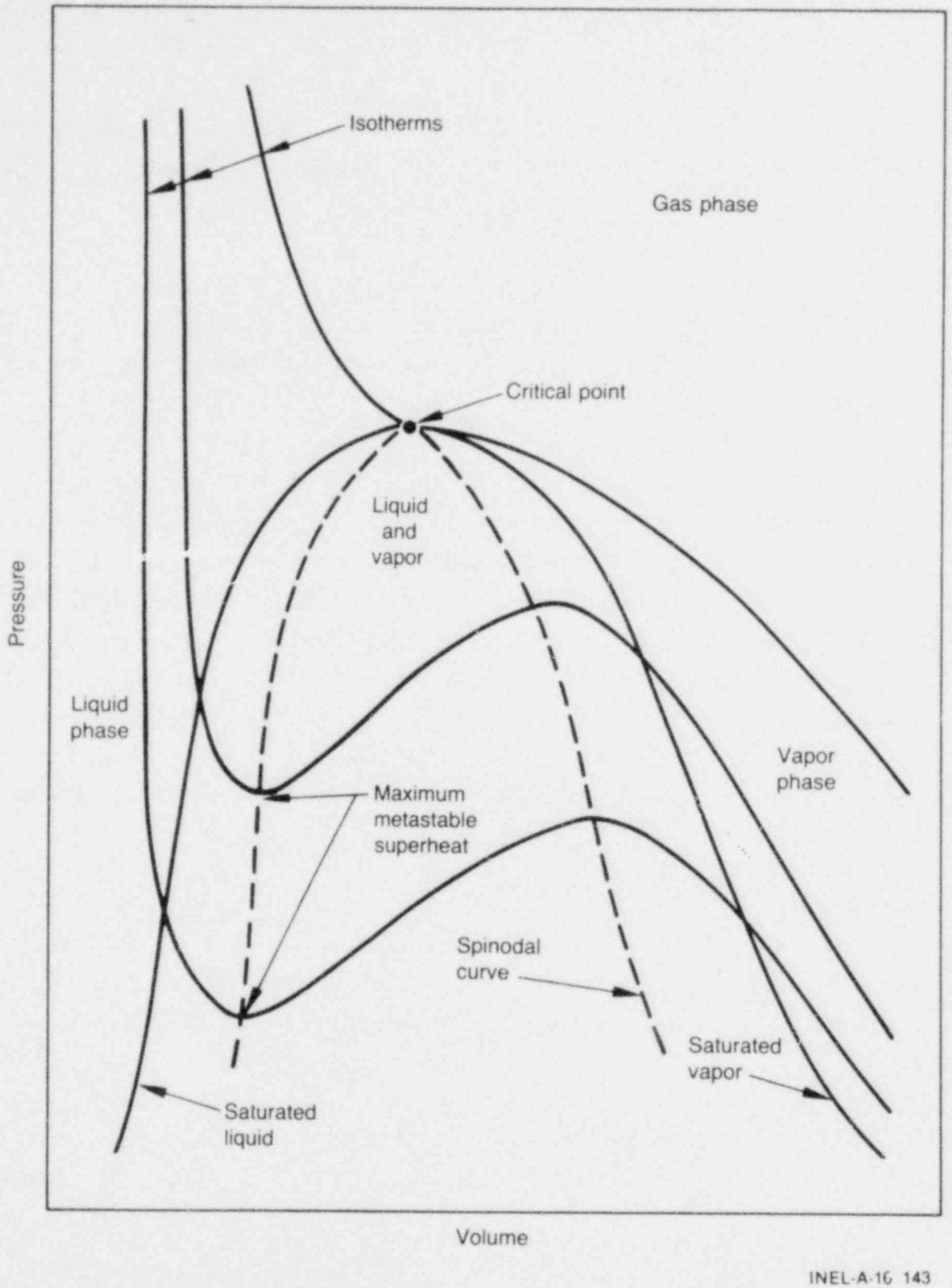

Figure A-2. Isotherms of a pure substance on a Pressure-Volume diagram.

where T_{sat} is the saturation temperature at a given pressure. Figure A-1 illustrates approximate values for $T_{max,s}$ (as calculated from the above empirical relationship) for water at various pressures.

MELTING TEMPERATURE (T_{mp}): The temperature at which heterogeneous solid-liquid phase change occurs at a given pressure. It is the temperature at which the solid and liquid phases of a substance may exist together in equlibrium, without either phase changing into the other.[A-9] It is the temperature at which a substance exhibits an increase in liquidity (or decrease in viscosity) in going from a solid to liquid state. For an amorphous solid (such as glass) no abrupt change in liquidity occurs at T_{mp}.

MINIMUM FILM BOILING TEMPERATURE (ΔT_{min}): The minimum superheat temperature of the heating surface, $(T_w - T_{sat})_{min}$, required to sustain film boiling. It may span a wide range of values depending upon the thermophysical nature of the heating surface and the boiling liquid. The wall temperature at the minimum point, $T_{W,min}$, may be viewed as the Leidenfrost temperature or rewet temperature whose range may be approximated by Equation (A-3).

QUENCH TEMPERATURE (T_q): The heater surface temperature at the onset of film boiling destabilization characterized by rapid cooling, where a significant increase in the surface heat transfer has occurred,[A-10,11] also referred to as the apparent rewet temperature[A-10,12] or apparent quenching temperature.[A-14]

REWET TEMPERATURE (T_{rw}): The heater surface temperature at which direct liquid/heater contact occurs and a liquid-vapor-heater triple interface is reestablished. For most applications, microscopic rewetting may be assumed nonexistent if the hot surface exceeds the Leidenfrost temperature (T_{Leid}).[A-10,11] Also referred to as the wetting temperature (T_{wet}).[A-15]

SATURATION TEMPERATURE (T_{sat}): The temperature at which the liquid and vapor phases of a substance are in thermodynamic equilibrium at a given pressure. Figure A-1 illustrates the saturation temperature for pure water at various pressures.

SPONTANEOUS NUCLEATION TEMPERATURE (T_{SN}): The maximum limit of superheat for a liquid at a given pressure, where possible interfacial vapor formation exist, as predicted from kinetic nucleation theory: heterogeneous nucleation (also see homogeneous nucleation temperature, T_{HN}).[A-3]

The effect of interfacial wetting characteristics must be considered in predicting T_{SN}. This is usually done by multiplying the work of vapor embryo formation, W (see Equation (A-2) by a wetting factor, $f(\theta)$:

$$f(\theta) = \frac{2 + 3\cos\theta - \cos^3}{4} \qquad \text{(A-6)}$$

where θ is the interfacial contact angle. For perfect wetting $\theta = 0$ and $f(\theta) = 1$ and, thus, $T_{SN} = T_{HN}$. Only for a high degree of nonwetting is T_{SN} significantly lower than T_{HN}. For complete nonwetting $\theta = 180^{o}$ and $f(\theta) = 0$ and, thus, $T_{SN} = T_{sat}$.

Therefore, the work required for spontaneous nucleation is less than that for homogeneous nucleation, and:

$$T_{sat} < T_{SN} \leq T_{HN} \qquad \text{(A-7)}$$

Values of the spontaneous nucleation temperature for pure water at atmospheric pressure as a function of interfacial wettability are given in Table A-1.

TABLE A-1. SPONTANEOUS NUCLEATION TEMPERATURES FOR PURE WATER AT ATMOSPHERIC PRESSURE AS A FUNCTION OF INTERFACIAL WETTABILITY

Contact Angle, (Degrees)	Wetting Factor $f(\theta)$, Equation (A-6)	Approximate T_{SN} (K)
0	1	578
90	0.50	568
135	0.060	541
150	0.013	513
180	0	373

SPUTTERING TEMPERATURE (T_o): The heater surface temperature in the region preceding a quench front (sputtering region).[A-16] It is considered to lie between the incipient boiling temperature (T_i) and the critical heat flux temperature (T_{CHF}, T_{DNB}).[A-16] The sputtering temperature is often approximated by[A-17] the Leidenfrost temperature or the rewet temperature. It has also been defined as the heater surface temperature at the quench front.[A-18,19] The sputtering temperature at various pressures is reported in Reference.[A-20]

REFERENCES

A-1. CRC Handbook of Chemistry and Physics, 55th edition, CRC Press, Cleveland, Ohio, 1974.

A-2. M. Volmer, "Kinetic der Phasenbildung," Die Chemische Reaktion, 4, 1939.

A-3. V. P. Skripov, Metastable Liquids, New York: John Wiley and Sons, 1974.

A-4. F. S. Gunnerson and A. W. Cronenberg, "On the Thermodynamic Superheat Limit for Liquid Metals and Its Relation to the Leidenfrost Tempera- ture," Journal of Heat Transfer, 100, 734, 1978.

A-5. W. S. Bradfield, "Liquid-Solid Contact in Stable Film Boiling," Industrial and Engineering Chemistry Fundamentals, 5, 2, May 1966, pp. 200-204.

A-6. K. J. Baumeister, F. F. Simon, R. E. Henry, "Role of the Surface in the Measurement of the Leidenfrost Temperature, Augmentation of Convective Heat and Mass Transfer, ASME Winter Meeting, New York. New York, December 2, 1970.

A-7. P. Spiegler et al., "Onset of Stable Film Boiling and the Foam Limit," International Journal of Heat Mass Transfer, 6, 1963, pp. 987-994.

A-8. J. H. Lienhard, "Correlation for the Limiting Liquid Superheat," Chemical Engineering Science, 31, 9, 1976, pp. 847-849.

A-9. J. J. Little and Ives Co., The Complete Book of Science, New York: Educational Publishers, 1963.

A-10. F. S. Gunnerson and T. R. Yackle, "Quenching and Rewetting of Nuclear Fuel Rods," (submitted for publication) Nuclear Technology, March 1980.

A-11. F. S. Gunnerson, "On the Prediction of Quench and Rewet Temperatures," Transaction of the American Nuclear Society, Las Vegas, Nevada, June 1980, p. 466.

A-12. A. K. Kim and Y. Lee, "A Correlation of Rewetting Temperature," Letters in Heat and Mass Transfer, 6, 1977--1979.

A-13. R. Martini and A. Premoli, "Bottom Flooding Experiments with Simple Geometries Under Different E.C.C. Conditions," Energia Nucleare, 20, 1973, pp. 540-553.

A-14. W. J. Chen, Y. Lee, D. C. Groenveld, "Measurement of Boiling Curves During Rewetting of a Hot Circular Duct," International Journal of Heat Mass Transfer, 22, 1979, pp. 973-976.

A-15. F. F. Simon and R. J. Simoneau, Transition from Film to Nucleate Boiling in Vertical Forced Flow, ASME publication 69-HT-26, 1969.

A-16. J. H. Linehan, P. A. Howard, M. A. Grolmes, "The Stationary Boiling Front in Liquid Film Cooling of a Vertical Heated Rod," Nuclear Engineering and Design, 52, 1979, pp. 201-218.

A-17. R. B. Duffey and D.T.C. Porthouse, Nuclear Engineering and Design, 25, 1973, p. 379.

A-18. M. W. E. Coney, "Calculations on the Rewetting of Hot Surfaces," Nuclear Engineering and Design, 31, 1974, pp. 246-259.

A-19. T. S. Thompson, "On the Process of Rewetting a Hot Surface by a Fall- ing Liquid Film," Nuclear Engineering and Design, 31, 1974, pp. 234-245.

A-20. A. W. Bennett, G. F. Hewitt, H. A. Kearsey, R.K.F. Keeys, The Wetting of Hot Surfaces by Water in a Steam Environment at High Pressure, AERE-R5146, 1966.

APPENDIX B

CRITICAL HEAT FLUX CORRELATIONS

APPENDIX B

CRITICIAL HEAT FLUX CORRELATIONS

The prediction of the critical heat flux has resisted all attempts at theoretical analysis from first principles. As a result, data have been gathered and empirical correlations developed to model the data. The evolution of such empirical critical heat flux correlations has paralleled the development of the test facilities to generate the necessary data.

Within Section 3 of this report, an assessment was made of the CHF correlations widely used in the nuclear industry to model the boiling transition behavior experienced during PBF experiments. A detailed listing of the more common CHF correlations, applicable to PWR-type conditions, follows.

1. Babcock & Wilcox, B&W-2[B-1]

$$\phi_{CHF} = \left[\frac{1.15509 - 0.40703\ (De)}{12.71 \quad (3.0545G')^{A}}\right] \left[(0.3702 \times 10^{8})\ (0.59137G')^{B} - 0.15208_{\chi}H_{fg}G\right] \Big/ F_{APk}$$

where

$$A = 0.71186 + (2.0729 \times 10^{-4})\ (P-2,000)$$
$$B = 0.834 + (6.8479 \times 10^{-4})\ (P-2,000)$$
$$G' = G/10^{6}$$

The B&W-2 correlation was developed from rod bundles in water data in the parametric ranges given by:

Equivalent diameter, De	0.2 to 0.5 in.
Heated length, L	72 in.
Pressure, P	2,000 to 2,400 psia
Mass flux, G	0.75×10^6 to 4.0×10^6 lbm/ft^2-hr
Local quality, X	-0.03 to 0.20

2. LOFT Correlation[B-2]

$$CHF = 0.11585G + 800P - 0.27442P^2 - 1.4383GX + 0.0002566\,GPX$$

The LOFT correlation is valid in the following parametric ranges:

Pressure, P	2,000 to 2,400 psia
Mass flux, G	0.75×10^6 to 2.5×10^6 lbm/ft^2-hr
Local quality,	-0.35 to 0.20

3. Westinghouse Company, W-3[B-3]

$$\Phi_{CHF} = 1.0 \times 10^6 \left\{ 2.022 - 4.302 \times 10^{-4}P + (0.1722 - 9.84 \times 10^{-5}P) \exp\left[(18.177 - 4.129 \times 10^{-3}P)X\right] \right\} (1.157 - 0.869X) \left\{ \left[0.1484 + X(-1.596 + 0.1729\,ABS(X))\right] G' + 1.037 \right\} \left[0.8258 + 7.94 \times 10^{-4}(H_f - H_{in})\right] \left[0.2664 + 0.8357 \exp(-3.151\,D_e)\right] / F_{APK}$$

where

$$G' = G/10^6$$

The W-3 correlation is valid in the following parametric ranges:

Equivalent diameter, D_e	0.2 to 0.7 in.
Heated length, L	10 to 144 in.
Pressure, P	1,000 to 2,400 psia
Mass flux, G	1.0×10^6 to 5.0×10^6 lbm/ft^2·hr
Local quality,	-0.15 to 0.15

4. CE-1 Correlation[B-4,5]

The CE-1 correlation is based on 731 data points from electrically heated rod bundles (14 x 14 and 16 x 16) and is given by:

$$\Phi_{CHF} = 10^6(b_1)\left(\frac{d}{d_m}\right)^{b_2}\left[(b_3 + b_4P)\left(\frac{G}{10^6}\right)^{(b_5 + b_6P)} - \left(\frac{G}{10_6}\right)(X)(h_{fg})\right] / \left(\frac{G}{10_6}\right)^{(b_7P + b_8\, G/10^6)}$$

where

$$\frac{d}{d_m} = 1.0$$

$$b_1 = 2.8922 \times 10^{-3}$$
$$b_2 = -0.50749$$
$$b_3 = 405.32$$
$$b_4 = -9.9290 \times 10^{-2}$$
$$b_5 = -0.67757$$
$$b_6 = 6.8235 \times 10^{-4}$$

$b_7 = 3.1240 \times 10^{-4}$

$b_8 = -8.3245 \times 10^{-2}$

The CE-1 correlation is valid in the following parametric ranges:

Pressure, P	1745 to 2415 psia
Local quality, χ	-0.16 to 0.20
Mass flux, G	1.0×10^6 to 3.0×10^6 lbm/ft^2-hr
Inlet temperature, T_{in}	451 to 633°F
Subchannel wetted Equivalent diameter, D_e	0.3588 to 0.5447 in.
Subchannel heated Equivalent diameter, D_H	0.4713 to 0.7837 in.
Heated length, L	84 to 144 in.

Axial Power Profile Factor (F_{APk})

The axial power profile factor is used in calculations for rods with a nonuniform heat flux and is calculated by the following equation.[B-3]

$$F_{APk} = \frac{A_1 \, C \int_0^{L_{DNB,N}} \phi(z) \exp\left[-C\,(L_{DNB,N} - z)\right] dz}{\phi_{local} \left[1 - \exp\left(-C\, L_{DNB,EU}\right)\right]}$$

where

$$\phi(z) = \frac{P_P}{\pi D} \sin\left(\frac{\pi z}{L}\right) \text{ and, } C = \frac{A_2 \, (1 - \chi)^{A_3}}{(G/10^6)^{A_4}}$$

For B&W-2		For W-3 and CE-1	
A_1	= 1.025	A_1	= 1.00
A_2	= 0.249	A_2	= 0.15
A_3	= 7.82	A_3	= 4.31
A_4	= 0.457	A_4	= 0.478

The values of F_{APk} in Table B-1 were calculated using these values:

P_P = $7.07 \times 10^4 \frac{Btu}{ft\text{-}hr}$

D = 0.03517 ft.

$L_{DNB,N}$ = 27.6 in.

$L_{DNB,EU}$ = 13.9 in.

L = 36 in.

TABLE B-1. AXIAL POWER FACTOR

Correlation	G(lbm/ft^2-hr)	X	F_{APk}
B&W-2	1.48×10^6 (2000 kg/m^2·s)	0.036	1.36
	8.11×10^5 (1100 kg/m^2·s)	0.094	0.73
W-3 and CE-1	1.48×10^6 (2000 kg/m^2·s)	0.036	1.44
	8.11×10^5 (1100 kg/m^2·s)	0.094	1.52

Cold-Wall Factor (F_{cw})

To compensate for the cold-wall effect believed to be present in our test geometries, the following cold-wall factor was used;[B-3]

$$F_{cw} = 1.0 - (1.0 - \frac{D_e}{D_H}) \left[13.76 - 1.372 \exp(1.78X) \right.$$

$$- 4.732 \left(\frac{G}{10^6}\right)^{-0.0535} - 0.0619 \left(\frac{P}{10^3}\right)^{0.14}$$

$$\left. - 8.509 (D_H)^{0.107} \right] \qquad \text{(B-6)}$$

Using the following values,

D_e = 0.22 in.

D_H = 0.55 in.

G = 1.48×10^6 lbm/ft^2·hr

P = 2103 psia

= 0.036

a cold-wall factor, F_{cw}, of approximately 0.4 is calculated.

REFERENCES

B-1. J. S. Gellerstedt et al., "Correlation of Critical Heat Flux in a Bundle Cooled by Pressurized Water," Two-Phase Flow and Heat Transfer in Rod Bundles, Winter Annual Meeting of the American Society of Mechanical Engineers, Los Angeles, California, November 1969, pp. 63-71.

B-2. S. A. Eide and R. G. Gottula, Evaluation and Results of LOFT Steady State Departure from Nucleate Boiling Tests, TREE-NUREG-1043, April 1977.

B-3. L. S. Tong, Boiling Crisis and Critical Heat Flux, TID-25887, August 1972.

B-4. Combustion Engineering, Inc., C-E Critical Heat Flux, CENPD-162-A, September 1976.

B-5. Combustion Engineering, Inc., C-E Critical Heat Flux, CENPD-162-A, Supplement 1-A, February 1977.

APPENDIX C

DATA BASE: CRITICAL HEAT FLUX AND QUENCH

APPENDIX C

DATA BASE: CRITICAL HEAT FLUX AND QUENCH

Contained within this appendix are the experimental data used in this report from all of the power-cooling-mismatch (PCM) and irradiation effects (IE) tests conducted, up to and including PR-1 (PCM-7 data was not available at the date of this publication). The PCM and IE tests were conducted in the Power Burst Facility at the Idaho National Engineering Laboratory.

The parametric ranges of the critical heat flux data in Table C-1 are as follows:

Mass flux	314 to 2750 kg/m^2 s
Peak rod power	40.5 to 71.0 kW/m
System pressure	12.7 to 15.6 MPa
Inlet temperature	575 to 610 K
Local quality	-0.035 to 0.239

The ranges of the quench data listed in Table C-2 are as follows:

Mass flux	345 to 2112 kg/m^2 s
Peak rod power	34.1 to 70.5 kW/m
System pressure	12.7 to 15.6 MPa
Inlet temperature	590 to 610 K
Maximum cladding temperature	668 to 1300 K
Time in film boiling	2.0 to 687 s

TABLE C-1. CRITICAL HEAT FLUX DATA

Test	PCM Cycle	Fuel Rod	System Pressure (MPa)	Coolant Inlet Temperature (K)	Elevation of DNB (m)	Peak Rod Power at Onset of DNB (kW/m)	Coolant Mass Flux at Onset of DNB (kg/m^2 s)	Local Critical Heat Flux (kW/m^2)	Local Quality
PCM-1	1	1	15.2	601	0.78 ± 0.1	52.0 ± 8%	1143 ± 5%	840 ± 18%	0.095
PCM-2[a,b]	8	8	13.6	600	0.686 ± 0.05	49.8 ± 8%	717 ± 8%	1057 ± 14%	0.231
	8	9	13.6	600	0.787 ± 0.05	52.3 ± 8%	917 ± 7%	855 ± 11%	0.208
	8	10	13.6	600	0.787 ± 0.05	52.7 ± 8%	975 ± 7%	861 ± 11%	0.195
PCM-2A[c]	2	1	14.7	600	[d]	53.4 ± 8%	693 ± 7%	[d]	[d]
	4	1	14.7	600	[d]	44.0 ± 8%	693 ± 7%	[d]	[d]
	8	1	14.7	600	[d]	53.4 ± 8%	715 ± 7%	[d]	[d]
	9	1	14.7	600	0.79 ± 0.1	59.8 ± 8%	809 ± 7%	772 ± 16%	0.239
PCM-3[e]	1	21	15.4	600	0.584 ± 0.05	49.5 ± 8%	971 ± 6%	1295 ± 16%	0.059
	3	21	15.4	600	0.686 ± 0.05	49.5 ± 8%	1127 ± 6%	1102 ± 14%	0.066
	4	21	15.4	600	0.686 ± 0.05	49.5 ± 8%	1011 ± 6%	1102 ± 14%	0.089
	5	11	15.4	600	0.737 ± 0.05	49.5 ± 8%	734 ± 8%	977 ± 12%	0.229
	5	21	15.4	600	0.686 ± 0.00	49.5 ± 8%	896 ± 7%	1102 ± 14%	0.116
PCM-4	1	15	15.1	600	0.686 ± 0.05	67.9 ± 8%	2112 ± 3%	1482 ± 14%	0.024
	2	15	15.1	600	0.635 ± 0.05	67.1 ± 8%	1973 ± 3%	1621 ± 15%	0.020
	3	15	15.1	600	0.686 ± 0.05	58.0 ± 8%	1863 ± 3%	1267 ± 14%	0.019
	4	14	15.1	600	0.787 ± 0.05	70.5 ± 8%	1909 ± 3%	1105 ± 11%	0.063
	4	15	15.1	600	0.686 ± 0.05	67.1 ± 8%	1967 ± 3%	1464 ± 14%	0.032
	4	16	15.1	600	0.787 ± 0.05	67.9 ± 8%	1852 ± 3%	1063 ± 11%	0.062
PCM-5[f]	1	1	15.5	593	0.58 ± 0.1	59.4 ± 12%	1055 ± 3%	1612 ± 18%	0.019
	1	3[g]	15.5	593	0.68 ± 0.1	62.1 ± 12%	1055 ± 3%	1422 ± 27%	0.024
	1	3[g]	15.5	593	0.68 ± 0.1	61.7 ± 12%	1055 ± 3%	1413 ± 27%	0.022
	1	3[g]	15.5	593	0.68 ± 0.1	61.4 ± 12%	1082 ± 3%	1407 ± 27%	0.016
	1	3[g]	15.5	593	0.68 ± 0.1	61.4 ± 12%	1092 ± 3%	1407 ± 27%	0.014

TABLE C-1. (continued)

Test	PCM Cycle	Fuel Rod	System Pressure (MPa)	Coolant Inlet Temperature (K)	Elevation of DNB (m)	Peak Rod Power at Onset of DNB (kW/m)	Coolant Mass Flux at Onset of DNB (kg/m^2 s)	Local Critical Heat Flux (kW/m^2)	Local Quality
	1	5	15.5	593	0.73 ± 0.05[h]	55.7 ± 12%	1082 ± 3%	1116 ± 27%	0.010
	1	6	15.5	593	0.68 ± 0.1	59.7 ± 12%	1108 ± 3%	1366 ± 27%	0.006
	1	8	15.5	593	0.68 ± 0.1[i]	60.7 ± 12%	1055 ± 3%	1390 ± 27%	0.019
8-1-RS[j]	3	1	13.5	600	0.74 ± 0.05	63.9 ± 8%[k]	1341 ± 4%	1241 ± 12%	0.056
	4	1	13.5	600	0.69 ± 0.05	65.9 ± 8%[k]	1353 ± 4%	1498 ± 14%	0.053
8-1-RF[j]	3	1	15.2	600	0.74 ± 0.05	59.4 ± 8%	605 ± 6%	1366 ± 12%	0.142
	4	1	15.2	600	0.74 ± 0.05	60.7 ± 8%	600 ± 6%	1396 ± 12%	0.150
	5	1	15.2	600	0.74 ± 0.05	61.0 ± 8%	568 ± 6%	1403 ± 12%	0.168
	6	1	15.2	600	0.74 ± 0.05	60.7 ± 8%	513 ± 7%	1396 ± 12%	0.194
CHF	1	1	15.2	603	0.667 ± 0.05	50.5 ± 8%	1262 ± 3%	1190 ± 14%	-0.007
Scoping[e]	3	1	15.2	603	0.667 ± 0.05	63.3 ± 8%	1387 ± 3%	1494 ± 14%	0.004
	4	1	15.2	603	0.533 ± 0.05	62.3 ± 8%	1364 ± 3%	1772 ± 16%	-0.021
	5	1	15.2	603	0.667 ± 0.05	58.4 ± 8%	1368 ± 3%	1379 ± 14%	-0.001
	6	1	15.2	603	0.667 ± 0.05	61.7 ± 8%	1383 ± 3%	1456 ± 14%	0.003
	7	1	15.2	603	0.58 ± 0.1	60.0 ± 8%	1358 ± 3%	1614 ± 20%	-0.015
PR-1[l,m]	7	1	12.7	594	d	43.0	590	d	d
	8	1	15.5	607	d	43.5	530	d	d
	8	3	15.5	607	d	43.0	509	d	d
	9	3	15.5	610	d	43.0	525	d	d
	14	3	13.0	593	d	43.5	380	d	d
	14	1	13.0	593	d	41.0	522	d	d
	15	1	13.1	593	d	44.0	442	d	d
	16	3	15.5	603	d	41.0	450	d	d
	16	1	15.5	603	d	41.0	590	d	d

TABLE C-1. (continued)

Test	PCM Cycle	Fuel Rod	System Pressure (MPa)	Coolant Inlet Temperature (K)	Elevation of DNB (m)	Peak Rod Power at Onset of DNB (kW/m)	Coolant Mass Flux at Onset of DNB (kg/m^2 s)	Local Critical Heat Flux (kW/m^2)	Local Quality
	17	1	15.6	604	d	41.5	498	d	d
	17	3	15.6	604	d	41.5	434	d	d
	17	4	15.6	604	d	41.5	360	d	d
PR-1[l,m]	20	3	12.9	593	d	42.3	322	d	d
	20	4	12.9	593	d	42.0	314	d	d
	21	1	15.4	606	d	41.0[n]	487[n]	d	d
	21	3	15.4	606	d	40.5	406	d	d
	22	1	15.0	575	d	46.0[n]	890[n]	d	d
	23	1	15.2	605	d	43.0[n]	550[n]	d	d
	23	3	15.2	605	d	43.0	340	d	d
	24	1	15.6	590	d	42.5[n]	810[n]	d	d
	25	4	15.5	590	d	52.0	345	d	d
IE ST-1	1	1	14.8	600	0.6 ± 0.1	67	2090	1890	-0.004
IE ST-2	1	5	15.2	600	0.6 ± 0.1	61	1280	1680	-0.035
	1	6	15.2	600	0.6 ± 0.1	61	1414	1680	a
IE-1	1	7	14.8	605	0.6 ± 0.1	68	2520	1950	o
	1	8	14.8	605	0.6 ± 0.1	63	1690	1810	0.003
	1	9	14.8	605	0.6 ± 0.1	64	1840	1840	-0.005
	1	10	14.8	605	0.6 ± 0.1	64	2030	1840	-0.016
IE-2	1	11	15.2	606	0.6 ± 0.1	65	2550	1830	0.011
	1	12	15.2	606	0.6 ± 0.1	65	2650	1840	0.008
	1	13	15.2	606	0.6 ± 0.1	62	2750	1760	0.001
	1	14	15.2	606	0.6 ± 0.1	61	2750	1730	0.000

TABLE C-1. (continued)

Test	PCM Cycle	Fuel Rod	System Pressure (MPa)	Coolant Inlet Temperature (K)	Elevation of DNB (m)	Peak Rod Power at Onset of DNB (kW/m)	Coolant Mass Flux at Onset of DNB (kg/m^2 s)	Local Critical Heat Flux (kW/m^2)	Local Quality
IE-3	1	15	15.2	606	0.6 ± 0.1	71	2110	2000	0.038
	1	16	15.2	606	0.6 ± 0.1	65	2160	1830	0.026
	1	17	15.2	606	0.6 ± 0.1	71	2290	2000	0.029
	1	18	15.2	606	0.6 ± 0.1	62	2100	1750	0.024
IE-5	1	19	15.2	605	0.6 ± 0.1	62	1275	1730	0.080
	1	20	15.2	605	0.6 ± 0.1	68	1315	1900	0.090
	1	21	15.2	605	0.6 ± 0.1	63	1210	1760	0.092
	1	22	15.2	605	0.6 ± 0.1	69	1800	1930	0.046

a. Rod 14 not instrumented.
b. Cycle 8 is the only usable data.
c. Cycle 1 did not reach film boiling, data not available on Cycles 3, 5, 6, and 7.
d. Data from LVDT, no local elevation.
e. No good data available on Cycle 2.
f. Rods 2, 4 not instrumented. Rods 7, 8 had no thermocouples. Rods 3, 9 had no LVDT.
g. Rod 3 underwent four separate DNB cycles.
h. Simultaneous DNB at 0.68 and 0.78 m elevations.
i. Best guess on elevation of DNB.
j. Good data not available on Cycles 1 and 2.
k. Suspected to be high values.
l. Test PR-1 used BWR-type rods.
m. Average (of four rods) test rod peak power.
n. Data from failed rod.
o. Data not available, function undefined (see Appendix D).

TABLE C-2. QUENCH DATA

Test	PCM Cycle	Fuel Rod	System Pressure (MPa)	Coolant Inlet Temperature (K)	Elevation of Quench (m)	Cladding Temperature at Quench (K)	Maximum Cladding Temperature during Cycle (K)	Coolant Mass Flux at Quench (kg/m^2 s)	Peak Rod[a] Power at Quench (kW/m)	Local[b] Quench Heat Flux (kW/m^2)	Time in Film Boiling (s)
PCM-1[c]											
PCM-2[d,e]	8	8	13.6	600	0.635	1210	1300	1462 ± 4%	43.2	1012	80
	8	8	13.6	600	0.686	1020	1170	1634 ± 4%	34.6	733	122
	8	9	13.6	600	0.787	910	915	1262 ± 5%	52.3	855	55
	8	10	13.6	600	0.787	875	875	803 ± 8%	52.7	861	54
PCM-2A[f,g]	2	1	14.7	600	0.787	645	645	798 ± 9%	53.5	692	372
	3	1	14.7	600	0.787	644	644	715 ± 8%	56.7	733	h
	4	1	14.7	600	0.787	648	648	704 ± 8%	56.7	733	813
	8	1	14.7	600	0.787	665	668	720 ± 8%	58.1	751	325[i]
	9	1	14.7	600	0.787	856	859	792 ± 8%	59.8	772	208
PCM-3	1	21	15.4	600	0.584	945	945	971 ± 6%	49.5	1295	10.0
	3	21	15.4	600	0.686	755	755	968 ± 6%	49.5	1102	5.0
	4	21	15.4	600	0.686	805	805	913 ± 7%	40.7	906	5.9
	5	11	15.4	600	0.635	695	695	740 ± 8%	49.9	1206	2.0
	5	11	15.4	600	0.686[j]	885[j]	885[j]	780 ± 8%	k	k	10.5[j]
	5	11	15.4	600	0.737[j]	890[j]	890[j]	734 ± 8%	k	k	21.5[j]
	5	21	15.4	600	0.635	810	810	751 ± 8%	49.5	1197	4.5
	5	21	15.4	600	0.584	1040	1080	844 ± 7%	k	k	28.0
	5	21	15.4	600	0.635	1080	1080	844 ± 7%	k	k	19.0
	5	21	15.4	600	0.686	1108	1108	844 ± 7%	k	k	56.0
	5	21	15.4	600	0.889	653	725	769 ± 8%	k	k	24.0
PCM-4[l]	1	15	15.1	600	0.635	727	727	2112 ± 3%	67.1	1621	22
	1	15	15.1	600	0.686	712	715	2112 ± 3%	65.6	1431	42
	2	15	15.1	600	0.635	703	703	1921 ± 3%	k	k	135
	3	15	15.1	600	0.686	730	730	1794 ± 4%	58.0	1260	195
	4	14	15.1	600	0.584	935	935	1678 ± 4%	70.5	1850	148
	4	14	15.1	600	0.686	860	920	1678 ± 4%	70.5	1538	148
	4	14	15.1	600	0.787	790	860	1678 ± 4%	70.5	1105	148
	4	15	15.1	600	0.635	980	1040	1637 ± 4%	k	k	212
	4	16[m]	15.1	600	0.686	1100	1100	1637 ± 4%	k	k	212

TABLE C-2. (continued)

Test	Rod Cycle	Fuel Rod	System Pressure (MPa)	Coolant Inlet Temperature (K)	Elevation Of Quench (m)	Cladding Temperature at Quench (K)	Maximum Cladding Temperature During Cycle (K)	Coolant Mass Flux at Quench (kg/m^2 s)	Peak Rod[a] Power at Quench (kW/m)	Local[b] Quench Heat Flux (kW/m^2)	Time in Film Boiling (s)
PCM-5	1	1[n]	15.5	593	0.58	980-1020[o]	1170	1161 ± 3%	36.0	977	670
	1	1[n]	15.5	593	0.68	798	1290	1414 ± 3%	34.1	781	647
	1	1[n]	15.5	593	0.78	775-800[o]	1120[p]	1161 ± 3%	36.0	609	629
	1	39,[r]	15.5	593	0.68	800	850	1055 ± 3%	62.5	1432	26.5
	1	39,[r]	15.5	593	0.68	820	825	1055 ± 3%	62.0	1420	25.5
	1	39,[r]	15.5	593	0.68	835	1010	1119 ± 3%	61.4	1406	48
	1	39,[r]	15.5	593	0.68	845-905[o]	1060	1098 ± 3%	60.6	1388	66
	1	39,[r]	15.5	593	0.78	880	1050	1113 ± 3%	61.2	1035	90
	1	5	15.5	593	0.68	900	1120	1098 ± 3%	56.1	1285	139
	1	5	15.5	593	0.78	770	1110	1108 ± 3%	56.4	954	210[s]
	1	6	15.5	593	0.68	850-875[o]	1000	1108 ± 3%	59.3	1359	43
	1	8	15.5	593	t	t	t	1108 ± 3%	59.0	t	310
8-1-RS[k]											
8-1-RF	3	1	15.2	600	0.74	692	692	607 ± 6%	k	k	5
	4	1	15.2	600	0.74	689	689	603 ± 6%	k	k	7
	5	1	15.2	600	0.74	668	668	569 ± 6%	k	k	7
	6	1	15.2	600	0.74	989	989	514 ± 7%	64.4	1440	44
CHF Scoping[k]											
PR-1[u,v]	7	1	12.7	594	t	t	t	424	36.0	t	h
	8	1	15.5	607	t	t	t	415	40.8	t	h
	8	3	15.5	607	t	t	t	377	41.0	t	h
	9	3	15.5	610	t	t	t	472	41.0	t	h
	14	1	13.0	593	t	t	t	522	40.8	t	h
	14	3	13.0	593	t	t	t	903	40.5	t	h
	15	1	13.1	593	t	t	t	482	42.5	t	h
	17	1	15.6	604	t	t	t	509	41.5	t	h
	17	3	15.6	604	t	t	t	472	41.5	t	h
	17	4	15.6	604	t	t	t	415	41.5	t	h
PR-1[u,v]	20	1	12.9	593	t	t	t	1080[w]	42.0[w]	t	h
	21	1	15.4	606	t	t	t	528[w]	39.0[w]	t	h
	21	3	15.4	606	t	t	t	467	39.0	t	h
	23	1	1[c] 2	606	t	t	t	483[w]	41.5[w]	t	h

TABLE C-2. (continued)

Test	PCM Cycle	Fuel Rod	System Pressure (MPa)	Coolant Inlet Temperature (K)	Elevation Of Quench (m)	Cladding Temperature at Quench (K)	Maximum Cladding Temperature during Cycle (K)	Coolant Mass Flux at Quench (kg/m^2 s)	Peak Rod[a] Power at Quench (kW/m)	Local[b] Quench Heat Flux (kW/m^2)	Time in Film Boiling (s)
	23	3	15.2	606	t	t	t	443	41.2	t	h
	24	1	15.6	590	t	t	t	1096[w]	43.5[w]	t	h
	25	1	15.5	590	t	t	t	426[w]	53.0[w]	t	h
	25	2	15.5	590	t	t	t	386	52.0	t	h
	25	3	15.5	590	t	t	t	406	53.0	t	h
	25	4	15.5	590	t	t	t	345	49.0	t	h

a. Uncertainty on peak rod power is 12%.
b. Uncertainty on local critical heat flux is 12% for PCM-5, 8% for all other tests.
c. No quench data available, thermocouples failed, flow rate blocked at 920 s.
d. Cycle 8 is the only good data.
e. Rod 14 not instrumented.
f. Only data from 0.787 m thermocouple was used.
g. Data not available for cycles 1, 5, 6, 7.
h. Data not available.
i. t comes from LVDT data.
j. Time of quench arrived at by using -200 slope method.
k. Reactor scram, data not available.
l. Rod 17 not instrumented.
m. All rods quenched except Rod 16 which rose in temperature from 700 to 1000 K at the time the other rods quenched (scram).
n. Total time in film boiling is 687 s.
o. Based on "best fit of asymptotes" or "-200 slope method", respectively.
p. Maximum cladding temperature immediately before quench is 880 K.
q. Rod 3 underwent four separate DNB cycles.
r. Total time in film boiling for Rod 3 is 229 s.
s. Total time in film boiling for Rod 5 is 210 s.
t. Data from LVDT, no local elevation, no quench temperatures.
u. Test PR-1 used BWR-type rods.
v. Quench indicated by rapid drop in LVDT trace.
w. Data from failed rod.

APPENDIX D

METHODOLOGY AND CALCULATIONS

APPENDIX D

METHODOLOGY AND CALCULATIONS

In this appendix the methodology and calculations of quality and error propagation are presented. In addition, a brief table of conversion factors commonly used in this study is given.

1. CALCULATION OF LOCAL QUALITY

There are several qualities that are of importance in the analysis of two-phase heat transfer. The quality χ of a liquid-vapor mixture in a non-flow system, or where no gross relative motion between the liquid and vapor phases exists, is defined as

$$\chi \equiv \frac{\text{mass of vapor in mixture}}{\text{total mass of mixture}} \tag{D-1}$$

or

$$\chi \equiv \frac{\rho_v \; x \; A}{(\rho_v A_x + \rho_L A_L)} \tag{D-2}$$

where ρ is density, A is cross sectional area and subscripts v and L refer to the vapor and liquid phases, respectively.

In a flow system, the quality at a given cross section is defined by

$$\chi = \frac{\text{mass-flow rate of vapor}}{\text{mass-flow rate of mixture}} \tag{D-3}$$

or

$$\chi = \frac{\rho_v A_v V_v}{(\rho_v A_v V_v + \rho_L A_L V_L)} \tag{D-4}$$

where V_v and V_L are the respective vapor and liquid velocities. Equation (D-4) can be rearranged to give a relationship between quality and void fraction (α), including the influence of interfacial slip, as

$$\alpha = \frac{1}{1 + \left(\frac{1 - \chi}{\chi}\right)\left(\frac{V_L}{V_v} S\right)} \qquad \text{(D-5)}$$

where S is an interfacial slip parameter. The effect of slip is to reduce the relative void fraction at a given quality. The interfacial slip parameter has been experimentally found to decrease with both system pressure and the volumetric flow rate and to increase with power density.

The quality which is extensively used within this study is the flow quality, given by Equation (D-3). In addition, the following assumptions are made:

1. There is no subcooled nucleate boiling

2. Vapor superheat is neglected

3. There is no slip at the liquid-vapor interface

4. Perfect cosine shaped power distribution.

In actuality, none of the above assumptions are always true, however, such assumptions are necessary to simplify the quality calculation.

The expression for quality at an elevation of Z is given by:

$$\chi = \frac{P_p L}{\pi h_{fg} G \rho_{in}} \left[\cos\left(\frac{\pi L_o}{L}\right) - \cos\left(\frac{\pi Z}{L}\right)\right] \qquad \text{(D-6)}$$

where the nonboiling height L_o is given by

$$L_o = \frac{L}{\pi} \arccos \left[1 - \frac{\pi \bar{C}_p \Delta T_{sc} G \bar{\rho}}{P_p L} \right] \qquad \text{(D-7)}$$

In essence, the above quality relationship assumes a homogeneous, equilibrium model and may best be viewed as a liquid-vapor distribution scaling parameter. Comparison of Equation (D-5) with quality calculations from subchannel code COBRA-IV[B-1] indicates favorable agreement.

Many of the critical heat flux correlations include one or more equivalent diameter terms. The two most common are the equivalent diameter based on wetted perimeter (D_e) and the equivalent diameter based on heated perimeter (D_H). The following equations were used to calculate these quantities:

$$D_H = \frac{4A}{P_c}, \qquad D_e = \frac{4A}{P_c + P_s} \qquad \text{(D-8)}$$

where

A = flow area
P_c = outside perimeter of cladding
P_s = inside perimeter of flow shroud.

2. ERROR ANALYSIS

Error estimates were made using a linear error propagation method.[D-2] The error is found using the equation

$$(\text{error})^2 = \left(\frac{\partial P}{\partial y}\right)^2 (\sigma z)^2 + \left(\frac{\partial P}{\partial y}\right)^2 (\sigma y)^2 . \qquad \text{(D-9)}$$

where

P = $f(Z,y)$ and ∂ is the associated uncertainty.

3. CONVERSION FACTORS

Table D-1 lists the conversion factors commonly used within this study.

TABLE D-1. CONVERSION FACTORS

$1 \frac{Btu}{ft^2\text{-}hr}$	=	$3.15 \times 10^{-3} \frac{kW}{m^2}$
$1 \frac{lbm}{ft^2\text{-}hr}$	=	$1.36 \times 10^{-3} \frac{kg}{m^2 \cdot s}$
$1 \frac{kW}{ft}$	=	$3.2808 \frac{kW}{m}$
1 gpm	=	$6.30 \times 10^{-2} \frac{l}{s}$
K	=	0.556 F + 255.37

REFERENCES

D-1. C. L. Wheeler et al., COBRA-IV-I: An Interim Version of COBRA for Thermal-Hydraulic Analysis of Rod Bundle Nuclear Fuel Elements and Cores, BNWL-1962, UC-32, March 1976.

D-2. M. G. Natrella, Experimental Statistics, Washington, D.C., U.S. National Bureau of Standards, August 1, 1963.